Aerosol Synthesis of Ceramic Particles by seed Growth: Analysis of process constraints

BY: **Chris Human**

DEGREE of MASTERS of SCIENCE
In
ENGINEERING SCIENCE
(Chemical Engineering)

at the

University of Stellenbosch

Supervisors: **Prof. SM Bradshaw**

AEROSOL SYNTHESIS OF CERAMIC PARTICLES BY SEED GROWTH: ANALYSIS OF PROCESS CONSTRAINTS

By

Chris Human

Supervised by:

Prof. Steven M. Bradshaw

SUBMITTED IN PARTIAL FULFILLMENT OF THE
REQUIREMENTS FOR THE DEGREE OF
MASTER OF CHEMICAL ENGINEERING
AT
THE UNIVERSITY OF STELLENBOSCH

MARCH 2002

DECLARATION

I, the undersigned, declare that the work contained in this thesis is my own original work and has not previously, in its entirety or in part, been submitted at any university for a degree.

Chris Human

Synopsis

Aerosol synthesis involves the formation of condensable product species by gas-phase reaction, and the simultaneous growth of particles by coagulation. For the production of ceramic particles, reaction temperatures higher than 700 K are commonly used, and a maximum fusible particle size is observed.

Coagulation-controlled growth yields spherical particles up to the maximum fusible size (approximately $< 50\ nm$). Such particles coalesce rapidly and completely upon collision with other particles, whereas larger particles reach a meta-stable equilibrium for solid-state coalescence. Agglomerates with weak Van der Waal's bonds between particles inevitably form in the cooling/collection process.

Coagulation of particles larger than the maximum fusible particle size yields agglomerates with significant neck growth between the primary particles.

Spherical ceramic particles in the order of 1 μm are favourable precursors for bulk electronic applications that require high purity. Such large spherical particles may possibly be produced in conditions of seed growth, which involves the deposition of small newly formed clusters onto larger existing particles.

The central focus of the present work is to evaluate whether spherical ceramic particles significantly larger than the maximum fusible size may be produced by seed growth. The evaluation is done by modelling of process constraints and interpretation of published results.

The modelling of constraints is based on a mathematical framework for comparison of different values of reactor design parameters. This framework comprises a simplified model system, a typology of quantities, and isolation of a set of independent design parameters. Comparison is done on the basis of fixed initial (seed) and final (product) particle sizes.

The reactor design framework is used to evaluate the hypothesis on spherical seed growth, by assessing whether a reactor can be designed that satisfies all the process constraints. Future extension of the framework may allow optimisation for seed growth in general.

The model system assumes laminar flow and isothermal conditions, and neglects the effect of reactor diameter on wall-deposition.

The constraints are graphically represented in terms of the design parameters of initial reactant concentration and seed concentration. The effects of different temperatures and pressures on the constraints are also investigated.

In a separate analysis, the suitability of turbulent flow for seed growth is assessed by calculating Brownian and turbulent collision coefficients for different colliding species. As turbulent intensity is increased, the seed coagulation rate is the first coagulation rate to be significantly enhanced by turbulence, resulting in a lowering of the maximum seed concentration allowed by the constraint for negligible seed coagulation. This tightening of a constraint by turbulence is the justification for considering only laminar flow for evaluating the hypothesis on spherical seed growth.

Quantitative application of the model of constraints, as well as experimental and modelling results from the literature, did not demonstrate that significant spherical seed growth is possible without seed coagulation (agglomeration).

As part of the conceptual effort in becoming familiar with aerosol reactor engineering, a simple two-mode plug-flow aerosol reactor model was developed, and verified with published results. This model has some novel value in that it translates the equations for aerosol dynamics into the terminology of reactor engineering.

Opsomming

Aerosol sintese behels die gelyktydige chemiese vorming van 'n kondenseerbare spesie en die groei van partikels deur koagulasie. Temperature hoër as $700\,K$ word gewoonlik vir die aerosol sintese van keramieke gebruik. Partikels bo 'n sekere grootte kan nie saamsmelt nie.

Koagulasie-beheerde groei lewer sferiese partikels tot en met die maksimum saamsmeltbare partikelgrootte (ongeveer $< 50\,nm$). Wanneer sulke partikels bots, smelt hulle vinnig en volledig saam. Groter partikels bereik egter 'n meta-stabiele ewewig vir vastestof samesmelting. Agglomerate met swak Van der Waal's bindinge tussen partikels vorm onvermydelik wanneer die aerosol afgekoel word en die produk versamel word.

Koagulasie van partikels groter as die maksimum saamsmeltbare grootte, lewer agglomerate met noemenswaardige nekvorming tussen primêre partikels.

Sferiese keramiekpartikels in die ordegrootte van $1\,\mu m$ is geskikte intermediêre produkte vir die vervaardiging van soliede eletroniese komponente waarvoor hoë materiaalsuiwerheid vereis word. Sulke groot sferiese partikels kan moontlik geproduseer word in toestande waar klein nuutgevormde partikels deponeer op groter bestaande partikels (saadpartikels).

Die hoof-fokus van die huidige werk is om vas te stel of sferiese keramiekpartikels wat noemenswaardig groter is as die maksimum saamsmeltbare grootte, geproduseer kan word met die metode van saadpartikel-groei. Die moontlikheid word ondersoek deur 'n model van prosesbeperkings te maak, en deur gepubliseerde resultate te vertolk.

Die model van prosesbeperkings is gegrond op 'n wiskundige raamwerk vir die vergelyking van verskillende waardes van reaktor ontwerp-parameters. Hierdie raamwerk bestaan uit 'n vereenvoudigde model-sisteem, 'n tipologie van verskillende soorte groothede, en die identifikasie van 'n stel onafhanklike ontwerp-parameters. Verskillende parameter-waardes word vergelyk vir dieselfde aanvanklike (saad) en resulterende (produk) partikelgroottes.

Die reaktorontwerp-raamwerk word gebruik om die hipotese van sferiese saadpartikel-groei te evalueer, deur vas te stel of 'n reaktor ontwerp kan word wat aan al die prosesbeperkings voldoen. Mettertydse verfyning van die raamwerk kan dit moontlik geskik maak vir die optimering van saadpartikel-groei in die algemeen.

Die model-sisteem is gebaseer op die aannames dat vloei laminêr en temperatuur konstant is, en die effek van reaktor-diameter op deponering op die reaktorwand word verontagsaam.

Die posesbeperkings word grafies voorgestel in terme van oorspronklike reaktant-konsentrasie en saadpartikel-konsentrasie. Die effek van verskillende temperature en drukke op die prosesbeperkings word ook ondersoek.

'n Systaande ondersoek word gedoen oor die toepaslikheid van turbulente vloei vir saadpartikel-groei, deur botsings-koeffisiënte vir Brown-beweging en turbulensie te vergelyk. Wanneer turbulensie verhoog word, styg die koaguleringstempo van saadpartikels beduidend voordat ander koaguleringstempo's beduidend toeneem. Dit noodsaak 'n verlaging in die maksimum toelaatbare saadpartikel-konsentrasie om saadpartikel-koagulasie te verhoed. Hierdie verskerping van 'n prosesbeperking deur turbulente vloei, is die rede hoekom slegs laminêre vloei beskou word in die evaluering van die hipotese van sferiese saadpartikel-groei.

Kwantitatiewe toepassing van die model van beperkings, asook eksperimentele en modellerings-resultate vanuit die literatuur, het nie getoon dat noemenswaardige groei van sferiese keramiekpartikels verkry kan word sonder saadpartikel-koagulasie (agglomerasie) nie.

As deel van die proses om aerosol reaktor-ingenieurswese konsepsueel onder beheer te kry, is 'n eenvoudige twee-modus propvloei aerosol reaktor model ontwikkel. Die resultate van die model is bevestig deur vergelyking met gepubliseerde resultate. Hierdie model het die nuwigheid dat dit die vergelykings vir aerosol dinamika uitdruk in die terminologie van reaktor-ingenieurswese.

Acknowledgements

The National Research Foundation of South Africa

for financially supporting this project (under grant 2043036).

Albert Visagie

for suggesting logarithmic transformation of differential equations when I had numerical problems.

Prof. Steven Bradshaw

for his abundant enthusiasm and commitment in guiding me.

Piet and Marlene Human

for their loving support.

Contents

List of Tables

List of Figures

Nomenclature

A	surface area	m^2
A_{gr}	reaction rate constant	s^{-1}
A_v	Avogadro number	$\#/mol$
c	velocity	m/s
C	concentration (of limiting reactant, unless indicated otherwise)	mol/m^3
C_0	initial concentration of limiting reactant	mol/m^3
d_a	agglomerate equivalent collision radius	m
d_i	particle/unit diameter	m
d_{melt}	maximum fusible particle size	m
d_p^*	critical nucleation particle size	m
d_{pg}	geometric average particle size	m
d_{pv}	volume-average particle size	m
D	reactor inner diameter	m
D	diffusivity	m^2/s
E_{gr}	activation energy for gas-phase reaction	$\frac{J}{mol \cdot K}$

f	minimum ratio between monomer consumption by m-p and m-m collisions, for constrained cluster growth	
f_F	fanning friction factor	
G	Gibbs free energy	J/mol
k	reaction rate constant	s^{-1}
k_B	Boltzmann's constant	$\frac{J}{K \cdot \#}$
ℓ_n	neck length	m
L	reactor length	m
m	number of molecules in a particle	$\#_m/\#$
m_{pp}	number of molecules in a primary particle in an agglomerate	$\#_m/\#_{pp}$
M_{pr}	production rate	t/a
MW_i	molecular weight	g/mol
n	number concentration	$\#/m^3$
n	particle distribution function	$\frac{\#}{m^3 \cdot m}$
n_{pp}	number of primary particles per agglomerate	$\#_{pp}/\#_a$

N	number flux of reaction or species (indicated by subscript)	$\#/s$
N_0	initial number flux of limiting reactant	$\#/s$
P	pressure	N/m^2
P	probability	$[0,1]$
r	reaction rate	$\frac{\#}{m^3 \cdot s}$ or $\frac{mol}{m^3 \cdot s}$
r	particle radius	m
r_0	tube radius ($= D/2$)	m
R	gas constant	$\frac{J}{mol \cdot K}$
$R_{c,s}$	rate of condensation onto a single particle	$\frac{\#_c}{\#_p \cdot s}$
S	supersaturation ratio	
t	time	s
T	temperature	K
u	velocity	m/s
v	molar volume	m^3/mol
V	volume	m
W_{dep_f}	average wall-deposition per volume of gas passing through the reactor	$[\#/m^3]$
x	neck radius	m

Non-Dimensional Parameters		
D_f	fractal dimension	
Kn	Knudsen number	
κ_c	collision rate constant	
κ_{gr}	reaction rate constant	
(l_0/d_1)	parameter for Brownian collisions	
Pe	Peclet number	
Pr	Prandtl number	
Re	Reynolds number	
$\left(\frac{W}{S}\right)$	local wall-to-seed deposition ratio	
X_{wd}	fractional yield loss to wall-deposition (in absence of seeds)	

Non-Dimensional Variables		
ϕ_i	number conversion of reaction i	[0,1]
γ_i	reaction rate i	
η_i	number concentration of species i	
LC_i	$= -\ln(1-\phi_i)$	
L_m	$= \ln(m_p)$	
x	position in reactor	

Greek Symbols		
α	constant	
α_i	stoichiometric coefficient	
β	iteration variable	$= \frac{C_{m_f}}{C_f}$
$\beta_{B_{ij}}$	Brownian collision coefficient	$\frac{m^3}{\#\cdot s}$
$\beta_{T_{ij}}$	turbulent collision coefficient	$\frac{m^3}{\#\cdot s}$
γ	surface tension	N/m
ε	fractional excess gas	
ε_d	turbulent energy dissipation rate	m^2/s^3
ϵ_{sc}	fractional seed coagulation	
ϵ_{te}	fractional thermodynamic entry length	
λ	mean free path of gas molecules	m
μ	viscosity	$N\cdot s/m^2$
μ	chemical potential	J/mol
θ	degree of coalescence	
ρ	density	kg/m^3
σ_g	geometric standard deviation	
σ_s	surface tension	N/m
τ	characteristic time	s
τ_{melt}	time for growth up to the maximum fusible particle size	s
τ_{res}	residence time	s
ψ	contact angle	0
ψ_e	dihedral angle	0

Abbreviations		
GDE	General dynamic equation for aerosols	
PSD	particle size distribution	
RTD	Residence time distribution	
STP	standard temperature and pressure	

Subscripts		
bg	bulk gas	
bp	by-product	
c	collision	
cap	capillary	
coag	coagulation	
cond	condensation	
dep	deposition	
f	final condition	
fd, h	hydrodynamically fully developed flow	
fd, t	thermodynamically fully developed flow	
g	gas	
gb	grain-boundary	
gr	gas-phase reaction	
m	monomer	
mm	monomer-monomer collision	
mp	monomer-particle collision	
M	metal-containing reactant	
O	oxidant reactant	
p	particle	
pp	particle-particle collision	
pr	product	
s	seed particle	
s	solid phase	
T	total	
sv	solid-vapour interface	
w	reactor wall	
0	original condition	
1	single molecule (monomer)	

Chapter 1

Introduction

The term 'advanced ceramics' is used to indicate ceramic materials with high purity, high homogeneity, and with specific microstructure. Advanced ceramics are usually synthetically produced by reactions with pure reactants.

Isolated ceramic particles are important as precursors for densification, as precursors for producing porous structures, or to be used as is. Common applications of advanced ceramic particles include: sintering to dense components (electronic, refractory and structural), sintering to porous components (membranes and catalysts), pigments, electro-optical applications (solar cells), and nano-scale electronics (single-electron memory/logic). Ceramics are favoured for their high temperature stability, inertness to various chemical environments, hardness, and semi-conductor properties. In the aforementioned applications, it is favourable to have particles with high purity and well-controlled particle size and morphology.

Nano-sized ($\sim 10\,nm$) ceramic particles have electrical and optical properties that change drastically with particle size. These particles are building blocks for emerging technologies that harness the special electrical and electro-optical properties pertaining to the specific particle sizes. Furthermore, miniaturisation technology in general (electrical, mechanical, chemical, bio-chemical) benefits from the high size resolution obtainable by constructing devices from such small particles.

Spherical ceramic particles in the order of $1\ \mu m$ are favourable precursors for bulk electronic applications that require high purity (such as producing ceramic substrates by sintering of powder).

Aerosol synthesis is a method for producing ceramic particles with controlled size and morphology. This process involves the formation of the ceramic by high-temperature reaction, and the simultaneous growth of particles by coagulation (collision and subsequent bonding of particles). The high reaction temperature results in a very pure product, which does not need calcination as post-processing (such as many wet chemistry methods of particle production require).

Coagulation-controlled growth produces spherical particles up to a certain size (approximately $< 50 nm$). Particles smaller than this 'maximum fusible particle size' coalesce rapidly and completely upon collision with other particles. Agglomerates with weak Van der Waal's bonds between particles inevitably form in the cooling/collection process, but these may be broken by light milling.

Particles larger than the maximum fusible size reach a meta-stable equilibrium for solid-state coalescence. Hence the coagulation of such particles yields agglomerate structures, with significant neck growth between the primary particles (which requires expensive milling to break up).

Zachariah and Dimitriou (1990) made the hypothesis that non-agglomerated (spherical) ceramic particles larger than the maximum fusible size may be produced in an aerosol reactor by seed particle growth. It is proposed that 'large' (non-fusible) particles may be grown by deposition of small fusible particles onto it, without coagulation of the larger (seed) particles (which will yield unwanted agglomerates). The evaluation of this hypothesis is the focal topic of the present work.

Gaining understanding of the relatively new technological field of aerosol reactor engineering is a major objective of the present research. Therefore the literature review is intentionally educational, and considerable attention is given to precise explanations and definition of terminology.

The literature review starts by introducing the reader to modelling concepts that are commonly used for aerosols. The most important concepts are the number conservation equation, the coagulation rate equation, the distinction between controlled nucleation and uninhibited coagulation, and the coalescence behaviour particles of different sizes.

Literature on experimental reactors are reviewed, with special attention given to seed growth reactors.

The extensive review of published aerosol reactor models classifies the models according to the assumptions and approximations on which they are based, and the different phenomena that they consider. Different methods for solving the model equations are also reviewed.

The above-mentioned study of published aerosol reactor models provides the basis for defining a new simple aerosol reactor model, with appropriate assumptions and approximations. The definition of the model system aims to give insight into more complex models in the literature.

The model equations are expressed in terms of dimensionless reaction conversions, as is typically done in reactor engineering (whereas published aerosol models are not expressed in this manner). The expression of output variables as reaction conversions aims to aid the interpretation of modelling results.

The numerical solution of the model equations is tailored for the scaling of the output variables (conversions scaled from 0 to 1 and asymptotically approaching 1). To this end, the model equations are transformed into a logarithmic domain (expressed in terms of 'logarithmic' variables: $-\ln|1-conversion|$), to obtain increased numerical resolution for conversions close to 1.

The main contribution of the present work is the evaluation of the hypothesis that spherical ceramic particles larger than the maximum fusible size may be produced by seed growth in an aerosol reactor. A model of constraints is developed which is used to evaluate whether reactor conditions for spherical seed growth exist. This evaluation is supported by interpretation of published experimental and modelling results for seed growth.

Seed growth is a particular regime of aerosol reactor operation, with certain limits (constraints). To derive expressions for these constraints, the hypothetical method of constant number spherical seed growth is first defined rigorously.

Thereafter a simple model system is defined, once again using the review of published models as a basis for making appropriate assumptions and approximations. Where necessary, modelling simplifications are justified by deductive discourses and/or mathematical analyses, e.g. to determine whether turbulent conditions should be considered.

A structured analysis of quantities is used to extract a small set of (five) independent design parameters, and the constraint equations are expressed in terms these.

The model of constraints is applied quantitatively for a range of values for the design parameters. The results are presented as graphs of inequalities (for the different constraints), from which it can be seen whether an allowable region for spherical seed growth exists. The initial (seed) and final (product) particle sizes are considered as fixed parameters for constructing each graph of constraints, so that the graphs can be used to identify and compare different process conditions for the same production requirement.

Part I

Literature Review and Analysis

Chapter 2

Modelling Principles for Aerosols

This chapter is an introduction to the number conservation principle (population balance) and some constitutive laws which form the basis for fundamental modelling of aerosol systems.

First, the terminology used for aerosol systems is defined.

2.1 Phenomena and Terminology for Particulate Systems

The terminology used in aerosol literature is often not precisely defined, and in some cases different authors use different terminology. The definition of terms presented here is based on that of Ramabhadran, Peterson and Seinfeld (1976), and Flagan and Lunden (1995). Ramabhadran et al. clearly distinguished between homogeneous nucleation, heterogeneous nucleation (condensation), and coagulation. Flagan and Lunden presented a clear definition of the different species and processes in the evolution of non-spherical particles.

2.1.1 Terms for Different Species

monomer	A single molecule not bound to any other molecules.
cluster	A small number of molecules bound together, that is not necessarily thermodynamically stable.
particle	Two or more molecules bound together, that are thermodynamically stable (i.e. larger than the critical nucleation particle size).
agglomerate	Two or more particles bound together, but not completely coalesced.
soft agglomerate	Primary particles weakly bound together by Van der Waal's forces. Such agglomerates are formed at low temperature.
hard agglomerate	Primary particles strongly bound together by neck formation. Such agglomerates are formed at high temperature.
aggregate	Same as agglomerate.
composite particle	Two or more particles bound together, with any degree of coalescence. Hence a collective term for agglomerates and for particles formed by the complete coalescence of two or more smaller particles.

Table 2.1: Glossary of Terms for Aerosol Species

Any single monomer, cluster, particle or agglomerate is referred to as one **unit**.

It is difficult to distinguish between the different species. For example: let three monomers combine, and let this unit again combine with another such unit, and let the resultant unit not coalesce completely. The final unit can be called either a particle, a cluster or an agglomerate/aggregate, and in each case satisfy the species definition.

A two-molecule unit (dimer) has properties much closer to that of a single (gaseous) molecule than to that of a molecule in the bulk solid phase.

The distinction between gas and solid phase is not sharp when very small particles are concerned. Rather, there is a gradual change from gas properties to solid properties as the particle size increases.

In this text, it is attempted to use only the terms *monomer*, *particle* and *agglomerate*. These terms are defined unambiguously:

Monomer: A single molecule not bound to any other molecules.

Particle: A completely coalesced unit consisting of multiple molecules. A particle is characterised by its size (number of molecules).

Agglomerate: An unit consisting of multiple individually distinguishable particles. An agglomerate is characterised by its size (number of molecules) and by the arrangement of the molecules (morphology).

In the aerosol synthesis of ceramics, the vapour pressure is typically so low that even particles consisting of a small number of molecules (e.g. tri-mers) are thermodynamically stable. Therefore the distinction between thermodynamically stable and unstable particles is not employed in the present work.

The term **cluster** is used where necessary to refer to the portion of smaller particles in a bi-modal particle size distribution, or to refer to the literature.

2.1.2 Terms for Different Phenomena

homogeneous nucleation	The formation of clusters larger than the critical nucleation particle size (see section 2.3).
heterogeneous nucleation	The combination of thermodynamically unstable particles with existing thermodynamically stable particles.
condensation	Same as heterogeneous nucleation.
collision	The collision of units.
coagulation	Particle collision, with subsequent binding and complete coalescence.
deposition	Collision, and subsequent binding and complete coalescence, of a small particle with a much larger particle.
wall-deposition	Collision and subsequent binding of particles with the reactor wall.
coalescence	The fusion of a particle to reduce the surface area.
sintering	Same as coalescence.
agglomeration	The combination of particles in which the the primary particles remain identifiable; coagulation without complete coalescence.

Table 2.2: Glossary of Terms for Aerosol Phenomena

2.2 The Population Balance

A conservation principle called the *population balance* (also called the *particle-number continuity equation*) is used to model particulate systems. This principle concerns the conservation of the number of discrete units. The book of Randolph and Larson (1998), *Theory of Particulate Processes*, gives a good introduction to the population balance.

A particle population is characterised according to the spatial and time dimensions (called the *external dimensions*) and the characteristic dimensions that describe each particle (called the *internal dimensions*, e.g. particle size, shape, age, etc.). The space spanned by the internal and external dimensions is called the *particle phase space.*

The *particle distribution function* (n) describes the particle density at any position in the internal and external dimensions.

The following simple example of Randolph and Larson (1998) is used to illustrate the use of the population balance. Consider a particulate system with the only internal dimension being particle size (L), and only external dimension being the length in the reactor (expressed as a reactor volume V).

The total number of particles with sizes L_1 to L_2 in the reactor space between positions V_1 and volume V_2 is:

$$N(L_1, L_2; V_1, V_2) = \int_{V_1}^{V_2} \int_{L_1}^{L_2} n(L, V)\, \mathrm{d}L\, \mathrm{d}V \tag{2.1}$$

The population balance for a stationary control volume is:

$$\frac{\partial n}{\partial t} + \nabla \cdot (\mathbf{v}n) - B + D = 0 \tag{2.2}$$

where B and D are the birth and death rates of particles. $\mathbf{v}$ is the vector phase space velocity, consisting of a internal coordinate component and a external coordinate component ($\mathbf{v} = \mathbf{v}_i + \mathbf{v}_e$).

For internal dimension L and external dimension V:

$$\mathbf{v} = \frac{\mathrm{d}L}{\mathrm{d}t}\mathbf{i}_L + \frac{\mathrm{d}V}{\mathrm{d}t}\mathbf{i}_V \tag{2.3}$$

where $\mathbf{i}_L$ and $\mathbf{i}_V$ are the unit vectors in the dimensions size and position.

Expanding the divergence term in (2.2):

$$\frac{\partial n}{\partial t} + \frac{\partial}{\partial L}\left(n\frac{\mathrm{d}L}{\mathrm{d}t}\right) + \frac{\partial}{\partial V}\left(n\frac{\mathrm{d}V}{\mathrm{d}t}\right) - B + D = 0 \tag{2.4}$$

This expression can be simplified by defining the growth rate as $G = \frac{\mathrm{d}L}{\mathrm{d}t}$ and defining the flow rate as $Q = \frac{\mathrm{d}V}{\mathrm{d}t}$:

$$\frac{\partial n}{\partial t} + \frac{\partial}{\partial L}(nG) + \frac{\partial}{\partial V}(nQ) - B + D = 0 \tag{2.5}$$

2.3 Nucleation

This section discusses the formation of solid particles or liquid droplets. Gaseous molecules must bind together to form a particle or droplet. This process is called nucleation.

Very small particles are thermodynamically unstable below a certain level of supersaturation of the gas. This is referred to as the thermodynamic barrier for nucleation.

It is necessary to evaluate how the free energy of the system changes with the size of a particle, to know whether the particle is thermodynamically stable. The change in free energy of the system depends on the free energy difference between gas and solid (or liquid) phase, and on the surface energy of the particle [Askeland (1996), p.216]:

$$\Delta G = \pi d_p^2 \sigma_s + \frac{\pi d_p^3 (G_s - G_g)}{6 v_s} \quad [J] \tag{2.6}$$

- If $\frac{\mathrm{d}\Delta G}{\mathrm{d}d_p} > 0$, then the free energy of the system is lower for a smaller particle. Hence it is thermodynamically favourable that the particle will become smaller (by evaporation). Such a particle is thermodynamically *unstable*.
- If $\frac{\mathrm{d}\Delta G}{\mathrm{d}d_p} < 0$, then the free energy of the system is lower for a larger particle. Hence particle growth is thermodynamically favourable.

$$\frac{\mathrm{d}\Delta G}{\mathrm{d}d_p} = 2\pi d_p \sigma_s - \frac{\pi d_p^2 (G_g - G_s)}{2v_s} \tag{2.7}$$

The particle size for which $\frac{\mathrm{d}\Delta G}{\mathrm{d}d_p} = 0$ is called the *critical nucleation particle size* (d_p^*).

For all particles larger than d_p^* particle growth is thermodynamically favourable. For all particles smaller than d_p^* particle growth is thermodynamically unfavourable. The only way that a particle can be formed is that a cluster of molecules larger than d_p^* forms. This is not possible according to the average energy of clusters of a certain size. However, all clusters of the same size do not have the same energy. There is a stochastic variation in the energies of equally sized clusters (or single molecules). One cluster (or molecule) will, for example, have a higher kinetic energy than another. Therefore, although the *average* free energy of a certain size of clusters does not allow particle growth, there will be some clusters of that size for which particle growth is thermodynamically favourable. The frequency of the formation of super-critical clusters ($d_p > d_p^*$) will depend on the critical nucleation particle size. The larger the critical size, the less frequent the formation of clusters of that size, and the slower the rate of particle formation. Particle formation that takes place by the stochastic formation of super-critical clusters is called *nucleation-controlled particle formation.*

If the critical cluster size is smaller than the size of a dimer, then the formation of all particle sizes is thermodynamically favourable. Particle formation under such conditions is called *coagulation-controlled particle formation* (or *uninhibited coagulation*), and is much faster than nucleation-controlled particle formation.

The *criterion for uninhibited coagulation* is:

$$d_p^* < d_2 \tag{2.8}$$

where d_2 is the spherical equivalent diameter of a dimer.

The criterion (2.8) is now expressed in terms of known variables. By setting equation (2.7) equal to zero the *critical nucleation particle size* can be calculated:

$$d_p^* = \frac{4\sigma_s v_s}{(G_s - G_g)} \tag{2.9}$$

An expression for $(G_s - G_g)$ is derived mathematically by thermodynamic analysis [such as is common in thermodynamics textbooks, e.g. Smith et al. (1996)].

At gas-solid equilibrium the free energy of a molecule in the gas phase is equal to the free energy of a molecule in the solid phase:

$$G'_g = G'_s \tag{2.10}$$

The free energy of the supersaturated gas is larger than the free energy of the gas at equilibrium:

$$G_g = G'_g + RT\ln(P/P') \tag{2.11}$$

$$= G'_s + RT\ln(P/P') \tag{2.12}$$

where P is the actual partial pressure of the product, and P' is the equilibrium partial pressure of the product.

Supersaturation (S) is defined as the ratio between the real concentration and the equilibrium concentration. Ideal gas behaviour is assumed, for which concentration is linearly dependant on partial pressure. Therefore:

$$S = P/P' \tag{2.13}$$

where P is the actual partial pressure of the species, and P' is the equilibrium partial pressure of the species.

When the gas is supersaturated, the solid still has the equilibrium free energy:

$$G_s = G'_s \tag{2.14}$$

Combining equations (2.12), (2.13) and (2.14) gives:

$$(G_s - G_g) = RT\ln(S) \tag{2.15}$$

Substituting (2.15) into (2.9) yields the so-called *Kelvin-equation* [Friedlander (1977)], which is the criterion for uninhibited coagulation:

$$d_p^* = \frac{4\sigma_s v_s}{RT\ln(S)} \tag{2.16}$$

At low pressure ideal gas behaviour can be assumed:

$$P = C_m RT \tag{2.17}$$

where C_m is the concentration of monomers.

Substituting (2.17) into (2.13):

$$S = \frac{C_m RT}{P'(T)} \tag{2.18}$$

2.4 Brownian Collisions

In this section an expression is derived for the frequency of collisions between monomers and particles, because of Brownian motion. A more general expression for collisions between particles of any size is frequently used in the literature [Seinfeld (1998), p. 661]. The derivation of the specific monomer-particle collision expression is much simpler, and gives insight into phenomena governing collision rates. This derivation is shown here to give the reader some insight into the modelling of collisions in aerosol systems.

2.4.1 Expression for Monomer-Particle Coagulation

Kodas and Friedlander (1988) proposed an aerosol reactor model which assumes that the only mechanism for particle growth is the coagulation of a monomer with a particle or another monomer.

The model calculates the nett condensation rate, i.e. the rate of condensation minus the rate of evaporation. The model represents zero particle formation for systems below the critical supersaturation point and particle formation by uninhibited coagulation above the critical saturation point, i.e. the model does not describe nucleation-driven particle formation (see section 2.3).

Note that this model does not describe coagulation of two *particles* (both consisting of two or more molecules). Thus this model is only appropriate for a system in which particle growth is dominated by condensation, and particle coagulation is negligible. Such a system will have a high monomer formation rate, and a low particle number density. Such conditions exist at the entry region of a flow-type aerosol reactor, where the particle number density is still low, and the reaction rate (monomer formation rate) is high.

Kodas and Friedlander state, without derivation, an expression for the rate at which vapour molecules (monomers) condense onto a single spherical particle (with diameter d_p):

$$R_{c,s} = 2\pi D_1 d_p \left[n_1 - n' S^{\left(\frac{d_p^*}{d_p}\right)} \right] F(\mathrm{Kn}) \quad \left[\#_c \, \#_p^{-1} \, s^{-1} \right] \tag{2.19}$$

D_1 = molecular diffusivity $[m^2/s]$

n_1 = monomer number concentration (bulk) $[\#_1/m^3]$

n' = monomer number concentration for gas–solid equilibrium $[\#_1/m^3]$

S = saturation ratio $= \dfrac{n_1}{n_{eq}}$

d_p^* = critical nucleation diameter [m]

Kn = Knudsen number

$$= \frac{\text{monomer mean free path}}{\text{monomer size}}$$

$F(\mathrm{Kn})$ is the Fuchs-Sutugin interpolation formula between the continuum regime and the kinetic theory regime. When the mean free path of fluid molecules is small with respect to their size, interaction between the particles is significant. It is then appropriate to model the fluid as continuous medium, and not as discrete non-interacting molecules. *Continuum* modelling is appropriate when: $\mathrm{Kn} = \frac{2\lambda}{d_p} \rightarrow 0$.

When the mean free path of fluid molecules is large with respect to their size, interaction between the particles is negligible. It is then appropriate to model the fluid as discrete non-interacting molecules, and not as a continuum. *Kinetic theory* modelling is appropriate when: $\mathrm{Kn} = \frac{2\lambda}{d_p} \rightarrow \infty$.

In sections 2.4.2 to 2.4.4 the expression (2.19) is derived from first principles. This derivation gives insight into important concepts in the modelling of aerosol systems, namely:

- Collision frequency
- Surface forces
- Gas saturation
- Continuum *vs.* kinetic theory regimes

Consider the transfer of monomers (with number concentration n) to the surface of a spherical particle with radius r_p. Assume that radial diffusion is the only mass transfer mechanism in a layer with thickness δ (arbitrarily small) around the sphere, and that the temperature is uniform within this layer.

The condensation rate expressions for the continuum (2.4.2) and molecular regimes (2.4.3) are derived separately, and then are then combined by an interpolation formula (2.4.4).

2.4.2 Derivation for Continuum Regime

Monomer transfer to the sphere is described by Fick's diffusion law (only valid for the continuum regime):

$$R_{c,s} = D_1 4\pi r^2 \frac{\mathrm{d}n}{dr} \tag{2.20}$$

where $r \geq r_p$ is the radial position measured from the centre of the spherical particle.

Solving the differential equation (2.20):

$$R_{c,s} \int \frac{\mathrm{d}r}{r^2} = 4\pi D_1 \int \mathrm{d}n + C \tag{2.21}$$

$$\frac{R_{c,s}}{r} = -4\pi D_1 n + C \tag{2.22}$$

$$\text{Thus} : n = n(r) \tag{2.23}$$

The constant C is solved by using the following boundary condition:

$$R_{c,s} = 0 \text{ for } n(r) = n_1 \tag{2.24}$$

This boundary condition represents the case when there are no gradient in monomer concentration, i.e. the monomer concentration is uniform for all r.

Substituting (2.24) into (2.23):

$$C = 4\pi D_1 n_1 \tag{2.25}$$

$$\frac{R_{c,s}}{r} = 4\pi D_1 [n_1 - n(r)] \tag{2.26}$$

$R_{c,s}$ is solved by substituting $r = r_p = \frac{d_p}{2}$:

$$R_{c,s} = 2\pi D_1 d_p [n_1 - n_{sf}] \tag{2.27}$$

where n_{sf} is the monomer concentration at the gas-solid interface (particle surface).

An expression for n_{sf} is derived by considering gas-solid equilibrium at the particle surface. The gas is assumed to be ideal, and consisting of the product species and an inert (non-condensing) gas. In such a system the inert gas has no influence on the gas-solid equilibrium, Hence the phase equilibrium is modelled by considering a system consisting only of product molecules, and the product partial vapour pressure is simply referred to as as the vapour pressure.

The vapour pressure exerted by the gas on the particle surface must be equal to the vapour pressure exerted by the particle surface on the gas. If this was not so, there would be an infinite driving force for condensation exerted by the gas on the surface $\left(\frac{dP}{dr} \rightarrow \infty \text{ at } r = \frac{d_p}{2}\right)$.

Therefore gas-solid equilibrium exists at the particle surface:

$$P_g = P_s = P_{sf} \tag{2.28}$$

where P_g is the vapour pressure exerted by the gas on the surface, P_s is the vapour pressure exerted by the surface on the gas, and P_{sf} is the vapour pressure for phase equilibrium at the *curved* particle surface.

Equilibrium vapour pressure (P') is defined for *flat* surfaces. Surface forces increase the internal pressure of a spherical particle, and therefore also increase the vapour pressure exerted by the surface. Therefore $P_{sf} \neq P'$ for a curved surface.

On a flat surface the surface force is perpendicular to the surface, and hence has no influence on the pressure under the surface.

On a curved surface the surface force has a component in the radial direction. The greater the curvature (smaller the particle) the greater the pressure increase due to this radial surface force. Mathematical expression of the radial component of the surface force on an infinitesimal circular piece of surface, gives the pressure increase due to curvature [Atkins (1994), pp. 963-964]. This is known as the Laplace equation:

$$\Delta P = \frac{2\sigma}{r} \tag{2.29}$$

Now that it is known what the pressure increase *inside* a particle (ΔP) due to particle curvature is, it is necessary to find the effect that this pressure increase has on the *vapour* pressure exerted by the *surface* of the particle (P_{sf}).

For a flat surface at phase equilibrium: $P_g = P_s = P_{sf} = P'$. To illustrate the change of P_{sf} with particle curvature, a virtual experiment is performed in which a flat surface is bent to the desired curvature, whilst always retaining phase equilibrium.

The chemical potential of all species at equilibrium are the same. Therefore:

$$\mu_s = \mu_g \tag{2.30}$$

$$\mathrm{d}\mu_s = \mathrm{d}\mu_g \tag{2.31}$$

$$\mathrm{d}\mu_s = v_s\,\mathrm{d}P_s \tag{2.32}$$

$$\mathrm{d}\mu_g = v_g\,\mathrm{d}P_g \tag{2.33}$$

$$= RT\frac{\mathrm{d}P_g}{P_g} \text{ (assume ideal gas)} \tag{2.34}$$

$$\int_{P'}^{P'+\Delta P} v_s\,\mathrm{d}P_s = RT\int_{P'}^{P_{sf}} \frac{\mathrm{d}P_g}{P_g} P_{sf} = P'\exp\left[\frac{v_s\Delta P}{RT}\right] \tag{2.35}$$

Substituting (2.29) into (2.35), and noting that $r = \frac{d_p}{2}$ at the particle surface:

$$P_{sf} = P'\exp\left[\frac{4v_s\sigma}{RTd_p}\right] \tag{2.36}$$

It is still necessary to express n_{sf} in equation (2.27) in terms of known variables. This is done by noting that $n \propto P$ for an ideal gas at constant temperature. Thus:

$$n_{sf} = n'\exp\left[\frac{4v_s\sigma}{RTd_p}\right] \tag{2.37}$$

where n' is the equilibrium monomer concentration (for a flat surface):

$$n' = \frac{P'}{RT} \tag{2.38}$$

Using equation (2.16):

$$\ln(S) = \frac{4v_s\sigma}{RTd_p^*} \tag{2.39}$$

Combining equations (2.39) and (2.37):

$$n_{sf} = n'S^{\frac{d_p^*}{d_p}} \tag{2.40}$$

Combining equations (2.23) and (2.40):

$$R_{c,s} = 4\pi D_1 d_p\left[n_1 - n'S^{\frac{d_p^*}{d_p}}\right] \tag{2.41}$$

2.4.3 Derivation for Kinetic Theory (Free Molecular) Regime

According to kinetic theory (for an ideal gas) the rate at which molecules collide with a plane of unit area is [Atkins (1994), pp. 819-820]:

$$Z_w = \frac{\text{number of collisions}}{m^2 \cdot s} = \frac{\bar{c}n}{4} \tag{2.42}$$

According to the kinetic theory, gaseous molecules have no interaction, therefore molecular collisions do not limit the diffusion rate, and the diffusion rate is extremely high (in the order of the mean kinetic velocity of the gas molecules). This implies that there negligible concentration gradients in the molecular regime.

The rate of condensation is equal to the rate at which molecules from the gas collide with the particle. Because of the lack of concentration gradients, the condensation rate is dependent only only the bulk gas concentration (n_1).

The rate of evaporation is equal to the rate at which gas molecules, with the same concentration as the equilibrium concentration at the gas-solid interface, will collide with the same area as that of the particle.

The nett condensation rate is the condensation rate minus the evaporation rate:

$$R_{c,s} = \pi d_p^2 \frac{\bar{c}n_1}{4} - \pi d_p^2 \frac{\bar{c}n_{sf}}{4} \tag{2.43}$$

Using the expression (2.40) for the equilibrium surface concentration:

$$R_{c,s} = \frac{\pi d_p^2 \bar{c}}{4} \left[n_1 - n' S^{\frac{d_p^*}{d_p}} \right] \tag{2.44}$$

2.4.4 Interpolation Between Continuum and Molecular Regimes

The Knudsen number is defined as:

$$\text{Kn} = \frac{2\lambda}{d_p} \tag{2.45}$$

where λ is the mean free path of monomers.

Using the kinetic theory, it can be shown [Atkins (1994), pp. 824-825] that the diffusivity of an ideal gas is a simple function of the mean free path and mean kinetic velocity of molecules:

$$D = \frac{\lambda \bar{c}}{3} \tag{2.46}$$

Substituting (2.46) into (2.45):

$$\mathrm{Kn} = \frac{6D_1}{\bar{c}_1 d_p} \tag{2.47}$$

where $\bar{c}_1$ is the mean monomer kinetic velocity.

The Fuchs-Sutugin formula for interpolating between the continuum and molecular regimes is:

$$F(\mathrm{Kn}) = \frac{1 + \mathrm{Kn}}{1 + 1.71\mathrm{Kn} + \frac{4}{3}\mathrm{Kn}^2} \tag{2.48}$$

The general condensation rate expression (2.19) reduces to the expressions for the continuum regime and the kinetic theory regime for limiting values of Kn:

- For the continuum regime $\mathrm{Kn} \to 0$, thus $F(\mathrm{Kn}) = 1$, and equation (2.19) reduces to equation (2.41).
- For the kinetic theory regime $\mathrm{Kn} \to \infty$, thus $F(\mathrm{Kn}) = \frac{3}{4\mathrm{Kn}} = \frac{d_p \bar{c}}{8D_1}$, and equation (2.19) reduces to equation (2.44).

2.4.5 Defining the Collision Coefficient for Monomer-Particle Collisions

The following expression is defined for the collision rate between monomers (referred to by subscript $_1$) and particles (referred to by subscript $_p$):

$$r_{1p} = \beta_{1p} n_1 n_p \ [\#_c \, \#_p^{-1} \, s^{-1}] \tag{2.49}$$

β_{1p} is called the collision coefficient (also called the coagulation coefficient) for collisions between monomers$_1$ and particles$_p$. The condensation expression (2.19) is used to find an expression for β_{1p}.

$$r_{1p} = R_{c,s} n_p = 2\pi D_1 d_p \left[n_1 - n_{eq} S^{\left(\frac{d_p^*}{d_p}\right)} \right] F(\mathrm{Kn}) n_2 \quad \left[\#_c \, \mathrm{m}^{-3} \, \mathrm{s}^{-1} \right] \tag{2.50}$$

If evaporation is assumed to be negligible:

$$r_{1p} = R_{c,s} n_p = 2\pi D_1 d_p n_1 n_p F(\mathrm{Kn}) \tag{2.51}$$

Therefore, in systems where evaporation is negligible (i.e. where the critical nucleation particle size is smaller than the size of a dimer):

$$\beta_{1p} = 2\pi D_1 d_p F(\mathrm{Kn}) \tag{2.52}$$

2.4.6 Fuchs Interpolation Formula for Brownian Collisions from Free-Molecular to Continuum Regimes

For collisions between particles of any size, the Fuchs expression is frequently used to describe the Brownian collision frequency [Seinfeld (1998), p.661]. This expression applies to the entire particle size spectrum, from the molecular to the continuum regime. The expression is not derived here. A similar expression for monomer-particle collisions only was rigorously derived in sections 2.4.1 to 2.4.5. This derivation gives some understanding of the form of the Fuchs expression, and the meaning of the variables therein.

The collision coefficient (β_{ij}) is defined by the following expression for the collision rate between species i and j:

$$r_{ij} = \beta_{ij} n_i n_j \ [\#_c \, m^{-3} \, s^{-1}] \tag{2.53}$$

The Fuchs expression for collisions between particles of sizes i and j is:

$$\beta_{ij} = 2\pi(D_{fi} + D_{fj})(d_{pi} + d_{pj}) \left[\frac{d_{pi} + d_{pj}}{d_{pi} + d_{pj} + 2g_{ij}} + \frac{8(D_{fi} + D_{fj})}{\bar{c}_{ij}(d_{pi} + d_{pj})} \right]^{-1} \tag{2.54}$$

D_{fi} is the particle diffusion coefficient:

$$D_{fi} = \frac{k_B T}{3\pi\mu d_{pi}} \left[\frac{5 + 4\mathrm{Kn}_i + 6\mathrm{Kn}_i^2 + 18\mathrm{Kn}_i^3}{5 - \mathrm{Kn}_i + (8 + \pi)\mathrm{Kn}_i^2} \right] \tag{2.55}$$

Kn_i is the particle Knudsen number:

$$\mathrm{Kn}_i = \frac{2\lambda}{d_{pi}} \tag{2.56}$$

The mean velocity of particles consisting of i molecules (with m_i molecules per particle) is:

$$\bar{c}_i = \left(\frac{8k_B A_v T}{\pi MW_{pr} \times 10^{-3} m_i} \right)^{\frac{1}{2}} \tag{2.57}$$

An average mean particle velocity for the two different particle size i and j is defined as:

$$\bar{c}_{ij} = \left(\bar{c}_i^2 + \bar{c}_j^2 \right)^{\frac{1}{2}} \tag{2.58}$$

The mean free path of the bulk gas is approximated according to the kinetic theory of gases [Seinfeld (1998), p.455]:

$$\lambda = \frac{2\mu}{P} \left(\frac{\pi k_B A_v T}{8MW_{bg} \times 10^{-3}} \right)^{\frac{1}{2}} \tag{2.59}$$

The mean free path of a particle consisting of i molecules is:

$$l_i = \frac{8D_{fi}}{\pi \bar{c}_i} \tag{2.60}$$

The particle size correction factor is defined as:

$$g_i = \left[\frac{(d_{pi} + l_i)^3 - (d_{pi}^2 + l_i^2)^{\frac{3}{2}}}{3 d_{pi} l_i} \right] - d_{pi} \tag{2.61}$$

The average particle size correction factor is defined as:

$$g_{ij} = \left(g_i^2 + g_j^2 \right)^{\frac{1}{2}} \tag{2.62}$$

2.5 Coalescence of Colliding Particles

The discussion of coalescence is limited to temperatures well below the melting/dissociation/sublimation temperature of the bulk solid phase (for both crystalline and glassy ceramics), as is typically encountered in the gas-phase synthesis of ceramic powders. This temperature restriction excludes the sintering mechanisms of evaporation-condensation and viscous flow. The possible sintering mechanisms for ceramics well below the melting/dissociation/sublimation temperature are surface, grain-boundary and lattice diffusion [Coblenz et al. (1980)]. However, these mechanisms do not adequately describe the coalescence of nano-scale particles.

Sections 2.5.1 and 2.5.2 apply to the coalescence of two equally-sized spherical particles. Section 2.5.3 applies to the coalescence of monomers and small clusters onto larger particles.

2.5.1 Very Small Particles, Non-Solid Behaviour

Sintering (coalescence) models which were developed for the bulk solid phase are known to significantly underestimate the sintering rate of particles smaller than about 10 nm [Ulrich and Subramanian (1977), Rogak (1997)]. Furthermore, these models do not allow for complete coalescence (see section 2.5.2). The rapid and complete coalescence of particles smaller than 10 nm occurs by mechanisms other than solid-state sintering. The maximum particle size that completely coalesces is called the *critical coalescence particle size* or the *maximum fusible particle size.* Experimental observations of the primary particles in hard agglomerates produced in aerosol reactors show a surprisingly narrow distribution of primary particle sizes, which has a weak dependence on material and formation process [Zachariah and Dimitriou (1990), Rogak (1997)]. It was hypothesised that this observed primary particle size has a strong relationship to the *critical coalescence particle size.*

The rapid and complete coalescence of very small particles can be explained by investigating the ratio between number of molecules on the surface of a particle to the number of molecules inside the particle (inside the surface layer of molecules). For TiO_2, a particle with 10 nm diameter consists of approximately 17000 molecules and has a surface-to-inside molecule ratio of 0.18. For such small particles, the lattice arrangement (for crystalline ceramics) or molecular network arrangement (for glassy ceramics) is severely disarranged because of the significant surface discontinuity. Therefore the properties of such small particles are very different from the properties associated with the bulk solid phase.

The exact mechanisms of coalescence of very small particles are unknown, but it is conceivable that a lack of atomic/molecular bonding structure allows atomic/molecular motion similar to that in a high-density fluid phase. An attempt to model such pseudo-fluid phase sintering of ceramics falls beyond the scope of this work. It is sufficient to note that the sintering of such very small particles is rapid and complete, and that it cannot be described by solid-state sintering models. Therefore it is frequently assumed that particle growth up to a certain critical particle size is spherical [Matsoukas and Friedlander (1991), Rogak and Flagan (1992), Flagan and Lunden (1995), Rogak (1997)].

2.5.2 Larger Particles with Properties of the Bulk Solid Phase

Ceramic particles that are large enough to have the lattice arrangement (for crystalline ceramics) or molecular network arrangement (for glassy ceramics) of the bulk solid phase, can sinter only by solid-state diffusion mechanisms. These mechanisms proceed by growth of the grain boundary (also called the *neck*) between the particles.

The thermodynamic driving force for sintering can be expressed as [Cannon and Carter (1989)]:

$$\Delta G_{tot} = \Delta(\gamma_{sv} A_{sv}) + \Delta(\gamma_{gb} A_{gb}) \tag{2.63}$$

where G_{tot} is the total Gibbs energy of the system, γ_i are the surface tensions for solid-vapour (sv) and grain-boundary (gb) interfaces respectively , and A_{sv} and A_{gb} are the corresponding surface areas.

It is common in sintering models to assume that the solid-vapour and grain-boundary surface tensions are constants, for a specific temperature.

The solid-vapour interface can be approximated as two sections. One section consists of the spherical surfaces of the two original particles, with radius r. The other section consists of the neck between the spherical particles, with neck length ℓ_n, neck radius x, and contact angle φ. This geometry is illustrated by figure 2.1. A contact angle less than 180^0 is caused by grain-boundary tension. Grain-boundary tension is the resistance to grain boundary growth associated with the positive difference between the energy at the imperfect grain-boundary and the energy in the perfect lattice structure. The equilibrium contact angle is called the *dihedral angle* (φ_e).

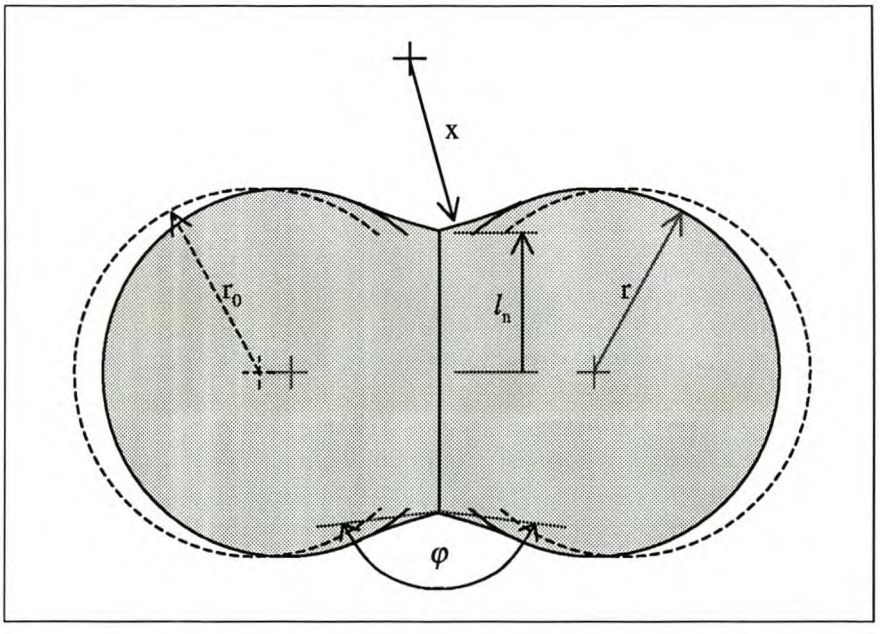

Figure 2.1: Approximate Geometry of Bi-Sphere Sintering

For this simplified geometry, the driving force for sintering is expressed as the sum of three terms:

$$\Delta G_{tot} = \gamma_{sv}\Delta A_{sphere} + \gamma_{sv}\Delta A_{neck} + \gamma_{gb}\Delta A_{gb} \tag{2.64}$$

where A_{sphere} and A_{neck} are the surface areas of the spherical and neck sections respectively, and A_{gb} is the grain boundary surface area.

Two different modelling approaches that are commonly used for the sintering of two solid spheres are described here. Each of these approaches simplifies the thermodynamic driving force by considering a certain term in equation 2.64 to be negligible, based on some conditions.

Negligible Grain-Boundary Energy: Neck Curvature Model

For a small neck radius, and small grain-boundary tension:

$$\left(\frac{\gamma_{sv}}{\gamma_{gb}}\right)\frac{\mathrm{d}A_{neck}}{\mathrm{d}A_{gb}} \gg 1 \tag{2.65}$$

It is suitable to model such initial-stage sintering ($x/r \ll 1$) of materials with small grain boundary tension (with dihedral angles not much smaller than 180°) by neglecting the grain-boundary energy, and by assuming homogeneous neck radius and constant particle radius. These assumptions were used by Coblenz et al. (1980) to model initial-stage solid-phase sintering. They developed expressions for the rate of change in the neck curvature, for different solid-state sintering mechanisms. Figure 2.2 illustrates the assumed geometry.

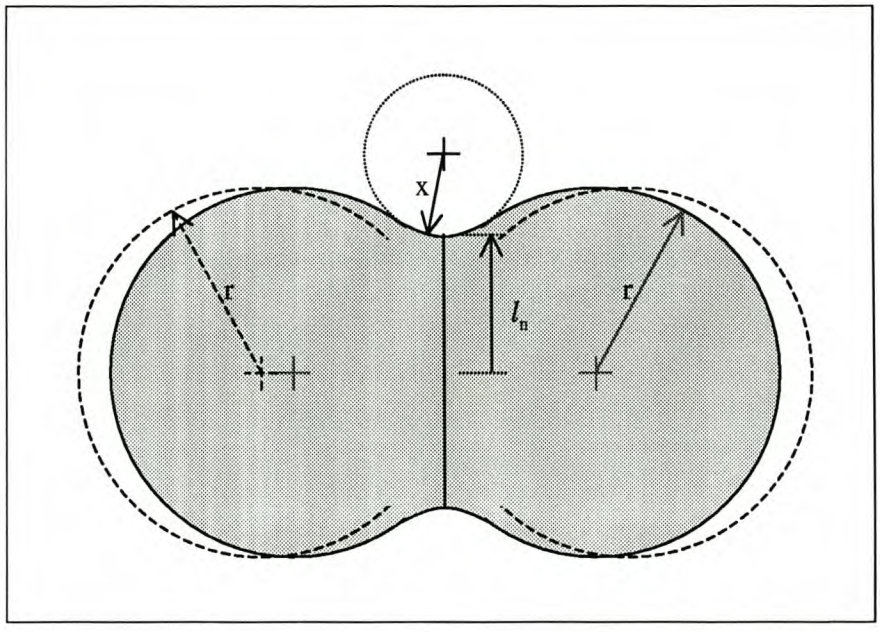

Figure 2.2: Negligible Grain-Boundary Energy: Neck Curvature Model

The *local driving force* for sintering, in terms of the neck curvature model, is the capillary pressure caused by the curvature in the neck [Chiang et al. (1997), p. 400]:

$$P_{capillary} = -\gamma_{sv}\left(\frac{1}{x} - \frac{1}{\ell_n}\right) \tag{2.66}$$

The *overall driving force for sintering* is the difference in the surface forces in the neck and on the spherical sections. The surface force on the spherical sections is described, in terms of increase in pressure inside a sphere, by the Laplace equation [Atkins (1994), pp. 963-964]:

$$P_{sphere} = \frac{2\gamma_{sv}}{r} \tag{2.67}$$

Coblenz et al. (1980) approximated the driving force for sintering for small neck radii (x), by noting that $x \ll \ell_n, r$. The resulting simplified driving force is:

$$P_{sintering} \approx P_{capillary} \approx -\frac{\gamma_{sv}}{x} \tag{2.68}$$

This approximation (based on $x \ll \ell_n$ and $x \ll r$) limits the models of Coblenz et al. (1980) to small neck radii. It is generally accepted that initial-stage solid-state sintering models are only valid for $x < 0.3 \times r$ [Flagan and Lunden (1995); Chiang et al. (1997), p. 400].

The local driving force for sintering, namely the capillary pressure in the neck, will decrease with increasing neck growth, and will be zero when $\ell_n = x$. Thereafter the surface pressure in the neck will become positive. Sintering will continue, but the the dominant driving force will now be the difference between the surface pressure on the spherical sections and in the neck section ($P_{sphere} - P_{neck}$). The distance over which atoms diffuse by this driving force is an order of magnitude greater than for capillary neck growth. Furthermore, the magnitude of the driving force is an order of magnitude smaller than for capillary neck growth. Therefore sintering beyond the geometry of $\ell_n = x$ will be dramatically slower than before. This may explain the paucity in the literature of neck curvature models for sintering beyond initial neck growth.

Negligible Neck Surface Energy: Contact Angle Relaxation Model

For crystalline ceramics, the grain-boundary surface tension is of the same order as the solid-vapour surface tension, in an air atmosphere at temperatures as high as 1800 K [Chiang et al. (1997), pp. 360-368]. This corresponds to dihedral angles in the order of 120^o.

For such systems, only a limited degree of neck radius formation is possible, before the dihedral angle dominates the geometry. Then:

$$\left(\frac{\sigma_{sv}}{\sigma_{gb}}\right)\frac{\mathrm{d}A_{neck}}{\mathrm{d}A_{gb}} \ll 1 \tag{2.69}$$

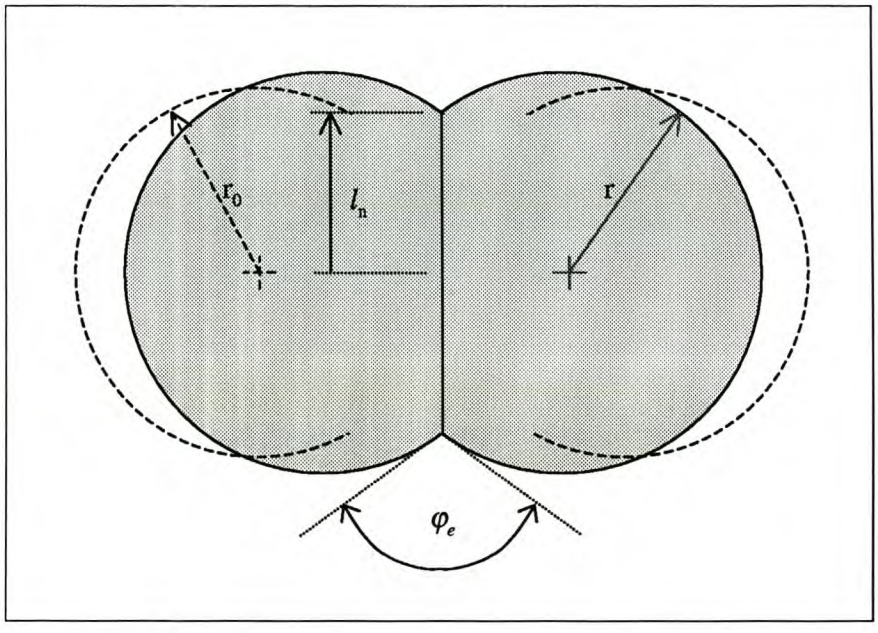

Figure 2.3: Negligible Neck Formation: Contact Angle Relaxation Model

There are two limiting geometries by which contact angle relaxation can be modelled, depending on the rate-limiting sintering mechanism [Cannon and Carter (1989)]:

- Surface diffusion and/or evaporation-condensation: Neck growth occurs without centre-to-centre approach, and the equilibrium particle curvature is non-spherical.
- Unconstrained grain-boundary and/or lattice diffusion: Neck growth occurs by centre-to-centre approach and the geometry is that of truncated spheres, with radius increasing as sintering progresses.

Figure 2.3 illustrates contact angle relaxation by unconstrained grain-boundary and/or lattice diffusion. In this geometry the formation of a neck radius is neglected, but rather the particle radius is allowed to increase, until the contact angle (φ) is equal to the dihedral angle (φ_e).

At this condition, the vector sum of solid-vapour and grain-boundary surface tensions at the circular vapour-solid-grain-boundary interface is zero. Therefore sintering stops when the contact angle is equal to the dihedral angle (the equilibrium contact angle) [Cannon and Carter (1989), Lange (1989), Kellet and Lange (1989)].

The dihedral angle is a function of the solid-vapour and grain-boundary surface tensions:

$$\cos\frac{\varphi_e}{2} = \frac{\gamma_{gb}}{2\gamma_{sv}} \tag{2.70}$$

Cannon and Carter (1989) modelled the kinetics of contact angle relaxation for a linear array of spheres, by solving the continuity equation for the grain-boundary diffusion flux. Thereby they calculated the metastable equilibrium geometries of arrays of solid-state spheres.

Coalescence in Aerosol Synthesis of Ceramics

Literature on aerosol synthesis of ceramics indicates that grain-boundary diffusion is often the limiting mechanism (see section 4.5.5), and evaporation-condensation is negligible at the relevant temperatures.

Both the neck curvature and contact-angle relaxation models predict a metastable end geometry, i.e. sintering equilibrium is reached before the surface area is completely minimised to produce a single sphere. These solid-state sintering models do not explain the rapid and complete coalescence of very small particles ($< 10\,nm$), as was discussed in section 2.5.1.

The importance of modelling the limited coalescence of larger particles, i.e. modelling simultaneous agglomeration and (limited) coalescence of agglomerates, may be evaluated by calculating the maximum possible contraction because of coalescence, and the corresponding decrease in collision rate. The reduction in spatial dimensions (contraction) of an agglomerate particle is the largest for the centre-to-centre approach illustrated by figure 2.3. For crystalline ceramics, dihedral angles are in the order of 120^o.

For a dihedral angle of $\varphi_e = 120°$, and using the centre-to-centre approach contact angle relaxation model, the maximum decrease in length of a bi-particle agglomerate is calculated to be 21% (shown by a scale-drawing in appendix A). Evaluation of the effect of contraction on agglomeration rate is not pursued in the present work.

2.5.3 Coalescence of Monomers and Small Clusters onto Larger Particles

Monomers and small clusters exhibit the non-solid behaviour discussed earlier. On collision with larger particles they will coalesce completely with the larger particles. This may allow the growth of spherical particles larger than the maximum fusible particle size (see section 4.5.7). The growth of seed particles by deposition of monomers and clusters is the focus of the present work, and is studied in detail in part II.

2.5.4 Summary of Ceramic Particle Coalescence

There exists a maximum particle size, called the *critical coalescence particle size* or the *maximum fusible particle size*, for which all smaller particles coalesce rapidly and completely upon collision with other particles. This phenomenon can be explained by the difference in the properties of such small particles with the macroscopic solid-phase properties.

For larger particles, with macroscopic solid-phase properties, solid-state sintering models predict a metastable end geometry, i.e. sintering equilibrium is reached before the surface area is completely minimised to produce a single sphere. Two common solid-state sintering models are the neck curvature model and the contact angle relaxation model. The applicability of these models depends on the dihedral angle of the material, and on the degree of coalescence that is modelled.

The theoretical justification for incomplete sintering of larger particles is supported by experimental observations. It was observed that primary particles in agglomerates collected from aerosol reactors have a surprisingly narrow size distribution, in the absence of growth by cluster deposition (see section 2.5.3) [Zachariah and Dimitriou (1990), Rogak (1997)]. Even though the primary particles in agglomerates have a broad age distribution, the 'oldest' primary particles appear not to have grown (by coalescence, in the absence of cluster deposition) more than the 'youngest' primary particles. This suggests that particles above a certain size do not have the ability to coalesce completely, within a realistic time scale.

2.6 Fractal-Like Agglomerate Particles

Meakin (1988) reviewed evidence that a wide variety of colloidal (aerosol, hydrosol, or other dispersions/suspensions) agglomerates can be described in terms of a fractal geometry. The fractal dimension for self-similar fractals is frequently used to describe colloidal agglomerates:

$$D_f = \frac{\log N}{\log \ell} \tag{2.71}$$

where N is the relative increase in the number of observed spherical particles with a relative increase in the radius of observation (around the centre of mass) of ℓ.

This equation can be transformed to the following form:

$$\frac{\mathrm{d}(\ln n_{pp})}{\mathrm{d}(\ln r)} = D_f \tag{2.72}$$

where n_{pp} is the number of equally sized spherical primary particles observed within a radius of r from the centre of mass of the agglomerate [Tandon and Rosner (1999)].

2.7 Summary of Principles for Aerosol Modelling

This chapter introduced the concept of the population balance, to describe a population of a discrete number of particles. This conservation principle forms the basis for any modelling of aerosol systems. It is supplemented by constitutive laws for phenomena taking place in aerosol reactors. The chapter introduced the constitutive laws for nucleation, collisions and coalescence.

Limited Contraction of Agglomerates by Coalescence

In the present work, the importance of the simultaneous modelling of agglomeration and coalescence of agglomerates, was evaluated by calculating the contraction of a bi-particle agglomerate by coalescence. The maximum possible contraction was found to be 21% for a dihedral angle of 120°, which is a typical value for crystalline ceramics. A future study may be to evaluate the decrease in collision rate because of decreased collision diameter, so as to indicate the incentive for calculating more accurate agglomeration rates (compared to simpler calculation of agglomeration rates by neglecting the contraction of agglomerates because of coalescence).

Chapter 3

Experimental Aerosol Reactors

This chapter discusses different aerosol reactor configurations, and some of the experimental observations made on these reactors.

The reactor configurations are discussed in terms of heating method (section 3.1), flow configuration (section 3.2), and reaction conditions (3.3). Section 3.4 discusses multi-stage reactors, which employ different conditions in the different stages. Section 3.5 briefly discusses aerosol measurement and the limitations thereof.

3.1 Heating Methods

3.1.1 Flame Synthesis

In this type of reactor the reactants are mixed with a combustible gas (usually a hydrocarbon gas) so that the heat needed to achieve a favourable temperature for reaction and particle growth is generated *in situ* [Pratsinis and Vemury (1996)].

3.1.2 Wall Heated Flow Reactors

The reaction temperature is achieved by heat transfer from the reactor walls [Okuyama et al. (1990); Xiong, Pratsinis and Weimer (1992); Sadataka et al. (1996)]. The walls can be heated by electrical elements or combustion heating.

3.1.3 Plasma Reactors

Solid and/or gaseous reactants are completely volatilised in the core of the plasma, with temperature in the order of $10^4 K$. Reaction and particle formation proceeds rapidly and the vapours are quenched ($\approx 10^6 K/s$) at the end of the plasma [Pratsinis and Vemury (1996); Flagan (1997)].

3.1.4 Laser Reactors

Rapid heating and cooling can be achieved in cold-wall reactors by heating the reactant with laser irradiation [Flagan (1997)].

3.2 Flow Configuration

Tubular aerosol reactors usually employ turbulent reactant mixing, carrier-gas induced transport, and rapid cooling at the end of the reactor.

An annular feed of 'sweep' gas around the reactant entrance is sometimes employed, to prevent deposits of the reactor walls [Xiong, Pratsinis and Weimer (1992)].

3.2.1 Reactant Mixing

Sadataka et al. (1996) performed experiments to prove that turbulent reactant mixing is needed to obtain complete reaction conversion and a narrow particle size distribution. They used a diffusion jet mixing reactor, in which the reactants were mixed under turbulent conditions in a cooled and narrow tube. The mixed reactants were then introduced to a much wider heated tube, where the reaction and particle growth took place. The flow in the heated reactor tube was non-turbulent. Note the distinction between *turbulent reactant mixing* (in the cooled entrance tube), and *non-turbulent particle formation and growth* (in the heated reactor tube). Turbulence (recirculation) in the particle formation and growth region would yield a wide particle size distribution. They found that increased turbulent reactant mixing results in a significant reduction in both the product particle size and the standard deviation.

3.2.2 Flow Pattern in Reaction Zone

The flow pattern in the tubular heated reactor is often laminar [Okuyama et al. (1990), Wilck and Stratmann (1997)].

Pratsinis and Vemury (1998) noted that there has been little progress in studying the effect of turbulence in aerosol reactors.

3.2.3 Product Cooling

Okuyama et al. (1990) cooled the product aerosol by dilution with N_2, by introducing the cold diluting gas through an porous tube at the end of the tubular reactor.

Xiong, Pratisinis and Weimer (1992) used an expanded cooling zone to facilitate rapid cooling of the aerosol at the reactor exit.

3.3 Reaction Conditions

Experimental aerosol reactors commonly use a large degree of reactant *dilution* [e.g. Kobata et al. (1991); Xiong, Pratsinis and Weimer(1992)]. The explanation for this dilution is that excess gas is needed to obtain forced flow of the aerosol. The excess gas (which is an excess of the most volatile reactant, or an inert gas) is used as a 'carrier' of the particles through the reactor.

The reaction *temperature* is between the vaporisation temperature of the least volatile reactant, and the melting temperature of the product.

3.4 Multi-Stage Reactors

3.4.1 Seeding

Seed particles (produced in a separate coagulation-controlled aerosol reactor) are introduced with the reactant mixture into the heated reactor, and the newly formed monomers and clusters deposit on the existing seeds, or may grow (by coagulation) to particles of comparable size to the seeds. Such aerosol reactor conditions allow spherical primary particles (which may or may not be part of agglomerates) to grow to sizes larger than the maximum fusible particle size (for the given reactor temperature).

Suppression of New Particle Formation

Several experimental studies (most of them accompanied by a theoretical study) have been conducted to determine the conditions (seed particle size and concentration, initial reactant concentration, temperature profile) that are required to suppress new particle formation [Alam and Flagan (1986), Wu and Flagan (1987) , Okuyama et al. (1990)].

Alam and Flagan (1986) proposed the benefit of suppressing new particle formation in terms of maximising particle growth. If new particle formation is *not* suppressed, there is a large increase in the total particle concentration [Wu and Flagan (1987) demonstrated an increase of more than three orders of magnitude]. Newly formed particles compete with seed particles for growth by monomer/cluster deposition, and since monomer production is limited to complete reaction conversion, less growth per particle is obtained.

It is *generally true* that changing the temperature profile so as to ensure suppression of new particle formation is beneficial for maximising the growth per particle (if the seed particle concentration and initial reactant concentration at STP are fixed). Hence, for a given seed particle concentration and initial reactant concentration, the problem of attaining the maximum amount of growth per particle (which is limited by complete reaction conversion) is reduced to determining a temperature profile for which new particle formation is suppressed.

Alam and Flagan (1986) determined such a suitable temperature profile theoretically. They used a 'clearance volume' model to describe the non-uniformities in the vapour caused by the presence of seed particles as mass transfer 'sinks'. They applied the temperature profile experimentally to obtain conditions of suppression of new particle formation.

They also conducted an experiment with the same temperature profile and reactant concentration as discussed above, but with a significantly lower seed concentration (2.7×10^{10} $\#/m^3$ *vs.* 1.02×10^{11} $\#/m^3$). In this case the observed product PSD was bimodal, indicating that new particle formation was *not* suppressed. Furthermore, the seed particle growth was much less than that obtained in conditions of suppression of new particle formation ($0.25 \rightarrow 5\ \mu m$ *vs.* $0.25 \rightarrow 10\ \mu m$).

However, it is *not generally true* that it is beneficial (for maximising the growth per particle) to have a high enough seed concentration so that new particle formation is suppressed (for fixed initial reactant concentration and temperature profile). This is illustrated by the results of Okuyama et al. (1990), as discussed below.

Okuyama et al. (1990) (figure 6) considered the reactor design problem from the perspective of fixed temperature profile and initial reactant concentration, and variable seed concentration. They experimentally observed that by lowering the seed particle concentration to the extent that new particle formation was *not* suppressed anymore, more growth per seed particle was obtained (see table 3.1). Note that they studied a different reaction and temperature profile that what was studied by Alam and Flagan (1986).

It may seem that the findings of Alam and Flagan (1986) and Okuyama et al. (1990) are contradictory. This apparent contradiction can arise from the misinterpretation of the effect of suppression of new particle formation in terms of only one dimension, namely that suppression of new particle formation would be generally good or bad.

The reactor optimisation problem is *not* one-dimensional in terms of 'extent of suppression of new particle formation'. All the design parameters (initial reactant concentration, seed concentration, temperature profile, ...) need to be considered in comparing different reactor designs. Furthermore, multiple performance indices need to be evaluated (yield, reactor volume, reactor temperature, ...). The focal topic of this thesis (part II) is to define this multidimensional reactor design problem as clearly as possible, so as to assess whether a reactor can be designed that satisfies all the constraints for attaining spherical seed growth.

Typical Initial and Final Particles Sizes for Seed Growth

Table 3.1 summarises the seed growth obtained in single reactors in different experimental studies. The following are indicated: initial and final particles sizes (d_{p_0} and d_{p_f}), the morphology of the particles (spherical or agglomerate), and whether new particle formation took place or was suppressed.

The values shown for the initial and final particle sizes are typical values reported in the relevant sources. Each literature source reports on multiple experiments with different particle sizes, and the singular values shown here are just for brevity.

In the case of Wu and Flagan (1987), the agglomerate structure yielded by the growth process is indicated (they succeeded in densifying the product agglomerates by operating the last section of the reactor at close to melting point, but this can be regarded as a separate process).

The initial and final particle sizes are shown for both of the sequential seed growth reactors that they used, for experiments where a high-temperature coalescence zone was not employed.

source of data	product	morphology	d_{p_0} [μm]	d_{p_f} [μm]	new particle formation
Alam & Flagan (1986)	Si	agglomerate	0.25	10	no
Wu & Flagan (1987)	Si	agglomerate	0.2	0.7	no
Wu & Flagan (1987)	Si	agglomerate	0.7	2	no
Okuyama et al. (1990)	TiO_2	not reported	0.053	0.064	no
Okuyama et al. (1990)	TiO_2	not reported	0.053	0.081	yes

Table 3.1: Summary of Particle Growth in Experimental Seed Growth Reactors

The dual sequential seed growth reactors of Wu & Flagan (1987) were an extension of the single seed growth reactor of Alam & Flagan (1986). The justification for adding another seed growth reactor was to obtain larger final particle sizes. Yet, the reported data on the dual seed growth reactors [Wu & Flagan (1987), figure 5] show less growth than for the single seed growth reactor [Alam & Flagan (1986)]. This may possibly be attributed to different measuring techniques to determine characteristic diameters for the agglomerate particles.

The latter work [Wu & Flagan (1987)] also reported the product particle size when the agglomerate particles were coalesced in a high temperature zone. The coalesced product particles were spherical with diameter of about 3 μm, which is close to the characteristic diameter reported for the agglomerate product particles. Hence Wu & Flagan (1987) successfully characterised the agglomerate particles in terms of an equivalent sphere diameter (proportional to mass).

3.4.2 Separate Particle Growth and Coalescence

Wu and Flagan (1987) developed a system of three reactors in series, to produce micron-sized silicon particles from silane reactant. The first reactor produced seed particles in coagulation-controlled conditions, and the subsequent two reactors were used to grow the seed particles by deposition of newly formed clusters onto the seeds. Two seed growth reactors were used, so as to be able to attain more particle growth (fresh reactant was added at the entry to each reactor). For reactor temperatures below 1100 K agglomerate particles were produced.

By increasing the temperature in the last section of the final reactor to 1723 K (with 1 s residence time at the increased temperature), the agglomerate particles were coalesced to form spherical particles with about 3 μm diameter.

Maisels, Kruis and Fissan (2000) and Fissan (2000) employed a twin-reactor (tube furnaces) configuration to produce spherical particles of PbS and Ag. In the first reactor particles were grown quickly at high concentration and intermediate temperature, at which conditions the growth was agglomeration-controlled. In the second reactor agglomerates were coalesced to form spherical particles, by employing high dilution and high temperature. They did not specify the conditions in the two reactors.

3.5 Measurement

Detailed description of aerosol measuring techniques falls outside the scope of this text. Common techniques for aerosol measurement are [Schmidt-Ott (2000)]:

- **optical particle counters**: Determine the number density of particles.
- **differential mobility analysis**: Particles are separated into different size sections according to their mobility in an electric field (the particles are charged prior to the separation).
- **quartz microbalance**: Measurement of particle mass.

Most of the aerosol modelling literature (see chapter 4) compares modelling results to experimental observations. However, this comparison is rudimentary, since the characterisation of nano-sized powders is limited by the measurement and sampling methods available. Ideally the distribution of particles size and shape should be measured *in situ*. Most experimental work measures only a limited number of particles that are collected at the end of reactor. Pratsinis (1998) noted that the development of *in situ* aerosol measuring techniques is one of the most important needs for advances in the aerosol synthesis of ceramic powders.

Chapter 4

Models for Aerosol Synthesis of Ceramic Powders

The first mathematical models for aerosol dynamics were based on the assumption of spherical particle growth, i.e. colliding particles would immediately coalesce completely. Only one internal dimension, particle size (in terms of volume, mass or diameter), was used, and only one external dimension, time. The models studied the evolution of the particle size distribution with time: $n(m_p, t)$. The differential equation that describes the evolution of $n(m_p, t)$ is called the general dynamic equation (GDE) for aerosols.

The early models incorporated the phenomena of nucleation, condensation (and evaporation) and coagulation. These models were initially developed for atmospheric aerosols, but are general enough to be applied to other particulate processes as well. The models of Seinfeld and co-workers [Ramabhadran, Peterson and Seinfeld (1976), Gelbard and Seinfeld (1978)] are examples of such models. Section 4.1 explains the general dynamic equation.

Section 4.2 presents different approximate functional forms of the particle size distribution (PSD) which are often employed to simplify the solution of the GDE. The way in which the PSD is represented determines (or strongly influences the choice of) the method employed to solve the GDE. Therefore the solution methods are discussed in conjunction with the functional representations of the PSD.

Section 4.3 discusses different approximate functional forms to describe the distribution of size and *morphology* of agglomerates.

Section 4.4 discusses models that considers more than one spatial dimension.

Section 4.5 discusses interactions between different gaseous and particulate species (referred to as population phenomena).

Section 4.6 discusses the phenomena imposed by the reactor conditions and physical constraints: turbulence and diffusion (flow variation), temperature variation, and particle deposition on the reactor walls.

Section 4.7 summarises and classifies the reviewed aerosol reactor models. The classification is presented in tables 4.1 and 4.2, and is a tool for quickly finding a published model for a specific application. The discussion in the sections 4.1 to 4.6 should be read with frequent consultation to this table, since the discussion and the table complement each other. The discussion contains some detailed descriptions that are not included in the table. Likewise, the table contains some technical information (in condensed format) that is not included in the discussion.

4.1 The General Dynamic Equation for Aerosols

A population balance is written for aerosol reactors to study the evolution of the particle distribution function $n(m_p, t)$, for an aerosol system with nucleation, condensation (and evaporation) and coagulation. Here the population balance is presented in a continuous particle size distribution function. For very small particles it is more appropriate to use the discrete form of the population balance, since particles consists of discrete numbers of molecules.

$$\begin{aligned}\rho\frac{\mathrm{d}[n(m_p,t)/\rho]}{\mathrm{d}t} &= \frac{1}{2}\int_{m_p^*}^{m_p}\beta((m_p-v),v)n((m_p-v),t)n(v,t)\mathrm{d}v \\ &\quad -n(m_p,t)\int_{m_p^*}^{\infty}\beta(m_p,v)n(v,t)\mathrm{d}v \\ &\quad +S(m_p^*,t)\delta(m_p-m_p^*) \\ &\quad +\frac{\partial}{\partial m_p}[I(m_p,t)n(m_p,t)] \end{aligned} \tag{4.1}$$

The terms in the population balance are explained by Flagan in the book by Weimer (1997). The following description is a slightly reworded version of that of Flagan.

The LHS of equation 4.1 denotes the change in time of the number density of particles of size m_p.

The terms on the RHS of equation 4.1 denote (in order):

- The formation of new particles of size m_p by collision (and subsequent binding and coalescence) of smaller particles. β is the collision coefficient.
- The consumption of particles of size m_p by collision (and subsequent bondage and coalescence) with other particles. β is the collision coefficient.
- The formation of new particles of size m_p^* by nucleation. S is the rate at which stable nuclei of size m_p^* are formed. $\delta(m_p - m_p^*)$ is the Kroenecker delta function.
- Particle growth or shrinkage because of condensation and evaporation. I is the time rate of change in particle mass because of condensation and evaporation.

4.2 Functional Representation of the Particle Size Distribution (PSD)

For spherical particles, the particle population is completely described (in terms of particle size and number density) by a discrete size distribution, incorporating every possible n-mer.

Particles can have a very large range of sizes in terms of the number of constituent monomers. To solve the GDE for so many discrete particle sizes, one has to solve an immense number of simultaneous differential equations, which is computationally exhaustive. Therefore simplified representations of the PSD are commonly employed.

The modelling of particle surface and/or shape adds additional complexity to the description of the particle population. Simplified functional representations are also used to incorporate this added dimensionality.

Subsections 4.2.1 to 4.2.4 discuss the development of aerosol models for spherical particle growth, according to the representation of the PSD.

Subsections 4.2.4 to 4.3.2 discuss models for the evolution of particle size as well as particle shape and/or surface area. These are discussed in more-or-less chronological order.

4.2.1 Moment Solution of the GDE

The PSD may be approximated according to a fixed functional format, of which the parameters can be inferred from the moments of this *continuous* PSD function. The error made by assuming a continuous PSD is small if the number of monomers per particle is large. This approach is also known as the *modal population balance.*

The *log-normal function* is often employed to represent the PSD. This function can be uniquely described in terms of the first three moments of the PSD. The population balance equations are written and solved in terms of these moments, and the (log-normal) PSD is then inferred from the moments.

The log-normal distribution is described in terms of particle volume as [Jain et al. (1997)]:

$$n(v,t) = \frac{1}{3\sqrt{2\pi}\ln\sigma_g}\exp\left(-\frac{\ln^2\left(\frac{v}{v_g}\right)}{18\ln^2\sigma_g}\right)\frac{1}{v} \tag{4.2}$$

with the average particle volume:

$$v_g = \frac{M_1^2}{M_0^{\frac{3}{2}}M_2^{\frac{1}{2}}} \tag{4.3}$$

and the geometric standard deviation in particle volume:

$$\ln^2\sigma_g = \frac{1}{9}\ln\left(\frac{M_0M_2}{M_1^2}\right) \tag{4.4}$$

The moments of the PSD are defined as:

$$M_i = \int_0^\infty n(v)\,v^i\,\mathrm{d}v \tag{4.5}$$

The model of Jain et al. (1997) shows, with derivation, how the population balance equations are written in terms of these moments.

Similarity Solution of the GDE

By using simplified functional forms to describe coagulation and condensation, and assuming a fixed functional form of the PSD, the GDE may be solved analytically. This was illustrated by Ramabhadran, Peterson and Seinfeld (1976). They used this analytical method to study the interaction of particle growth by coagulation and condensation.

4.2.2 Continuous Representation of PSD

The representation of the PSD can be simplified by approximating particle size as a continuous function, whereas it is actually a discrete function of integer number of molecules. This approximation is applicable for particles with large numbers of constituent molecules, which is indeed the case for particles in the nano-metre size range. The draw-back of this approximation is that the dynamics of small clusters are inaccurately modelled.

The population balance for a continuous PSD, with *unspecified functional form*, is very complex. The resulting equations are of a non-linear integro-partial-differential type, in two or more dimensions. Solutions for such equations have been obtained, but with great numerical effort. Gelbard and Seinfeld (1978) used the method of collocation in finite element techniques to solve the GDE for a continuous PSD.

Modern approaches were the wavelet-Galerkin method of Chen, Hwang and Shih (1996), and the Galerkin and collocation methods of Nicmanis and Hounslow (1998).

4.2.3 Monodisperse Approximation of PSD

Wu et al. (1988) developed a simplified reaction-coagulation (SRC) model which represented the particle size distribution as two monodisperse modes. The *nuclei* mode represents particles that were formed by homogeneous nucleation. The *seed* mode represents seed particles which were initially introduced in the reactant mixture, and that grow by deposition of newly formed nuclei onto the seeds.

Okuyama et al. (1990) extended the SRC model of Wu et al. by approximating the PSD as four distinct modes: a *monomer* mode, a *cluster* mode, a *particle* mode, and a *seed* mode.

Kruis et al. (1993) studied agglomerate dynamics by assuming a monodisperse agglomerate population, in terms of the number of spherical primary particles constituting an agglomerate and the size of the primary particles. They assumed a constant mass fractal dimension ($D_f = 1.8$) to describe the agglomerate structure. This value of the mass fractal dimension is common for agglomerate-agglomerate coagulation (i.e. when there is no spherical particles left in the system) in the free-molecular and continuum regimes.

Pratsinis and Spicer (1998) used a simple model for the evolution of monodisperse spherical particles, to study the effect of simultaneous gas-phase and surface reaction.

4.2.4 Sectional Representation of PSD

The discretised population balance (DPB) models the PSD as a finite number of particle size intervals (sections) [Gelbard et al. (1980); Hounslow (1990); Zachariah and Dimitriou (1990); Xiong and Pratsinis (1991)].

Discrete-Sectional Representation of PSD

Another form of discretised population balance is the discrete-sectional model. This model incorporates units with number of molecules from 1 to N (the *discrete* part of the PSD model). For units greater than size N, particles are characterised according to a finite number of size intervals (the *sectional* part of the PSD). This approach was used by Landgrebe et al. (1990), Kobata et al. (1991), and Rogak and Flagan (1992).

The discrete-sectional approach has the advantage of modelling small-particle dynamics accurately, whereas the simple DPB, such as that of Gelbard et al. (1980), can cause significant errors in modelling small-particle dynamics.

4.2.5 Discrete Representation of PSD

The most accurate way to represent particles of different sizes, is to represent each particle with the discrete number of molecules of which it is constituted. The solution of the large array of simultaneous differential equations for this representation is numerically exhaustive. Therefore stochastic Monte Carlo simulation is employed to reduce the numerical effort.

Smith and Matsoukas (1998) used a novel Monte Carlo technique to model the coagulation of spherical particles. In coagulating systems, the number of particles decrease over several orders of magnitude. The common implementation of the Monte Carlo technique is based on a constant system volume. In such implementation the model accuracy decreases the further the coagulation commences, because the number of particles in the simulation decreases dramatically. Smith and Matsoukas made the novel implementation of basing their Monte Carlo simulation on a constant particle number (and thus constant accuracy), by allowing the system volume to change. Their method samples a constant number of particles of the particle population. For each time increment a different volume is sampled so that the particle number remains constant.

Kostolgou and Konstandopoulos (2000) extended the Monte Carlo technique of Smith and Matsoukas to model simultaneous agglomeration and restructuring of fractal-like particles. They assumed that the agglomerate surface remained constant, i.e. that coalescence is negligible.

Kruis, Maisels and Fissan (2000) verified Monte-Carlo simulations of particle collision (and combination) in aerosol reactors with analytical results (for simplified collision frequency functions) and with the results of a sectional model (for a realistic functional form for the collision frequency). They applied their model to chemical reaction in coagulating droplets, and to coating of particles with smaller particles of another material. Their model did not incorporate particle shape, and is therefore not applicable to fractal-like agglomerate particles.

4.3 Representation of Agglomerates

4.3.1 Incorporating Coalescence

Ulrich and Subramanian (1977) *de-coupled* the coalescence and agglomeration rate equations and assumed monodisperse agglomerate and primary particle (spherical) size. This model yielded a simple solution for evolution of the agglomerates in terms of number of primary particles and size of (spherical) primary particles.

Koch and Friendlander (1989) modelled the evolution of particle size and surface area for an initially monodisperse spherical particle population undergoing collision and coalescence. Unlike Ulrich and Subramanian (1977), they solved the *coupled* coalescence and agglomeration rate equations, and they incorporated *polydispersity* in the volume and surface area of agglomerates. They neglected the effect of agglomerate on collision rate. They solved their model equations analytically in terms of moments of the volume and surface area distribution, only for the free-molecular regime (i.e. particle diameters much less than the gas free mean path).

4.3.2 Incorporating Fractal Structure

Mountain and Mulholland (1986) substituted for the particle volume in the Brownian coagulation (spherical growth) rate equations for the free molecular and continuum limits respectively, by functions of the agglomerate volume and fractal dimension (as defined in section 2.6). In this way they accounted for the increased collision frequency of agglomerates over that of equal-volume spheres, because of the open structure of the agglomerates.

Matsoukas and Friedlander (1991) employed the assumptions of fixed primary particle size and constant fractal dimension to determine self-preserving agglomerate size distributions for the free-molecular regime. The defined an agglomerate collision radius (r_c) as a function of primary particle size (r_0), number of primary particles per agglomerate (v/v_0) and fractal dimension (D_f) to calculate Brownian collision frequencies of agglomerates:

$$r_c = r_0 \left(\frac{v}{v_0}\right)^{\frac{1}{D_f}} \tag{4.6}$$

where v is the total agglomerate volume, and v_o is the volume of a spherical primary particle (assuming that all the primary particles in the agglomerate have the same size).

Rogak and Flagan (1992) also employed assumptions of fixed primary particle size and constant fractal dimension to model agglomerate growth. They developed a collision frequency function based on an absorbing sphere collision model. This model applies to collisions from the free molecular regime to the continuum regime, and particularly to the transition between these regimes. The evolution of agglomerate particle size was solved by the discrete-sectional approach.

Rogak (1997) performed similar modelling to Rogak and Flagan (1992), except that he allowed the primary particle size to increase by collisions with particles smaller than the maximum fusible particle size. Thereby he obtained predictions of the evolution of agglomerate particles under conditions where fusible species (small clusters) are still being formed by gas-phase reaction after agglomeration (coagulation without coalescence) has commenced. Such conditions allow the growth of agglomerates with primary particles larger than the *maximum fusible particle size* (see section 2.5).

Variable Fractal Structure

Kostoglou and Konstandopoulos (2000) modelled the evolution of particle mass and structure (according the fractal dimension) for an agglomerating aerosol with negligible coalescence, i.e. they modelled simultaneous agglomeration and *invariant-area restructuring* of agglomerates. They concluded that the reduction of agglomerate fractal dimension because of Brownian restructuring is significant. However, they do not show how they derived and calculated the Brownian restructuring rate.

4.3.3 Incorporating Coalescence and Fractal Structure

Xiong, Pratsinis and Weimer (1992) numerically solved the simultaneous agglomeration and coalescence equations for a two-dimensional sectional representation of the PSD. Their model is valid from the whole spectrum particle sizes from the free-molecular regime to the continuum regime. They accounted for the effect of agglomerate structure on collision rate by inferring the *'surface fractal dimension'* (not to be confused with the *fractal dimension* as defined in section 2.6) from agglomerate surface and volume, and using an empirical surface area scaling factor associated with a certain 'open-ness' of the agglomerate structure. A similar approach was followed by Lee et al. (2001).

Kruis et al. (1993) modelled the evolution of agglomerate particles undergoing collision and coalescence. They employed a constant fractal dimension ($D_f = 1.8$) to account for agglomerates structure. They incorporated D_f in the calculation of collision rates by substituting for spherical particle radius in the Fuchs Bronian collision frequency function (interpolation between free-molecular and continuum regimes, see section 2.4.6) by the agglomerate collision radius function proposed by Matsoukas and Friedlander (1991).

Their model represented the particle population as monodisperse agglomerate particles, with spherical primary particles. Their model successfully accounted for the enhanced collision rate of agglomerate particles. The equations that they used for coalescence kinetics are discussed in section 4.5.5.

Tandon and Rosner (1999) demonstrated how Monte Carlo simulation can be used to model simultaneous agglomeration (in the continuum regime) and coalescence, with constant fractal dimension, to predict the distribution of particle size and surface area. They identified a self-preserving asymptotic shape of the joint population distribution function, in terms of re-scaled particle volume and area. Rosner and Yu (2001) did the same modelling for agglomeration in the free-molecular regime. They also identified a self-preserving asymptote of the joint population distribution function.

Jeong and Choi (2001) performed similar modelling to that of Xiong, Pratsinis and Weimer (1992), but they simplified the modelling by approximating the distribution of particle volume and surface as one-dimensional. For each section of particle volume, the corresponding average particle surface is used. This approximation facilitated a 1/1000 decrease in computational time, compared to the more accurate two-dimensional model of Xiong, Pratsinis and Weimer (1992).

4.4 Spatial Dimensions

Okuyama et al. (1990, 1992) modelled convective (laminar flow) and diffusive transport in a wall-heated (tubular) aerosol reactor. Their model included radial diffusion and a parabolic radial velocity profile (for laminar flow). Hence the model is spatially two-dimensional.

Wilck and Stratmann (1997) developed a spatially two-dimensional aerosol reactor model with modal approximation of the PSD (i.e. in terms of moments of the PSD). They applied the model to a laminar flow aerosol reactor. They showed that the reactor wall temperature profile has an pronounced effect on the results of simulations and experiments alike.

Bensberg et al. (1999) developed a spatially two-dimensional model for a laminar co-flow diffusion flame reactor, where the one reactant is introduced in the middle of the tubular reactor and the other reactor is introduced in a annulus around the central inlet. They approximated the PSD as a unimodal log-normal function. The model incorporated convective and diffusive particle transport.

A recent development is the integration of aerosol dynamics into computational flow dynamics models (this has not been reviewed for the present study).

4.5 Population Phenomena

4.5.1 Chemical Reaction

It is common in the literature to assume perfect instantaneous mixing of reactants, and first-order reaction kinetics for the limiting reactants. The chemical reaction $TiCl_4 + O_2 \rightarrow TiO_2 + Cl_2$ is, for example, modelled as a first-order equation by Jain et al. (1997) and Pratsinis and Spicer (1998).

4.5.2 Nucleation

The equilibrium vapour pressures of metal oxides, borides and nitrides are typically so low that the critical size for nucleation is less than the molecular size of the product [Landgrebe, Pratsinis and Mastrangelo (1990)]. In the gas-phase production of such powders, there is therefore no barrier for nucleation, and the nucleation rate is simply the rate of formation of product monomers by chemical reaction. Such formation processes are called *coagulation-controlled particle formation* or *uninhibited coagulation*, in contrast to *nucleation-controlled particle formation* [Sadataka et al. (1996)].

Classical nucleation theory (as described in section 2.3) does not apply well to systems in which the critical nucleation particle size is close to the size of a monomer. More specifically, the surface tension of the bulk solid phase does not apply to small n-mers. However, it is commonly accepted in the literature that aerosol synthesis of ceramic powders occurs by uninhibited coagulation, and therefore most of the models for ceramic systems do not consider nucleation dynamics.

There do exist some cases of controlled nucleation in aerosol synthesis of ceramics, such as the gas-phase synthesis of non-oxide ceramics like AlN [Kusters and Pratsinis (1995)]. Such a process requires a high enough temperature so that the ceramic vapour pressure is significant.

Aerosol synthesis of ceramics in nucleation-controlled conditions has received little attention in the literature. The present work also focuses only on uninhibited coagulation. However, the following short discussion of nucleation-controlled processes is given, as an analogy will be made between these processes and a limiting case of uninhibited coagulation.

Nucleation-Controlled Particle Synthesis

For *non-ceramic materials*, Kodas and Friedlander (1988) modelled an aerosol system in which the particle concentration varies along the length of a tubular reactor only as the result of nucleation. The nucleation rate is a function of the supersaturation (of monomers) and the critical nucleation particle size. They applied the model numerically to the aerosol synthesis of NH_4Cl at approximately $300K$. They implicitly assumed that inter-particle coagulation was negligible. (Section 2.4.1 gives the rate expression that they used for combination of monomers with particles of any size.)

They concluded that a narrow particle size distribution can be obtained by separating particle formation (by homogeneous nucleation) and condensational particle growth (by heterogeneous nucleation). A high monomer formation rate ensures that new particle formation takes place in only a small section near the entrance of the reactor, and thereafter the controlling phenomenon is particle growth by heterogeneous nucleation (i.e. the combination of sub-critical clusters with super-critical particles). In the particle growth section, the particle number concentration does not vary with length in the reactor. They noted that an upper limit for monomer formation rate is set by coagulation of particles, but they did not discuss or quantify this limit. This limit is explained here: too high a monomer formation rate results in too high a particle concentration which would cause significant inter-particle coagulation, which would spread out the size distribution.

The models in section 4.5.7 describe a limiting case of uninhibited coagulation, where new particle formation is suppressed. This is analogous to the controlled nucleation that was discussed in the preceding paragraphs.

4.5.3 Coagulation

The term coagulation is used to describe collisions and subsequent bonding between particles of any size (sticking probability=1). This term is often used for a special case in which the bonding of particles yields immediate coalescence compared with the time scale of collisions. In this case particles are always spherical. The rate equations for spherical particle coagulation were discussed in section 2.4.6.

Henceforth, spherical particle coagulation will be called simply coagulation (this is the way the term is used in the literature), whereas coagulation without immediate and complete coalescence is called agglomeration.

- **(spherical) coagulation**: the combination of particles of any size, with immediate and complete coalescence of colliding particles (i.e. the particles are smaller than the critical fusion particle size).
- **agglomeration**: the combination of particles of any size, without immediate and complete coalescence of colliding particles (i.e. the particles are larger than the critical fusible particle size).

Agglomeration (see section 4.3)

Agglomerates are composite particles in which the primary particles are identifiable.

Kruis et al. (1993) modelled the dynamics of agglomerate particles undergoing simultaneous coagulation and coalescence. They characterised agglomerates according to the number and size of the primary particles. They assumed that primary particles and agglomerates have monodisperse size distributions, and that the fractal dimension of agglomerates does not change with coalescence.

For spherical particles the particle diameter is used to determine the collision frequency function (equation 2.54). However, for (non-spherical) agglomerate particles an *equivalent collision diameter* is required.

Matsoukas and Friedlander (1991) and Rogak and Flagan (1992) developed expressions for the equivalent collision diameters of agglomerate particles. The expression by Matsoukas and Friedlander is simpler, but less accurate, than that of Rogak and Flagan. The former expression has also been used by Kruis et al. (1993).

For agglomerate particles, d_p in equation 2.54 is substituted with the equivalent collision diameter [Matsoukas and Friedlander (1991), Kruis et al. (1993)]:

$$d_a = d_{pp}(n_{pp})^{\frac{1}{D_f}} \tag{4.7}$$

where d_{pp} is the diameter of the (spherical) primary particles which constitutes the agglomerate particle, and n_{pp} is the number of primary particles in the agglomerate.

D_f is the fractal dimension of an agglomerate, as defined in section 2.6. It is often assumed that the fractal dimension of agglomerates does not change with coalescence (see table 4.2: representation of PSD: V, A and constant D_f). This assumption is justified by the fact that agglomerates have a open structure. The primary particles in such an open structure are not able to move so as to relax the open structure (and thus increase the fractal dimension).

Kruis et al. (1993) concluded from their simulations that the size of primary particles in an agglomerate is insensitive to the fractal dimension. The number of primary particles in an agglomerate is significantly affected by the fractal dimension, since more open agglomerates (with a lower fractal dimension) are more effective at scavenging particles.

4.5.4 Surface Reaction

Jain et al. (1997) added the complexity of simultaneous surface and gas-phase reaction to classical aerosol models, which consider particle growth by coagulation only. The modelling was simplified by assuming a log-normal particle size distribution, and solving the moments of the PSD. The model was solved specifically for the aerosol reaction $TiCl_4 + O_2 \rightarrow TiO_2 + 2Cl_2$.

Jain et al. concluded that surface reaction is *not* an important growth mechanism in laboratory and commercial-scale production of titania particles via the reaction $Ti\,Cl_4 + O_2 \rightarrow Ti\,O_2 + 2\,Cl_2$. They showed that, in general, surface reaction narrows the size distribution.

However, they found that the geometric standard deviation of the PSD cannot be narrower than 1.32 (the self-preserving limit for coagulation of spherical particles in the continuum regime, assuming a log-normal PSD) under realistic reaction conditions.

The model of Pratsinis and Spicer (1998) is the same as above, except that the model is even simpler by assuming a monodisperse PSD. They compared experimental results of other workers with their model. They showed, like Jain et al., that in cases where surface reaction was predominant, the PSD is narrower than expected.

4.5.5 Coalescence

Knowledge about the coalescence of colliding particles is critical in the design of aerosol reactors for the production of spherical particles. However, solid-state sintering models were traditionally developed for large particles, which could be considered to have the properties of the bulk solid phase. These sintering models do not apply to nano-sized particles, in which the lattice arrangement (for crystalline ceramics) or molecular network arrangement (for glassy ceramics) is severely disarranged because of the surface discontinuity. The sintering of ceramics was discussed in section 2.5.

It is conceivable that the coalescence of very small ($< 30nm$) particles occurs by some fluid flow mechanism, even at temperatures well below the melting/dissociation/sublimation temperature of the bulk solid phase, and the resulting particles are therefore spherical. This was discussed in section 2.5.1.

The Critical Particle Size for Coalescence

There exists some critical particle size, above which only limited coalescence is obtained [Rogak and Flagan (1992)]. This particle size has some temperature dependance.

Particles larger than this critical size exhibit the properties of the bulk solid phase. For such 'true' solid phase particles, the sintering models discussed in section 2.5.2 show that complete sintering is impossible for crystalline materials with a dihedral angle significantly less than 180^o, and that the sintering rate of non-crystalline materials is dramatically reduced when the neck radius has grown to the same value as the neck length.

In the present work, it is suggested that the *critical coalescence particle size* (also called the *maximum fusible particle size*) be determined experimentally in the following manner:

- Ensure that monomer formation (and therefore growth by cluster deposition, see sections 2.5.3 and 4.5.7) has ceased by the time that agglomeration commences. This implies that the time for almost complete reaction conversion (τ_{gr}) should be much less than the time for growth up to the maximum fusible particle size (τ_{melt}):

$$\tau_{gr} \ll \tau_{melt} \tag{4.8}$$

  1. $\tau_{gr} = \tau_{gr}(T)$ may be calculated from the reaction kinetics, e.g. for first-order reaction and 99% reaction conversion: $\tau_{gr} = \frac{1}{k} \ln |C_0/C| = \frac{1}{k} \ln |100|$.
  2. $\tau_{melt} = \tau_{melt}(T, d_{melt}, C_0)$ is dependent on the maximum fusible particle size (d_{melt}), which is the quantity that has to be determined by the experiment.
     (a) To design the experiment, a conservatively small value of d_{melt} should be guessed to evaluate equation 4.8. With the guessed value of d_{melt}, τ_{melt} may be calculated with a dynamic aerosol reactor model, by increasing the residence time until $d_p = d_{melt}$.
     (b) If the inequality (equation 4.8) is violated for the specified conditions (T, d_{melt}, C_0), then the initial reactant concentration (C_0) should be lowered to satisfy the inequality.
     (c) After d_{melt} has been determined experimentally, equation 4.8 should be checked again, and if the inequality is violated, the experiment should be repeated for a lower C_0. This procedure should be repeated, if necessary, until the inequality is satisfied.

- Ensure that the residence time is long enough for significant agglomeration to occur:

$$\tau_{res} > \tau_{melt} \gg \tau_{gr} \tag{4.9}$$

- The observed average primary particle size is the maximum fusible particle size corresponding to the temperature that was employed in the aerosol reactor.

Soft and Hard Agglomerates

Flagan and Lunden (1995) explained the difference between soft and hard agglomerates:

- In *soft agglomerates*, the primary particles are weakly bound together by Van der Waal's forces.

  Soft agglomerates form when an aerosol is rapidly cooled, and there is insufficient time for colliding particles to coalesce with significant neck growth.

  Soft agglomerates can easily be broken up into their constituent primary particles, and therefore do not pose a problem for the production of spherical particles.

- In *hard agglomerates*, the primary particles are strongly bound together as the result of neck growth.

  Hard agglomerates typically form when an aerosol is slowly cooled, allowing time for colliding particles to coalesce with significant neck growth.

  Hard agglomerates cannot easily be broken up into their constituent primary particles. Therefore the formation of hard agglomerates must be avoided in aerosol reactors for the production of spherical particles.

Modelling Simultaneous Agglomerate Formation and Coalescence

Several studies have been performed to model the decrease in agglomerate surface area because of neck formation, for primary particles larger than the critical coalescence particle size (see section 2.5.1). The sintering models in section 2.5.2 indicated that complete coalescence is often impossible, or extremely slow.

For crystalline ceramics the sintering continues only until the contact angle reaches value of the dihedral angle , which is approximately 120°.

For non-crystalline ceramics the sintering rate is dramatically reduced when a geometry is reached where the neck radius is the same as the neck length ($\ell_n = x$), resulting in incomplete sintering for realistic sintering times in an aerosol reactor (order of seconds).

Therefore, for both crystalline and non-crystalline ceramics, the number of identifiable primary particles does not change with sintering.

The following discussion gives a brief explanation of the simultaneous agglomeration and coalescence studies that have been done, and the limitations thereof. It is advised that this explanation be read with frequent reference to section 4.3.

Koch and Friedlander (1990) stated the following expression to relate the change in agglomerate surface area with coalescence time, for coalescence by the viscous flow mechanism, and long sintering times:

$$\frac{da}{dt} = -\frac{(a - a_s)}{\tau_f} \quad (t \gg \tau_f) \tag{4.10}$$

where τ_f is called the characteristic time for coalescence by viscous flow.

This expression has also been applied to other coalescence mechanisms, due to its simplicity [Kruis et al. (1993) and Flagan and Lunden (1995)]. In such cases the characteristic sintering times are calculated by more accurate and complex models for the specific sintering mechanisms. Then equation 4.10 is used to *interpolate* between zero coalescence and the *degree of coalescence associated with the characteristic sintering time.*

Equation 4.10 is a linear approximation for the change in surface area of two attached particles which are initially spherical, between $t = 0$ (no coalescence) and $t = \tau_f$ (some critical degree of coalescence which has to be defined).

Integration of equation 4.10 gives the degree of coalescence (θ, defined by equation 4.13) as a function of time:

$$\int_{2a_p}^{a} \frac{da}{a - a_s} = -\int_0^t \frac{dt}{\tau_f} \tag{4.11}$$

$$\ln\left[\frac{a - a_s}{2a_p - a_s}\right] = -\frac{t}{\tau_f} \tag{4.12}$$

$$\frac{a - a_s}{2a_p - a_s} = \exp\left(-\frac{t}{\tau_f}\right) = 1 - \theta \tag{4.13}$$

By substituting $t = \tau_f$ in equation 4.13, it can be shown that the characteristic sintering time corresponds to a 63% degree of coalescence. This value is also used by Kruis et al. (1993), who stated that τ_f is 'the time needed to reduce by about 63% the excess surface area of the aggregate over that of an equal mass sphere'. This statement corresponds to the definition of the degree of coalescence (θ) by equation 4.13.

Kobata et al. (1991) used the model of Coblenz et al. (1980), for initial-stage sintering by neck growth (according to the neck curvature model, see figure 2.2) through the grain-boundary diffusion mechanism, to calculate a characteristic sintering time.

They defined the characteristic sintering time as the time after which the 'curvature between the the spheres disappears'. This is interpreted as the time when the neck radius (x) is the same as the neck length (ℓ_n), which implies zero local driving force for coalescence by capillary pressure in the neck (see equation 2.66).

Kobata et al. (1991) proposed that the state of zero curvature between the spheres corresponds to a ratio between the neck length (ℓ_n) and the initial particle radius (r_i) of 0.83. Calculations in the present work (illustrated by a scale drawing in appendix B) shows that $\ell_n/r_i = 0.814$ (the reason for this slight discrepancy is unknown.)

In the present work it was verified (the calculation is not shown) that the degree of coalescence corresponding to $\ell_n/r_i = 0.83$, based on the neck curvature model, is approximately 63%. Hence the characteristic sintering time defined by Kobata et al. (1991) is the same as the characteristic sintering time defined by the viscous flow coalescence rate expression (equation 4.10).

However, the derivation of the sintering rate expression of Coblenz et al. (1980) was done with the assumption of small neck radius. This sintering rate expression applies only to neck radii $x/r < 0.3$ (see section 2.5.2). For $\ell_n/r_i = 0.814$ or $\ell_n/r_i = 0.83$: $x/r_i > 0.8$. Kobata et al. (1991) extrapolated the sintering rate expression of Coblenz et al. (1980) far outside its applicable range.

Kruis et al. (1993) used the expression of Kobata et al. (1991), for the characteristic sintering time, without correction of the extrapolation of the sintering rate expression beyond its applicable range. Kruis et al. used this characteristic sintering time to interpolate with the approximate coalescence rate expression (equation 4.10) for coalescence times between $t = 0$ and $t = \tau_f$. However, the model used to calculate τ_f [Coblenz et al. (1980)] was used far outside its applicable range.

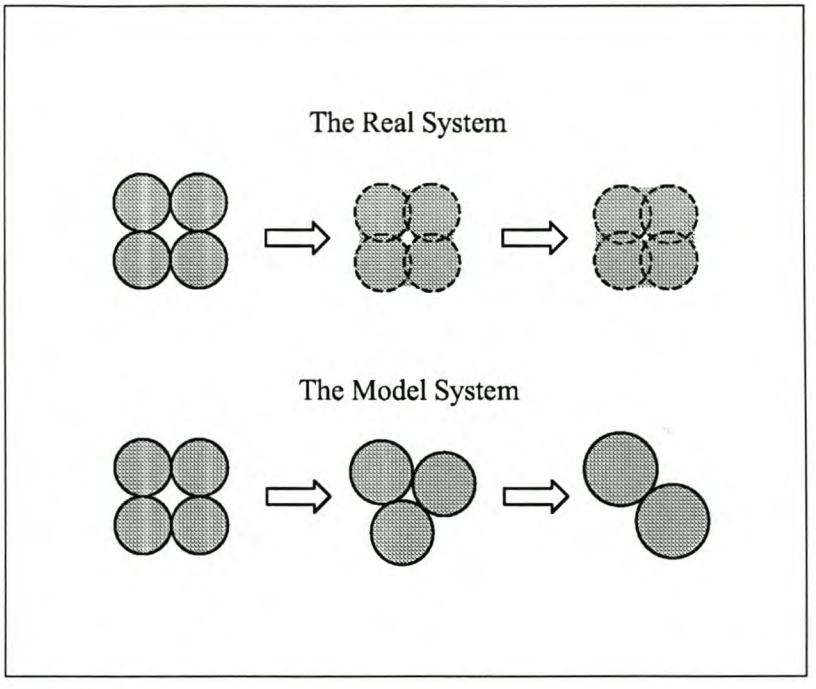

Figure 4.1: Coalescence in the Real System and the Model System

The model of Kruis et al. (1993) represents agglomerates as consisting of equally-sized spherical primary particles. In the 'model system', the surface area of an agglomerate is reduced, whilst maintaining the same mass, by decreasing the number of primary particles and increasing the size (mass) of primary particles. In the real system, primary particles of agglomerates do not coalesce completely (as explained in section 2.5), and the number and mass of primary particles remains constant. Yet, the abstract ('model system') representation of Kruis et al. (1993) effectively accounts for the decrease in the spatial dimensions of agglomerates because of coalescence. This enables the model to account for decreased collision rates compared to less accurate models in which coalescence is neglected.

Figure 4.1 illustrates how coalescence occurs in the real system by neck-formation, compared with the representation of agglomerates by the model of Kruis et al. (1993). Note that in the model system, the number of primary particles is not limited to integers.

Inadequacies of Models for Simultaneous Agglomeration and Coalescence

It is evident from the literature review that there is scope for improving the modelling of simultaneous agglomeration and coalescence in aerosol reactors:

- It is necessary to develop sintering models that apply to nano-size particles that have different properties from the bulk solid phase (see section 2.5.1).
- Experimental determination of sintering parameters is needed [Xiong et al. (1992)].
- Discrepancies in the application of sintering rate expressions need to be resolved.

4.5.6 Restructuring of Fractal-Like Agglomerates

This was discussed in section 4.3.2

4.5.7 Growth of Seed Particles

Alam and Flagan (1986) used a 'clearance volume' model to describe the non-uniformities in the vapour caused by the presence of seed particles as mass transfer 'sinks' for newly formed monomers and clusters. They used this model to evaluate whether a chosen temperature profile would result in suppression of new particle formation (for fixed seed particle size and concentration, and fixed initial reactant concentration). They experimentally implemented such a theoretically verified temperature profile, and suppression of new particle formation was observed as predicted.

Wu et al. (1988) modelled gas-phase reaction and coagulation in the presence of seed particles. They neglected evaporation from clusters because of the low saturation vapour pressure of ceramics, i.e. they assumed that uninhibited coagulation occurs. They showed that a slow reaction rate (low enough temperature and reactant concentration) is needed to ensure that seed growth occurs only by the addition of clusters to the seeds. They called the required condition the *'suppression of homogeneous nucleation'*. (This term may be misinterpreted as indicating nucleation-controlled particle formation, as opposed to the assumption of uninhibited coagulation.)

Wu et al. (1988) demonstrated that seed particles can be formed *in situ* by 'homogeneous nucleation', by initial slow reaction. The reaction rate can then be gradually increased (by increasing temperature) as the seed particles become larger and thus more effective in scavenging newly formed nuclei. In this way, according to their modelling results, relatively uniformly sized sub-micron particles can be produced in a single-stage reactor.

Zachariah and Dimitriou (1990) did similar modelling, with the specific purpose of finding a way to prevent the formation of fractal-like agglomerates with strong bonds between the primary particles. They noted that it has been experimentally observed that the primary particles of such agglomerates have a narrow size distribution, and attributed this to the fact only particles smaller than a certain limit (in the order of $10\,nm$) have enough surface free energy to coalesce completely upon collision with other particles.

They proposed that particles ($> 100\,nm$) which are not strongly bound in agglomerate structures can be produced by introducing seed particles (order of $100\,nm$) into the reactant mixture, and by using a sufficiently slow monomer formation rate (achieved by the choice of reactor temperature and reactant concentration). Spherical particles larger than the critical coalescence particle size can be formed by combination of smaller (fusible) particles with larger (non-fusible) particles. It is necessary that the smaller particles do not continue growing by themselves to form particles of comparable size to the larger particles. This would spread out the particle size distribution, and it would increase the particle concentration and possibly lead to coagulation. Therefore the monomer formation rate should be kept low enough so that all newly formed particles collide and coalesce with seed particles (newly formed particles are 'scavenged' by existing particles), before the new particles grow beyond the critical size for coalescence.

They investigated the constraint of 'suppression of homogeneous nucleation' (defined similarly to Wu et al. (1988)), but they did not investigate seed particle coagulation (which would produce unwanted agglomerates).

They employed numerical simulation to develop an empirical expression for the maximum monomer source rate for 'suppression of homogeneous nucleation', as a function of the size and concentration of the existing seed particles (for $T = 1000\,K$, $P = 1\,atm$). Their model assumed that there is no thermodynamic barrier for nucleation, because of the low vapour pressure and high levels of supersaturation typical in aerosol synthesis of ceramics.

Zachariah and Dimitriou (1990) modified the typical coagulation model by assuming that a collision between two small clusters (< 7 molecules) does not produce a stable complex cluster unless it it stabilised by a third body. The three-body coagulation model that they employed for small clusters predicted slower cluster growth than the usual bi-collider coagulation model. They noted that the difference in the predicted PSD of these two models merits further study in the mechanism(s) of small cluster growth, but they did not discuss this topic further.

The empirical expression (for the material and conditions which were specified earlier) of Zachariah and Dimitriou (1990) for the maximum monomer source rate, for 'suppression of homogeneous nucleation', is:

$$R_m(max) = 1.21 \times 10^{16} d_s^{4.7} N_s^{2.72} \ [\# \cdot cm^{-3} s^{-1}] \tag{4.14}$$

where d_s $[cm]$ and N_s $[\#/cm^3]$ are the seed particle diameter and number concentration respectively.

4.6 Reactor Phenomena

This section discusses the the flow of mass and energy in the reactor, which is determined by the reactor configuration and conditions.

4.6.1 Turbulence

The model of Xiong and Pratsinis (1991) described coagulation because of simultaneous Brownian and turbulent motion. Most other aerosol models assume laminar flow, and therefore consider only Brownian coagulation. However, according to Pratsinis and Vemury (1996), aerosol synthesis of ceramic powders can only be economically viable at turbulent conditions, because of the increased reaction and coagulation rates in turbulent conditions.

In appendix D an expression (equation D.20) is derived to determine the reactor diameter for a specified Reynolds number (Re) and production rate (characterised by the initial number flow rate of the limiting reactant: N_0 $[\#/s]$):

$$D \propto \frac{N_0}{Re} \tag{4.15}$$

This expression indicates that a smaller reactor diameter is required for a higher Reynolds number. This may explain the high length-to-diameter ratio and flow velocity that Xiong and Pratsinis (1991) chose for their simulations on turbulent coagulation:

- **length**: $L = 125\,m$
- **diameter**: $D = 0.25\,m$
- **flow velocity**: $u \approx 150\,m/s \propto N_0$
  (gas flow rate $= 176\,mol/s$, $T = 2000\,K$, $P = 4\,atm$)

Correspondence with Prof. R.C. Flagan (October 2001) indicated that reactors with such length and diameter are employed in industry in the cooling phase of TiO_2-agglomerate synthesis, where the long reactor length is realised by folded tubes. This method of cooling is preferable to more efficient heat exchangers, since the latter will rapidly be fouled by the high particle concentrations.

4.6.2 Diffusion

Lee et al. (2001) included the phenomenon of axial particle diffusion in their model of the evolution of particle volume and surface area. They concluded that particle diffusion significantly influences the particle size distribution. However, it is not possible to infer from their data whether or not diffusion broadens the size distribution. Their data represent bi-modal size distributions, which were obtained because of simultaneous chemical reaction and particle growth (i.e. the characteristic time for chemical reaction was of the same order as the residence time).

4.6.3 Temperature Variation

Many of the reviewed models accounted for temperature profiles with a constant heating rate (at the start of the reactor) and a constant cooling rate (at the end of the reactor), e.g. Kruis et al. (1993). However, there are more models that assume isothermal conditions (see tables 4.1 and 4.2).

4.6.4 Wall-Deposition

Sadataka et al. (1996) claimed that wall deposition causes $70-90\%$ yield loss in experimental aerosol reactors. This figure included deposition in the feed nozzle and deposition of reactant.

The modelling and experiments of Okuyama et al. (1992) indicated that wall-deposition is significant (in the order of 50%) when the reaction rate is slow, because of the high diffusivity of small species.

Wall-deposition is less important in industrial scale reactors, for which greater reactor diameters are employed.

Wall-Deposition without Simultaneous Particle Growth Dynamics

Chang, Ranade and Gentry (1990) developed an experimental set-up to study thermophoretic wall-deposition. They generated an aerosol with certain particle size, and then introduced this aerosol into a thermophoretic cell.

They conducted modelling which showed how deposition increases with decreasing particle size, and increases with increasing temperature gradient. They also showed that diffusional (non-thermophoretic) wall-deposition is negligible for particles larger than 0.01 μm.

Gomez and Rosner (1993) measured thermophoretic diffusivities of particles (including agglomerate particles) in a counter-flow diffusion flame, in which a particle stagnation plane was established.

Simultaneous Wall-Deposition and Particle Growth Dynamics

Park and Rosner (1989) modelled simultaneous particle coagulation and wall deposition within the thermal boundary layer adjacent to the collecting surface. This model is tailored for applications with intentional particle deposition, such as the manufacture of optical wave-guides. Their modelling showed that coagulation has little influence on the total mass deposition rate (compared to modelling in which coagulation is neglected), but that it significantly broadens the PSD of the depositing particles.

Okuyama et al. (1990) modelled simultaneous chemical reaction, coagulation, and convective (laminar flow) and diffusive transport in a wall-heated (tubular) aerosol reactor. They showed that new particle formation can be suppressed by *seed particles* and slow chemical reaction rate (see section 4.5.7). Such suppression of new particle formation, due to scavenging of clusters by seed particles, reduces wall-deposition compared to the same reactor conditions without seed particles.

4.7 Summary of Aerosol Models

Tables 4.1 and 4.2 summarise the models in the literature that are used for spherical and agglomerate particle growth. Models are are classified according to:

- Representation of the PSD (as discussed in section 4.2): *functional form* of the PSD, and incorporation of *particle area/shape* in the model.
- Applicability to continuum and free-molecular regimes (see section 2.4.1).
- Number of spatial dimensions (as discussed in section 4.4).
- Population phenomena (as discussed in section 4.5).
- Reactor phenomena (as discussed in section 4.6).
- Method by which the model equations are solved (as discussed in section 4.2).

Yr	Representation of PSD										Size Scale		Spatial Dimensions	Population Phenomena								Reactor				Solution		
	functional form						area/shape																					
	monodisperse	moments/self-preserving PSD	sectional	discrete-sectional	continuous	discrete	V & A	V & A, constant D_f	V & A [$D_s=f(V,A)$]	V &D_f	free-molecular regime	continuum regime		chemical reaction	nucleation	condensation	surface reaction	coagulation	seed particles	coalescence	restructuring	turbulence	diffusion	temperature variation	wall-deposition	analytical	numerical solution of DEs	stochastic simulation
76 Ramabhadran, Peterson and Seinfeld													1								*[Analytical solution of GDE.]*						
78 Gelbard and Seinfeld													1								*[Collocation method in finite element solution of the GDE.]*						
80 Gelbard, Tambour and Seinfeld													1								*[Sectional solution of GDE.]*						
88 Kodas and Friedlender													1				*[Nucleation-controlled aerosol process.]*										
88 Wu et al.													1				*[Simple reaction-coagulation (SRC) model.]*										
89 Park and Rosner													2				*[Effect of coagulation on depositing particles.]*										
90 Okuyama et al.							*[Reaction, coagulation and wall deposition in the presence of seed particles.]*						2														
90 Hounslow													1								*[Discretised population balance.]*						
90 Zachariah and Dimitriou													1				*[Controlled nucleation for suppression of agglomerate formation.]*										
91 Xiong and Pratsinis													1								*[Study transition from Brownian to turbulent coagulation.]*						
92 Okuyama et al.													2				*[Reaction, coagulation and wall deposition.]*										
97 Jain et al.													1				*[Simultaneous surface and gas-phase reaction.]*										
98 Pratsinis and Spicer													1				*[Simultaneous surface and gas-phase reaction.]*										
98 Smith and Matsoukas													1														
99 Bensberg et al.													2								*[2D spatial model of flame synthesis.]*						
00 Kruis, Maisels and Fissan													1														

[Constant-Number Monte Carlo Simulation of Population Balances.]

[Direct Monte Carlo simulation for particle coagulation.]

Table 4.1: Aerosol Modelling Literature: Spherical Particle Growth

Yr	Representation of PSD										Size		Spatial Dimensions	Population Phenomena								Reactor				Solution		
	functional form						area/shape				Scale																	
	monodisperse	moments/self-preserving PSD	sectional	discrete-sectional	continuous	discrete	V & A	V & A, constant D_f	V & A [D_s=f(V,A)]	V &D_f	free-molecular regime	continuum regime		chemical reaction	nucleation	condensation	surface reaction	coagulation	seed particles	coalescence	restructuring	turbulence	diffusion	temperature variation	wall-deposition	analytical	numerical solution of DEs	stochastic simulation
77 Ulrich and Subramanian	■						■				■		1					■		■						■		
	[De-coupled coalescence and agglomeration rate equations.]																											
86 Mountain and Mulholland						■				■	■	■	1					■										■
								[Increased collision frequency of agglomerates compared to spheres.]																				
89 Koch and Friedlander		■					■				■		1					■		■				■			■	
														[Effect of coalescence on coagulating aerosol.]														
91 Matsoukas and Friedlander		■						■			■		1					■										
								[Collision radius function of number&size of prim. particles & D_f.]																				
92 Rogak and Flagan			■					■			■	■	1					■		■							■	
														[Study fundamentals of fractal agglomerates.]														
92 Xiong, Pratsinis and Weimer			■						■		■	■	1	■				■		■							■	
																						[2D-sectional model.]						
93 Kruis et al.	■							■			■	■	1					■		■							■	
	[Structure-dependant monodisperse (SDM) model for coagulation and coalescence.]																											
97 Rogak			■					■			■	■	1	■				■									■	
														[Fusible species still forms after agglomeration has commenced.]														
99 Tandon and Rosner						■		■				■	1					■		■								■
								[Monte-Carlo simulation for 2D PSD, in terms of volume and surface.]																				
00 Tsantilis and Pratsinis		■						■			■	■	1	■				■		■							■	
																						[2D-sectional model.]						
00 Kostoglou and Konstandopoulos						■			■	■	■	■	1					■			■							■
														[Invariant-area restructuring of fractal aggregates.]														
01 Lee et al.		■						■			■	■	1	■				■		■			■	■			■	
								[Evaluate different coalescence models; study effect of axial diffusion.]																				
01 Rosner and Yu						■		■			■		1					■		■								■
								[Monte-Carlo simulation for 2D PSD, in terms of volume and surface.]																				
01 Jeong and Choi	■							■			■	■	1					■		■							■	
	[Approximate distribution of particle volume and surface as 1-dimensional.]																											

Table 4.2: Aerosol Modelling Literature: Agglomerate Growth

Chapter 5

Reactor Design Criteria and Research Needs in Aerosol Reactor Engineering

5.1 Aerosol Reactor Design Criteria

This section is concerned with *general design criteria* for the aerosol synthesis of *spherical ceramic particles*. The choice of reaction route depends on the specific material to be synthesised, and is therefore not discussed here (although it is indeed an important process design consideration). The focus here is on *criteria for choosing favourable process conditions*. Separate discussions are given for reactor design criteria for coagulation-controlled growth and for seed growth.

Only explicit propositions of criteria for aerosol reactor design are reviewed here. A more comprehensive review of the state-of-the-art in aerosol reactor engineering is given in chapters 3 and 4.

The design criteria typically rely on some measures of tolerance. For example: the guideline to separate particle formation and growth depends on how much separation is considered to be enough, and on how much separation is possible. Such criteria cannot be quantitatively evaluated on their own, but would rather be evaluated as part of a formal optimisation problem definition. This would include a comprehensive definition of different process constraints and multiple objective functions (which may be combined into a single cost function).

The reviewed literature does not attempt to integrate the different criteria into an reactor optimisation algorithm. Ongoing expansion of the understanding, measurability (on-line measuring instruments) and predictability (faster, more accurate numerical models) of aerosol reactors, may in the future allow the application of an integrated optimisation algorithm for aerosol reactor design.

5.1.1 Coagulation-Controlled Particle Growth

Coagulation-controlled particle growth refers to particle formation and growth by uninhibited coagulation, where coalescence is rapid and complete (and hence spherical particles are produced).

Landgrebe, Pratsinis and Mastrangelo (1990) employed dimensionless modelling to plot *nomographs* to relate dimensionless particle concentration, mean particle diameter and standard deviation to *dimensionless residence time* and *dimensionless reaction time* (the two coordinates of the nomographs). The non-dimensional nature of the nomographs (and the underlying model) allows them to be applied to different process conditions and reaction routes. However, the application of the nomographs is restricted by the modelling assumptions, namely spherical particle growth, isothermal conditions and first-order reaction.

Sadataka et al. (1996) proposed criteria for the generation of nearly monodisperse aerosols, in terms of characteristic times. Their experimental work was discussed in section 3.2.1.

They used the following *performance criteria* for aerosol reactors in their analysis:

- Reaction conversion
- Particle production yield
- Average particle size
- Particle size distribution
- Particle purity

The following *characteristic times* were specified:

- Diffusion time: τ_D
- Residence time: τ_r
- Reaction time: τ_P
- Reactant mixing time: τ_m

Sadataka et al. (1996) proposed the following criteria for producing ultrafine particles with a narrow size distribution:

- *Nucleation should be carried out under reaction control*: $\tau_P > \tau_m$. This ensures that particle formation occurs homogeneously in a small volume near the reactor entrance.
- *Ensure complete reaction*: $\tau_r > \tau_P$
- *Minimise particle deposition on reactor wall*: $\tau_D > \tau_r$
- *No recirculation flow*: Particle formation and growth should take place under plug flow conditions.

Flagan and Lunden (1995) stated that the formation of hard agglomerates (with significant neck formation between primary particles) can be prevented by rapidly cooling the aerosol before the particle size is large enough (and the temperature low enough) so that the characteristic coalescence time is greater than the characteristic collision time. Rapid cooling prevents neck formation when particles agglomerate during the cooling process. They also showed that high reactor pressure increases growth rates.

5.1.2 Seed Growth by Cluster Scavenging

Seed growth by cluster scavenging refers to a special case of uninhibited coagulation where a bi-modal PSD is established, without overlap between the modes, and larger particles (seeds) grow by deposition of smaller particles (clusters) onto it. This was discussed in section 4.5.7. Such conditions can be achieved either by introducing seed particles into the reactor, or by *in situ* seed formation.

Kodas and Friedlander (1988) developed criteria for the generation of nearly monodisperse aerosols, in terms of non-dimensional parameters. They developed these criteria for seed growth in nucleation-limited systems and not for uninhibited coagulation. Yet, because of the similarity between these two processes (see section 4.5.7) their criteria may be of use also for uninhibited coagulation.

- *Separate nucleation and growth*: The nucleation time (time during which new particles are formed) should be much less than the time for growth by coagulation (residence time). This can be achieved by operating at high reaction rate (monomer formation rate). This criterion can be translated for uninhibited coagulation as: *separate seed formation and growth.*

- *Operate with a narrow residence time distribution*: A broad residence time distribution results in a broad particle size distribution. This can be minimised by using a plug-flow reactor configuration with minimal mixing effects.

- *Minimise monomer concentration gradients*: Limit the radial diffusion of monomers to ensure radially homogeneous monomer concentration (and therefore homogeneous particle growth). This criterion is met if the time for nucleation is much less than the time for monomer diffusion to the walls (which can be achieved by increasing the reaction rate, reactor diameter, and/or operating pressure).

Okuyama et al. (1990) conducted experiments and modelled reaction, coagulation and wall-deposition in a laminar-flow aerosol reactor, in the presence of seed particles (presumedly spherical, but this is not explicitly stated). They proposed that new particle formation should be suppressed for producing particles with a narrow size distribution. The criterion for suppression of new particle formation is described in terms of seed particle size and concentration, and monomer formation rate:

- *Seed particle concentration*: The number concentration of seed particles should be of the same order of magnitude as the number concentration of product particles that would be formed under the same conditions without any seed particles.

- *Size of seed particles*: The larger the seed particles, the lower is the concentration of seed particles needed to suppress new particle formation.

- *Slow chemical reaction*: The chemical reaction rate should be slow enough so that the growth of particles in the cluster mode is constrained. This can be achieved by choosing a low enough temperature and reactant concentration.

Alam and Flagan (1986) used a 'clearance volume' model to predict whether a chosen temperature profile would ensure suppression of new particle formation.

Zachariah and Dimitriou (1990) proposed an empirical expression for the maximum monomer source rate for suppression of new particle formation, as a function of seed particle size and concentration (see equations and 4.14).

5.1.3 Common Reactor Design Criteria

The following criteria for the production of spherical particles with narrow size distributions are commonly accepted:

- Turbulent reactant mixing at low temperature.
- Non-turbulent particle growth.
- Rapid cooling at reactor exit.

5.2 Research Needs in Aerosol Synthesis of Ceramic Powders

This section reviews explicit statements in the literature on how the field of aerosol reactor engineering may be advanced in the future.

Stamatakis et al. (1991) noted that the high particle concentrations in aerosol reactors make conventional measurement and control impossible with the current (1991) measurement technology. They concluded that accurate on-line measurement, coupled with appropriate control strategies (models), are needed for real-time optimisation of aerosol reactors.

Gurav et al. (1993) emphasised the need for scale-up of aerosol processes for higher production rates, whilst maintaining powder quality.

Kusters and Pratsinis (1995) noted that although aerosol synthesis of particles is used on a significant commercial scale, there is a lack of formal process control of these processes. They attributed this lack of rational control procedures to the following:

- A lack of accurate models for particle dynamics.
- The inadequacy (in terms of speed) of measuring techniques for particle characterisation.

Pratsinis (1998) reiterated that the development *in situ* particle and temperature measurement instruments is a major need for the advancement of particle production by aerosol synthesis.

Chapter 6

Exemplary 2-Mode Plug-Flow Aerosol Reactor Model

An aerosol reactor model is developed to describe simultaneous monomer formation and coagulation as simply as possible. The model considers (one-dimensional) plug-flow through an isothermal and isobaric tubular reactor, and the PSD is represented by monomers and monodisperse particles. The model equations are derived in a manner that is typical of reactor engineering.

This model is novel in the manner of derivation and expression of equations, but the set of assumptions and approximations is a simplification of that being used by some existing models (which are more complex). Hence the numerical output is not a novel contribution, but the manner of presentation of results is novel. The model is a valuable tool for gaining understanding into more complex models presented in the literature.

The model is applied to typical aerosol reactor conditions, so as to allow comparison with published results.

6.1 Novel Aspects of the Model

The model equations are derived in non-dimensional form, as is common in reactor modelling. Reaction conversions are the non-dimensional variables that are used to describe the different phenomena ('reactions') in the process.

The novelty of the model equations is that *reaction conversions are defined in a sequential manner*, in analogy to the sequential phenomena in the process (reactants/products are indicated with *italics* and 'reactions' are indicated with **boldface**):

- *Reactant* enters the reactor.
- **Gas-phase reaction** creates *monomers*.
- *Monomers* are 'reactants' for **monomer-monomer and monomer-particle collisions**, of which the product is *particles*.
- *Particles* are 'reactants' for **monomer-particle and particle-particle collisions**, of which the product is *particles*.

The sequential definition of reaction conversions promotes interpretation of the reaction conversions, and ensures that the numerical values of the conversions will not differ by orders of magnitude. The last point is important for accuracy and speed of numerical simulation.

Another novel aspect is that the *final equations are transformed to logarithmic form*. This ensures that the asymptotic behaviour of reaction conversions (with an upper limit of 1), is represented in a numerically more tractable manner. For example, it is numerically more accurate to model changes in $-\ln(1-\phi)$, where $\phi \rightarrow 1$, than to model changes in ϕ.

The sequential definition of reaction conversions and the logarithmic transformation have the drawback that the model equations would become excessively complex if more phenomena or modes were to be added to the model. For the present two-mode model this is not a problem, but the form of the model equations may hinder expansion of the model to include more phenomena and/or modes.

6.2 Classification of the Model

The model system is defined in a manner similar to the classification of aerosol models in the literature (see chapter 4).

6.2.1 Functional Representation of the PSD

The PSD is described as two modes: one describing the concentration of monomers, and the other describing the concentration and size of particles. The particle size is assumed to be monodisperse.

This representation of the PSD as a small number of discrete (and monodisperse) modes is similar to the reaction-coagulation (SRC) model of Wu et al. (1988) and the extended SRC model of Okuyama et al. (1990). This model excludes the cluster-mode (for clusters of approximately 5 molecules) that both these SRC models have, and is therefore likely to be less accurate.

6.2.2 Spatial Dimensions

Perfect plug flow is assumed, therefore the model is one-dimensional with respect to residence time or position in the reactor.

6.2.3 Population Phenomena

The model describes simultaneous chemical reaction and coagulation.

6.2.4 Other Assumptions

- A large excess of non-limiting reactant is used.
- Perfect mixing, and no reaction, of reactants before entering the reactor.
- Isothermal and isobaric reactor.
- Non-turbulent flow.
- Steady-state conditions.
- No deposition of reactant, monomers or particles on reactor walls.

- First-order reaction kinetics, and stoichiometric ratio between limiting reactant and product is unity.
- Colliding particles immediately coalesce completely, hence particles are spherical.
- Condensation of reactant and subsequent chemical reaction on the surface of particles (or monomers) is negligible.

The first assumption in this list is based on the fact that experimental aerosol reactors commonly use a large degree of reactant dilution, in the order of 0.01 mole of limiting reactant to 1 mole total gas, [e.g. Kobata, and Kusakabe and Morooka (1991); Xiong, Pratsinis and Weimer (1992)]. A large degree of reactant dilution (excess gas) is necessary to obtain forced flow of the aerosol. The excess gas (which is an excess of the most volatile reactant, and/or an inert gas) is used as a 'carrier' of the particles through the reactor.

6.3 Description of the Model System

6.3.1 Species in the Model System

The different **species in the model system** are:

- oxidant reactant (in excess) [O]
- metal-containing reactant (limiting reactant) [M]
- product monomer [m]
- product particle [p]

Each single entity of a species is called a **unit**.

6.3.2 Reactions in the Model System

There are different phenomena which cause change in the number (and size in the case of particles) of the different species. These are called the **reactions affecting the species**:

- gas-phase (chemical) reaction [gr]
- coagulation (collision and bondage) [$mm/mp/pp$]

Gas-Phase Reaction Stoichiometry

The following general chemical equation applies to many ceramic synthesis reactions:

$$\alpha_M M + \alpha_O O \rightarrow m + \alpha_{bp}(byproduct\ gas)$$

M is the metal-containing reactant, O is the the oxidant reactant, and m is a product monomer. α_i is the stoichiometric coefficient.

The stoichiometric coefficients are evaluated for the reaction $TiCl_4 + O_2 \rightarrow TiO_2 + 2Cl_2$, to which the model is numerically applied. Hence $\alpha_M = \alpha_O = 1$.

Furthermore, a large excess of non-limiting reactant (O) is assumed. A typical published value for the fractional excess gas is $\varepsilon = 1000$ [Pratsinis and Spicer (1998)]. For such high reactant dilution, the contributions of reactant M and byproduct gas to the overall gas concentration are negligible.

Gas-Phase Reaction Kinetics

It is assumed that the gas-phase reaction rate is dependent only on the limiting reactant (M), because a large excess of the other reactant (O) is specified, and that reaction kinetics are first-order.

6.4 Variables to Describe the System

6.4.1 Independent Variable: Position

The model is one-dimensional in terms of position in the reactor, which may be characterised according to volume (V) or time (t). Non-dimensional position is defined as the ratio of time to residence time:

Definition 6.1 (Non-Dimensional Position)

$$x = \frac{t}{\tau_{res}}$$

6.4.2 Dependent Variables: Reaction Fluxes

Reaction fluxes are used as a complete set of variables to describe the system.

Definition 6.2 (Reaction Flux) $N_i\,[\#/s]$ *is the cumulative flux (up to a certain reactor volume) at which the reaction* i *produces product units.*

$$N_i = \int_0^V r_i \, \mathrm{d}V$$

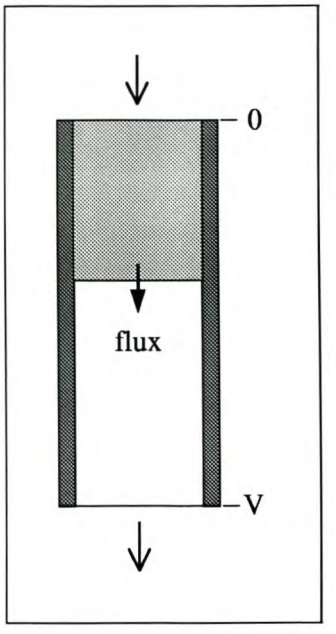

The necessary fluxes to describe the system are:

- Flux of chemical (gas-phase) reaction: N_{gr}
- Flux of monomer-monomer collisions: N_{mm}
- Flux of monomer-particle collisions: N_{mp}
- Flux of particle-particle collisions: N_{pp}

6.4.3 Reaction Conversions

Non-dimensionalisation transforms the reaction fluxes to reaction conversions. These will be used instead of the fluxes to describe the system.

The initial flux of the limiting reactant $N_0\,[\#/s]$ is used to non-dimensionalise the fluxes.

The reactions $gr/mm/mp/pp$ take place in a sequential manner:

- The product of reaction gr (monomer) is the reactant for reactions mm and mp.
- The product of reactions mm, mp and pp (particle) is the reactant for reaction pp.

A 'reverse reaction' that will cause a unit to decrease in size is not possible, e.g. for an particle to break up into smaller particles. In analogy to the sequential reactions, the *reaction conversions are also defined in a sequential manner.* This promotes interpretation of the reaction conversions, and ensures that the numerical values of the conversions will not differ by orders of magnitude. The last point has great practical importance, since numerical integration algorithms are not reliable when the numerical values of the variables differ by orders of magnitude.

Definition 6.3 (Reaction Conversion) *ϕ_i is the ratio between the flux of reaction i (N_i) multiplied by the stoichiometric coefficient (α_i)of the reactant of reaction i, and the flux (N_j) of the reaction that produces the reactant for reaction i.*
For the gas-phase reaction $N_j = N_0$.

$$\phi_i = \frac{\alpha_i N_i}{N_j(\text{formation of reactant})}$$

According to this general definition, the conversions for the different reactions are individually defined:

- Gas-phase reaction:

$$\phi_{gr} = \frac{\alpha_M N_{gr}}{N_0} \tag{6.1}$$

- Coagulation:

$$\phi_{mm} = \frac{2N_{mm}}{N_{gr}} = \frac{2\alpha_M N_{mm}}{N_0 \phi_{gr}} \tag{6.2}$$

$$\phi_{mp} = \frac{N_{mp}}{N_{gr}} = \frac{\alpha_M N_{mp}}{N_0 \phi_{gr}} \tag{6.3}$$

$$\phi_{pp} = \frac{N_{pp}}{N_{mm}} = \frac{\alpha_M N_{pp}}{N_0 \left(\frac{1}{2}\phi_{gr}\phi_{mm}\right)} \tag{6.4}$$

6.4.4 Particle Characteristic Variables

These variables are the directly measurable properties of the aerosol. They describe the aerosol at any point in the reactor in terms of concentrations and particle size. Characteristic non-dimensional variables are defined for concentrations (for O, M, m, and p) and particle size. These characteristic variables are written in terms of the reaction conversions.

In order to derive equations for the characteristic variables in terms of reaction conversions, equations for the *species* fluxes and *species* concentrations in terms of reaction conversions are first derived.

Species Fluxes in Terms of Conversions

$$N_M = N_0(1-\phi_{gr}) \tag{6.5}$$

$$N_O = \frac{\alpha_O}{\alpha_M} N_0(1+\varepsilon-\phi_{gr}) \approx \frac{\alpha_O}{\alpha_M} N_0\varepsilon \tag{6.6}$$

$$N_m = \frac{N_0}{\alpha_M}\phi_{gr}(1-\phi_{mm}-\phi_{mp}) \tag{6.7}$$

$$N_p = \frac{N_0}{\alpha_M}(\tfrac{1}{2}\phi_{gr}\phi_{mm})(1-\phi_{pp}) \tag{6.8}$$

Note the approximation of the flux of the oxidant (excess) reactant as a constant (equation 6.6). This approximation is based on a large excess of oxidant reactant ($\varepsilon \gg 1$).

Assume large excess oxidant reactant:

$$\varepsilon \gg 1$$

Species Number Concentrations

The number concentration of a species is written in terms of species flux and velocity:

$$n_i = \frac{N_i}{Au} \tag{6.9}$$

where N_i is the number flux of species i, A is the cross-sectional area of the reactor, and u is the linear velocity of flow.

Based on large excess gas, it is assumed that the total gas flux (N_T) is constant though-out the reactor.

Assume constant total gas flux N_T [#/s]

$$N_T \approx N_0 + N_O \approx N_0 \left(\frac{\alpha_O}{\alpha_M} \varepsilon + 1 \right) \tag{6.10}$$

It is assumed that the gas mixture behaves as an ideal gas. This is a reasonable approximation, because in this work the model is only applied to atmospheric pressure reactors.

Assume ideal gas

The reactant gases, monomers and particles all have the same velocity at the same cross-section in the (model system) reactor, because ideal plug flow is assumed. In equations 6.11 to 6.13 the velocity of flow is derived:

$$u = \frac{N_T}{A n_T} \tag{6.11}$$

$$n_T = \frac{P}{k_B T} \tag{6.12}$$

$$u = \frac{k_B T}{AP} N_T \tag{6.13}$$

where n_T is the total gas number concentration.

Equation 6.14 shows how the number concentration of any species i is determined, and equation 6.15 shows how the species concentration is non-dimensionalised:

$$n_i = \frac{N_i}{N_T} n_T \tag{6.14}$$

$$\eta_i = \frac{n_i}{n_T} \tag{6.15}$$

Combination of equations 6.10, 6.14 and 6.15 gives the simplified expression for non-dimensional concentration:

$$\eta_i = \frac{N_i}{N_0\left(\frac{\alpha_O}{\alpha_M}\varepsilon + 1\right)} \approx \left(\frac{N_i}{N_0}\right)\frac{\alpha_M}{\alpha_O\varepsilon} \qquad (\varepsilon \gg 1) \tag{6.16}$$

The species fluxes (N_i) are substituted in terms of reaction conversions (using equations 6.5 to 6.8) to express the dimensionless number concentrations:

$$\eta_M = (1-\phi_{gr})\frac{\alpha_M}{\alpha_O\varepsilon} \tag{6.17}$$

$$\eta_O \approx \left(\frac{\alpha_O}{\alpha_M}\varepsilon\right)\frac{\alpha_M}{\alpha_O\varepsilon} = 1 \tag{6.18}$$

$$\eta_m \approx \left(\frac{\phi_{gr}(1-\phi_{mm}-\phi_{mp})}{\alpha_M}\right)\frac{\alpha_M}{\alpha_O\varepsilon} = \frac{\phi_{gr}(1-\phi_{mm}-\phi_{mp})}{\alpha_O\varepsilon} \tag{6.19}$$

$$\eta_p \approx \frac{(\frac{1}{2}\phi_{gr}\phi_{mm})(1-\phi_{pp})}{\alpha_O\varepsilon} \tag{6.20}$$

Particle Size

> **Definition 6.4 (Particle Size)** $\mathbf{m_p}$ *is the number of molecules per particle.*

Particle size is determined by dividing the total number of molecules in particles by the number of particles. This is expressed in terms of reactions fluxes by dividing the sum of reaction fluxes (scaled by stoichiometric coefficients) that add new molecules to the mode of particles by the sum of reaction fluxes that increases (or decreases) the number flux of particles.

$$m_p = \frac{2N_{mm} + N_{mp}}{N_{mm} - N_{pp}} \tag{6.21}$$

Substitution in terms of reaction conversions (using equation 6.2 to 6.4) gives:

$$m_p = \frac{\phi_{gr}(\phi_{mm} + \phi_{mp})}{(\frac{1}{2}\phi_{gr}\phi_{mm})(1 - \phi_{pp})} \tag{6.22}$$

$$= 2\left[\frac{(\phi_{mm} + \phi_{mp})}{\phi_{mm}(1 - \phi_{pp})}\right] \tag{6.23}$$

Particle diameter is needed to model collisions, and is inferred from the particle size (m_p):

$$d_p = \left[\frac{6m_p v_1}{\pi}\right]^{\frac{1}{3}} \tag{6.24}$$

$$a_p = \pi^{\frac{1}{3}}(6m_p v_1)^{\frac{2}{3}} \tag{6.25}$$

where v_1 is the volume of a single molecule in the solid phase.

6.5 Equations for the Different Phenomena

This section gives the rate expressions for the phenomena of chemical reaction and coagulation, and non-dimensionalises these expressions.

6.5.1 Gas-phase Reaction

The following expressions for reaction rate apply to the reaction $TiCl_4 + O_2 \rightarrow TiO_2 + 2Cl_2$, to which the model is numerically applied. A large excess of non-limiting reactant (O_2) and first-order reaction kinetics are assumed. The concentration of the metal-containing (limiting) reactant is referred to as C_M.

$$r_{gr} = k_{gr}(T)C_M \left[\frac{mol}{m^3 s}\right] \tag{6.26}$$

$$k_{gr} = A_{gr} \exp\left(\frac{-E_{gr}}{k_B A_v T}\right) \tag{6.27}$$

Definition 6.5 (Non-Dimensional Gas-Phase Reaction Rate) *γ_g is the gas-phase reaction rate divided by the constant gas-phase reaction rate that would be necessary to consume all the initial limiting reactant (M), in one reactor volume.*

$$\gamma_{gr} = \left(\frac{VA_v}{N_0}\right) r_{gr} \tag{6.28}$$

$$= \left(\frac{VA_v}{N_0}\right) k_{gr} C_M \tag{6.29}$$

$$= \kappa_{gr} \eta_M \tag{6.30}$$

The non-dimensional number concentration (η_M) was defined in section 6.4.4. The non-dimensional parameter κ_{gr} is now defined. This definition is derived by combining equations 6.29 and 6.30. The derivation is not straightforward, and is shown in equations 6.31 to 6.38.

Definition 6.6 (Non-Dim. Gas-Phase Reaction Rate Constant)

$$\kappa_{gr} = k_{gr} \tau_{res} \varepsilon$$

Derivation of κ_{gr} (refer to section 6.4.4 if needed):

$$\kappa_{gr} = \left(\frac{VA_v}{N_0}\right) A_{gr} \frac{C_M}{\eta_M} \tag{6.31}$$

$$C_M = C_T \frac{C_M}{C_T} \tag{6.32}$$

$$= \left(\frac{P}{k_B A_v T}\right) \left[\frac{(1-\phi_{gr})}{(1-\phi_{gr}) + (1+\varepsilon-\phi_{gr})}\right] \tag{6.33}$$

$$\approx \left(\frac{P}{k_B A_v T}\right) \frac{(1-\phi_{gr})}{\varepsilon} \qquad (\varepsilon \gg 1) \tag{6.34}$$

$$\eta_M = \frac{(1-\phi_{gr})}{\varepsilon} \tag{6.35}$$

$$N_0 = C_{M_0}\tfrac{\pi}{4}D^2uA_v \tag{6.36}$$

$$\approx \left(\frac{P}{k_BA_vT}\right)\left(\frac{1}{\varepsilon}\right)\frac{\pi}{4}D^2uA_v = \left(\frac{P}{k_BT}\right)\left(\frac{1}{\varepsilon}\right)\frac{\pi}{4}D^2u \tag{6.37}$$

$$\kappa_{gr} = \frac{VA_{gr}\varepsilon}{\frac{\pi}{4}D^2u} \tag{6.38}$$

6.5.2 Collisions

The Fuchs expression for Brownian collision (section 2.4.6) is non-dimensionalised:

$$\tilde{\beta}_{Bij} = \left(\frac{3\pi\mu}{k_BT}\right)\beta_{Bij} \ , \ ij = mm/mp/pp \tag{6.39}$$

$$= 2\pi(\tilde{D}_{fi}+\tilde{D}_{fj})(m_{ci}^{\frac{1}{3}}+m_{cj}^{\frac{1}{3}}) \tag{6.40}$$

$$\times\left[\frac{(m_i^{\frac{1}{3}}+m_j^{\frac{1}{3}})}{(m_i^{\frac{1}{3}}+m_j^{\frac{1}{3}}+2\tilde{g}_{ij})}+\pi\left(\frac{l_0}{d_1}\right)\frac{(\tilde{D}_{fi}+\tilde{D}_{fj})}{\tilde{c}_{ij}(m_i^{\frac{1}{3}}+m_j^{\frac{1}{3}})}\right]^{-1} \tag{6.41}$$

$$\tilde{D}_{fi} = \left(\frac{3\pi\mu}{k_BT}\right)\left(\frac{6v_1}{\pi}\right)^{\frac{1}{3}}D_{fi} \ , \ i = m/p \tag{6.42}$$

$$= \frac{1}{m_{ci}^{\frac{1}{3}}}\left[\frac{5+4\mathrm{Kn}_i+6\mathrm{Kn}_i^2+18\mathrm{Kn}_i^3}{5-\mathrm{Kn}_i+(8+\pi)\mathrm{Kn}_i^2}\right] \tag{6.43}$$

$$\mathrm{Kn}_i = \frac{\mathrm{Kn}_0}{(m_i)^{\frac{1}{3}}} \ , \ i = m/p \tag{6.44}$$

$$\tilde{c}_i = \left(\frac{\pi MW\times10^{-3}}{8k_BTA_v}\right)^{\frac{1}{2}}\bar{c}_i \ , \ i = m/p \tag{6.45}$$

$$= \left(\frac{1}{m_i}\right)^{\frac{1}{2}} \tag{6.46}$$

$$\tilde{c}_{ij} = (\tilde{c}_i^2+\tilde{c}_j^2)^{\frac{1}{2}} \ , \ ij = mm/mp/pp \tag{6.47}$$

$$\tilde{g}_i = \left(\frac{\pi}{6v_1}\right)^{\frac{1}{3}}g_i \ , \ i = m/p \tag{6.48}$$

$$= \left\{ \frac{\left[m_i^{\frac{1}{3}} + \left(\frac{l_0}{d_1}\right)\left(\frac{\tilde{D}_{fi}}{\tilde{c}_i}\right)\right]^3 - \left[m_i^{\frac{2}{3}} + \left(\frac{l_0}{d_1}\right)^2 \left(\frac{\tilde{D}_{fi}}{\tilde{c}_i}\right)^2\right]^{\frac{3}{2}}}{3m_i^{\frac{1}{3}}\left(\frac{\tilde{D}_{fi}}{\tilde{c}_i}\right)} \right\} \left(\frac{d_1}{l_0}\right) - m_i^{\frac{1}{3}} \quad (6.49)$$

$$\tilde{g}_{ij} = (\tilde{g}_i^2 + \tilde{g}_j^2)^{\frac{1}{2}} \ , \ ij = mm/mp/pp \quad (6.50)$$

where m_m is the number of molecules per monomer: $m_m = 1$.

The non-dimensional parameters used in equations 6.39 to 6.50 are now defined. These definitions are derived by comparing equations 6.39 to 6.50 with their dimensional equivalents in section 2.4.6.

Definition 6.7 (Non-Dim. Parameter for Brownian Collision)

$$\left(\frac{l_0}{d_1}\right) = \frac{8D_{f_0}}{\pi \bar{c}_{1_0} d_1} \quad (6.51)$$

$$= \left(\frac{8}{\pi}\right)\frac{k_B T}{3\pi\mu}\left(\frac{\pi}{6v_1}\right)^{\frac{1}{3}}\left(\frac{\pi MW_{pr}\times 10^{-3}}{8k_B A_v T}\right)^{\frac{1}{2}}\left(\frac{\pi}{6v_1}\right)^{\frac{1}{3}} \quad (6.52)$$

$$= \left[\frac{1}{3\pi}\left(\frac{\pi}{6}\right)^{\frac{2}{3}}\left(\frac{8k_B}{\pi A_v \times 10^3}\right)^{\frac{1}{2}}\right]\frac{(TMW_{pr}m_i)^{\frac{1}{2}}}{\mu v_1^{\frac{2}{3}}} \quad (6.53)$$

Definition 6.8 (Knudsen number)

$$\mathrm{Kn}_0 = \frac{2\lambda_0}{d_1} \quad (6.54)$$

$$= \frac{4\mu}{P}\left(\frac{\pi k_B A_v T}{8MW_O \times 10^{-3}}\right)^{\frac{1}{2}}\left(\frac{\pi}{6v_1}\right)^{\frac{1}{3}} \quad (6.55)$$

$$= \left[(2\pi k_B A_v \times 10^3)^{\frac{1}{2}}\left(\frac{\pi}{6}\right)^{\frac{1}{3}}\right]\frac{\mu}{P v_1^{\frac{1}{3}}}\left(\frac{T}{MW_O}\right)^{\frac{1}{2}} \quad (6.56)$$

Collision rate is calculated as:

$$r_{ij} = \beta_{Bij} n_i n_j \left[\frac{\#}{m^3 s}\right] \tag{6.57}$$

$$ij = mm/mp/pp$$

non-dimensional collision rate : γ_{ij} is the collision rate of species i and j, divided by the constant gas-phase reaction rate that would be necessary to consume all the initial limiting reactant (M), in one reactor volume.

$$\gamma_{ij} = \left(\frac{V}{N_0}\right) r_{ij} \tag{6.58}$$

$$ij = mm/mp/pp$$

$$\gamma_{mm} = \kappa_c \tilde{\beta}_{Bmm} \eta_m^2 \tag{6.59}$$

$$\gamma_{mp} = \kappa_c \tilde{\beta}_{Bmp} \eta_m \eta_p \tag{6.60}$$

$$\gamma_{pp} = \kappa_c \tilde{\beta}_{Bpp} \eta_p^2 \tag{6.61}$$

Another non-dimensional parameter (in addition to those defined by equations 6.53 and 6.56) is defined to characterise collision rates. This parameter is called the **non-dimensional collision rate constant**.

$$\kappa_c = \left[\frac{1}{6\pi}\right] \frac{\tau_{res} P \varepsilon}{\mu} \tag{6.62}$$

6.6 Conservation Equations

In the derivation is the conservation equations, the stoichiometric coefficients corresponding to the equation $TiCl_4 + O_2 \rightarrow TiO_2 + 2Cl_2$ are used: $\alpha_M = 1$, $\alpha_O = 1$.

6.6.1 Conversions

Gas-Phase Reaction

$$\frac{dN_{gr}}{dV} = -r_{gr}A_v \tag{6.63}$$

$$\frac{d\phi_{gr}}{dx} = \left(\frac{VA_v}{N_0}\right) r_{gr} = \gamma_{gr} \tag{6.64}$$

Monomer-Monomer Collision

$$\frac{dN_{mm}}{dV} = r_{mm} \tag{6.65}$$

$$\frac{1}{2}\frac{d}{dx}(\phi_{gr}\phi_{mm}) = \gamma_{mm} \tag{6.66}$$

$$= \frac{1}{2}\left[\phi_{gr}\frac{d\phi_{mm}}{dx} + \phi_{mm}\frac{d\phi_{gr}}{dx}\right] \tag{6.67}$$

$$\frac{d\phi_{mm}}{dx} = \frac{2\gamma_{mm} - \phi_{mm}\gamma_{gr}}{\phi_{gr}} \tag{6.68}$$

Monomer-Particle Collision

$$\frac{dN_{mp}}{dV} = r_{mp} \tag{6.69}$$

$$\frac{d}{dx}(\phi_{gr}\phi_{mp}) = \gamma_{mp} \tag{6.70}$$

$$= \left[\phi_{gr}\frac{d\phi_{mp}}{dx} + \phi_{mp}\frac{d\phi_{gr}}{dx}\right] \tag{6.71}$$

$$\frac{d\phi_{mp}}{dx} = \frac{\gamma_{mp} - \phi_{mp}\gamma_{gr}}{\phi_{gr}} \tag{6.72}$$

Particle-Particle Collision

$$\frac{\mathrm{d}N_{pp}}{\mathrm{d}V} = r_{pp} \tag{6.73}$$

$$\frac{1}{2}\frac{\mathrm{d}}{\mathrm{d}x}(\phi_{gr}\phi_{mm}\phi_{pp}) = \gamma_{pp} \tag{6.74}$$

$$= \frac{1}{2}\left[\phi_{gr}\phi_{mm}\frac{\mathrm{d}\phi_{pp}}{\mathrm{d}x} + \phi_{gr}\phi_{pp}\frac{\mathrm{d}\phi_{mm}}{\mathrm{d}x} + \phi_{mm}\phi_{pp}\frac{\mathrm{d}\phi_{gr}}{\mathrm{d}x}\right] \tag{6.75}$$

$$= \frac{1}{2}\left[\phi_{gr}\phi_{mm}\frac{\mathrm{d}\phi_{pp}}{\mathrm{d}x} + \phi_{gr}\phi_{pp}\frac{2\gamma_{mm} - \phi_{mm}\gamma_{gr}}{\phi_{gr}} + \phi_{mm}\phi_{pp}\gamma_{gr}\right] \tag{6.76}$$

$$\frac{\mathrm{d}\phi_{pp}}{\mathrm{d}x} = \frac{2\gamma_{pp} - \phi_{pp}(2\gamma_{mm} - \phi_{mm}\gamma_{gr}) - \phi_{mm}\phi_{pp}\gamma_{gr}}{\phi_{gr}\phi_{mm}} \tag{6.77}$$

$$= \frac{2\gamma_{pp} - 2\phi_{pp}\gamma_{mm}}{\phi_{gr}\phi_{mm}} \tag{6.78}$$

6.6.2 Particle Size

$$m_p = 2\left[\frac{1 + \frac{\phi_{mp}}{\phi_{mm}}}{1 - \phi_{pp}}\right] \tag{6.79}$$

$$\frac{\mathrm{d}m_p}{\mathrm{d}x} = 2\left[\frac{\left(\frac{1}{\phi_{mm}}\frac{\mathrm{d}\phi_{mp}}{\mathrm{d}x} - \frac{\phi_{mp}}{\phi_{mm}^2}\frac{\mathrm{d}\phi_{mm}}{\mathrm{d}x}\right)}{1 - \phi_{pp}} + \frac{\left(1 + \frac{\phi_{mp}}{\phi_{mm}}\right)}{(1 - \phi_{pp})^2}\frac{\mathrm{d}\phi_{pp}}{\mathrm{d}x}\right] \tag{6.80}$$

$$\frac{\mathrm{d}m_p}{\mathrm{d}x} = 2\left[\frac{\left(\frac{\gamma_{mp} - \phi_{mp}\gamma_{gr}}{\phi_{gr}\phi_{mm}} - \frac{\phi_{mp}(2\gamma_{mm} - \phi_{mm}\gamma_{gr})}{\phi_{gr}\phi_{mm}^2}\right)}{1 - \phi_{pp}} + \frac{\left(1 + \frac{\phi_{mp}}{\phi_{mm}}\right)(2\gamma_{pp} - 2\phi_{pp}\gamma_{mm})}{\phi_{gr}\phi_{mm}(1 - \phi_{pp})^2}\right] \tag{6.81}$$

$$= \frac{(2\gamma_{mm} + \gamma_{mp}) + (\gamma_{pp} - \gamma_{mm})m_p}{\frac{1}{2}\phi_{gr}\phi_{mm}(1 - \phi_{pp})} \tag{6.82}$$

6.6.3 Equations in Logarithmic Form for Increased Resolution

The differential equations were not numerically tractable when particle coagulation proceeded beyond a certain point, because of the decimal precision error of $(1-\phi_{pp}) \approx 0$, with subsequent division by zero. This numerical problem was solved by transforming the differential equations logarithmic form.

The following four logarithmic transformations of reaction conversions are used as a complete set of variables to describe the system:

$$LC_g = -\ln(1-\phi_{gr}) \tag{6.83}$$

$$L_m = \ln(m_p) \tag{6.84}$$

$$LC_{mp} = -\ln[1-(\phi_{mm}+\phi_{mp})] \tag{6.85}$$

$$LC_{pp} = -\ln(1-\phi_{pp}) \tag{6.86}$$

The differential equations for number conversions are now rewritten in terms of these four logarithmic variables:

$$\frac{\mathrm{d}LC_g}{\mathrm{d}x} = \frac{1}{(1-\phi_{gr})}\frac{\mathrm{d}\phi_{gr}}{\mathrm{d}x} \tag{6.87}$$

$$= \frac{\gamma_{gr}}{\exp(-LC_g)} \tag{6.88}$$

$$\frac{\mathrm{d}L_m}{\mathrm{d}x} = \frac{1}{m_p}\frac{\mathrm{d}m_p}{\mathrm{d}x} \tag{6.89}$$

$$= \frac{(2\gamma_{mm}+\gamma_{mp})+(\gamma_{pp}-\gamma_{mm})m_p}{\phi_{gr}(\phi_{mm}+\phi_{mp})} \tag{6.90}$$

$$\frac{\mathrm{d}LC_{mp}}{\mathrm{d}x} = \frac{1}{(1-\phi_{mm}-\phi_{mp})}\frac{\mathrm{d}}{\mathrm{d}x}(\phi_{mm}\phi_{mp}) \tag{6.91}$$

$$= \frac{2\gamma_{mm}+\gamma_{mp}-\gamma_{gr}(\phi_{mm}+\phi_{mp})}{\phi_{gr}\exp(-LC_{mp})} \tag{6.92}$$

$$\frac{\mathrm{d}LC_{pp}}{\mathrm{d}x} = \frac{1}{(1-\phi_{pp})}\frac{\mathrm{d}\phi_{pp}}{\mathrm{d}x} \tag{6.93}$$

$$= \frac{\gamma_{pp}-\phi_{pp}\gamma_{mm}}{\frac{1}{2}\phi_{gr}\phi_{mm}\exp(-LC_{pp})} \tag{6.94}$$

The conversions (ϕ) are inferred from their logarithmic counterparts with the following equations:

$$\phi_{gr} = 1 - \exp(-LC_g) \tag{6.95}$$

$$\phi_{mm} + \phi_{mp} = 1 - \exp(-LC_{mp}) \tag{6.96}$$

$$\phi_{mm} = \frac{2(\phi_{mm} + \phi_{mp})}{\exp(L_m - LC_{pp})} \tag{6.97}$$

$$\phi_{pp} = 1 - \exp(-LC_{pp}) \tag{6.98}$$

6.7 Simulation

6.7.1 Evaluation of Simulation Parameters

The simulation is performed for the same reaction and conditions that were modelled by Pratsinis and Spicer (1998), so as to allow comparison with their results.

$$\begin{aligned} TiCl_4 + O_2 &\rightarrow TiO_2 + 2Cl_2 \\ T &= 1000K \\ P &= 1\,atm \\ k &= 8.26 \times 10^4 \exp\left(-\frac{10681}{T}\right)\,[s^{-1}] \\ MW_{bg} &= 32\,g/mol\ \ (O_2) \\ \varepsilon &= 1000 \\ \tau_{res} &= 10\,s \end{aligned}$$

6.7.2 Numerical Integration Algorithm

The integration is performed with a stiff differential equation solver, using the variable order method (MatLab ODE15s). The code for the simulation is given in appendix C.

The computational efficiency of the numerical model may be evaluated by considering the number of intervals required to obtain an accurate solution, as well as the number of intensive calculations required for each interval:

- The integration algorithm used 162 intervals to obtain the required accuracy (scalar relative error tolerance is 1×10^{-3} and vector of absolute error tolerances is 1×10^{-6}).
- Four exponential terms (and no logarithms) need to be evaluated for each interval. The code may be optimised further by employing auxiliary variables for repetitively used exponential terms. The current code gives a rapid solution (about $2s$), and therefore such optimisation has not yet been performed.

6.7.3 Initial Conditions for Simulation

The initial conditions that are used have to be non-zero, to prevent division by zero. Therefore, very small values of ϕ_{gr} and ϕ_{mm} are used as initial conditions:

- $-\ln(1-\phi_{gr_0}) = -\ln(1-10^{-5})$
- $\ln(m_{p_0}) = \ln 1 = 0$
- $-\ln[1-(\phi_{mm_0}+\phi_{mp_0})] = -\ln(1-10^{-6})$
- $-\ln(1-\phi_{pp_0}) = -\ln(1-0) = 0$

6.8 Results and Discussion

Figure 6.1 presents the output variables from the numerical simulation. The independent variable is non-dimensional position (x). The dependent variables are the logarithmic transforms of sequential reaction conversions ($-\ln[1-\phi_i]$), and the logarithm of particle size ($\ln[m_p]$).

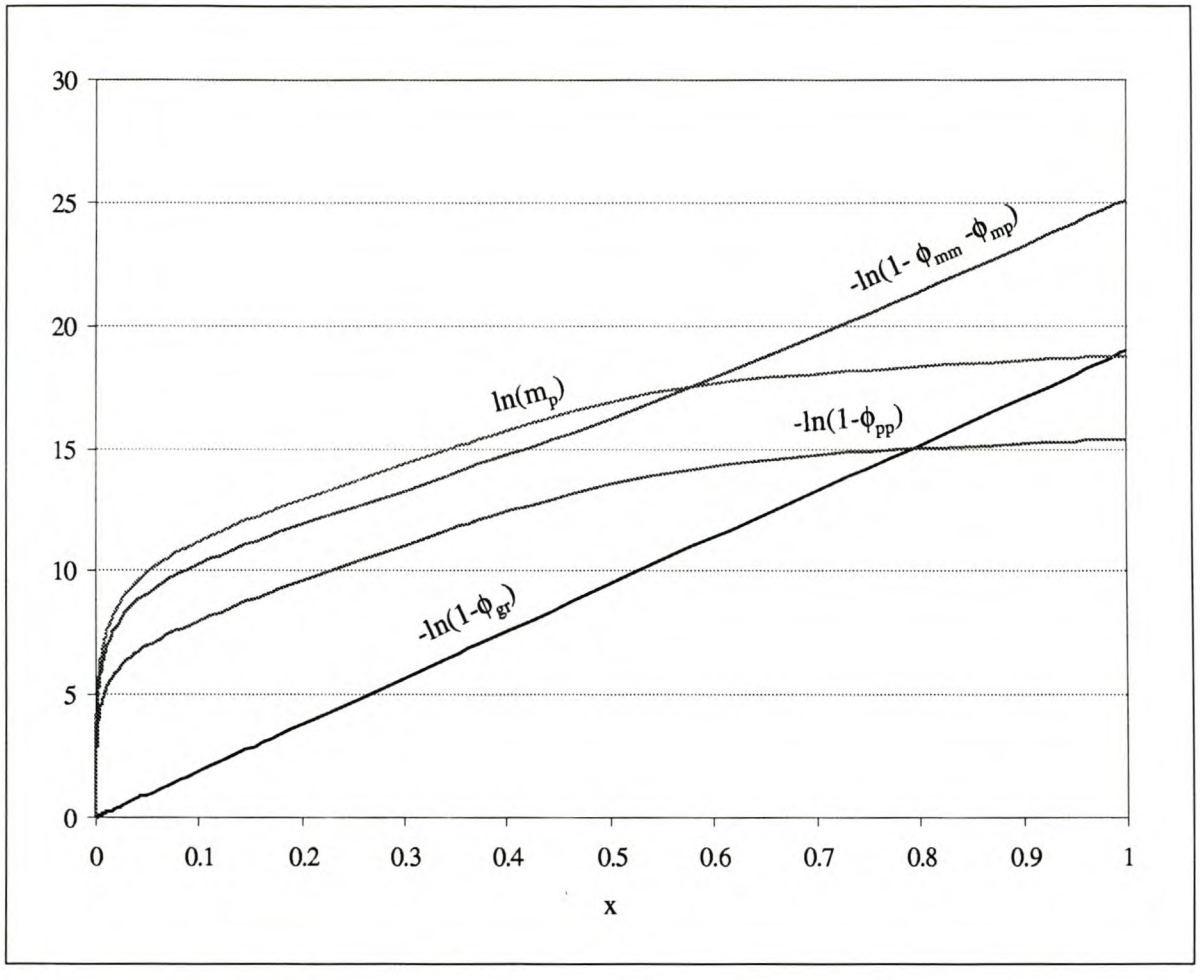

Figure 6.1: Output from Numerical Simulation ($x = \frac{t}{\tau_{res}}$, $\tau_{res} = 10\ s$)

The dependent output variables have a gradual increase with position x, except for $x < 0.05$, and are scaled between 0 and 25. This is an indication of good numerical tractability for the greatest part of the residence time of the reactor. However, because of the steep gradients for $x < 0.05$, smaller numerical intervals are required to model the initial particle formation.

Note that: $\ln(m_p) - [-\ln(1 - \phi_{pp})] \approx constant$, after $x = 0.3$. This trend is interpreted by considering equation 6.79: $\ln(m_p) = \ln\left[2\left(1 + \frac{\phi_{mp}}{\phi_{mm}}\right)\right] - \ln(1 - \phi_{pp})$. On the following page, the evolution of $\frac{\phi_{mp}}{\phi_{mm}}$ with time in the reactor is investigated, so as to determine the relationship between m_p and ϕ_{pp}.

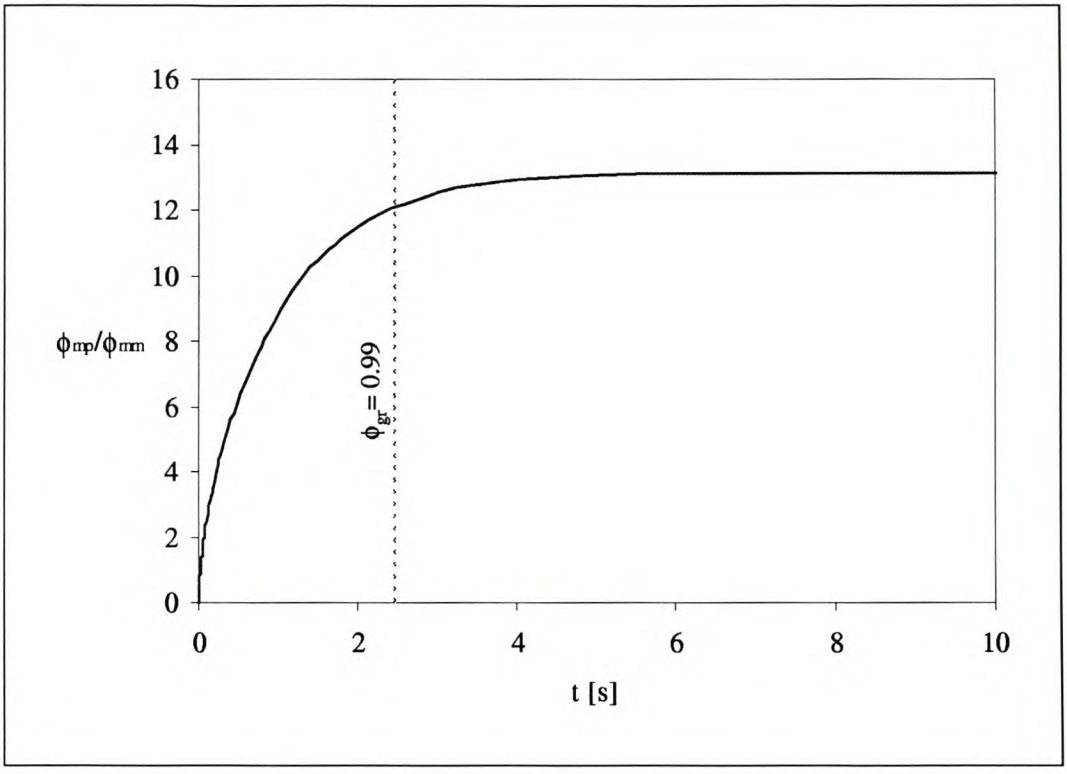

Figure 6.2: Comparison of Monomer-Monomer and Particle-Particle Conversions

Figure 6.2 shows the change of $\frac{\phi_{mp}}{\phi_{mm}}$ with time in the reactor. The increasing value of $\frac{\phi_{mp}}{\phi_{mm}}$ shows that monomers are progressively more consumed by collisions with particles, rather than by monomer-monomer collisions.

Shortly after (99%) complete gas-phase reaction conversion, $\frac{\phi_{mp}}{\phi_{mm}} \approx constant$. For $t > 3s$, equation 6.79 simplifies to: $\ln(m_p) = constant - \ln(1 - \phi_{pp})$. This explains the trend observed on the previous page. The interpretation of the trend is that after $t = 3\ s$, the evolution of particle size and concentration is determined solely by particle collisions. This type of growth is commonly referred to as *coagulation-controlled growth.*

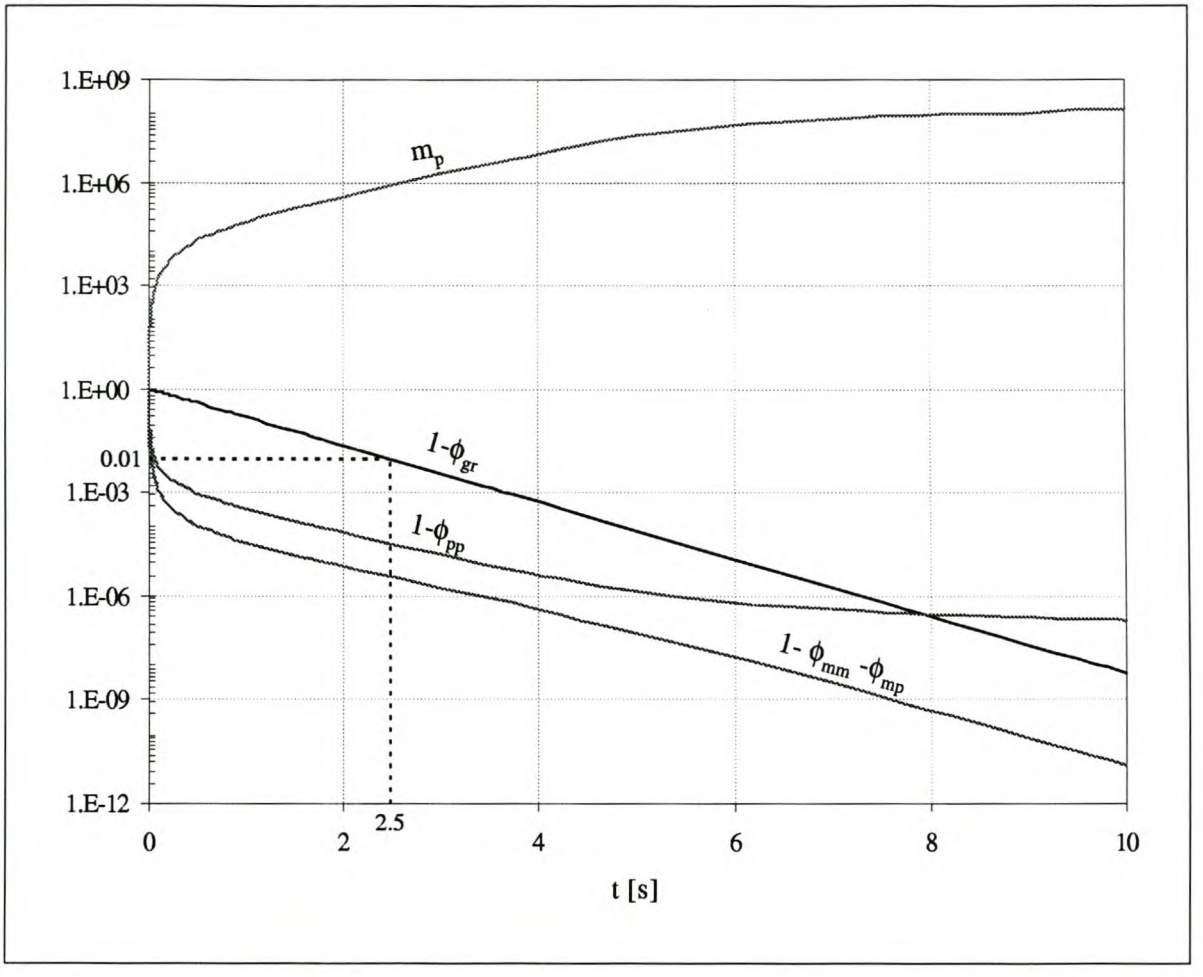

Figure 6.3: Evolution of Conversions with Residence Time

Figure 6.3 translates the output variables into a more conventional form. The independent variable is time (t). The dependent variables are the sequential reaction conversions (ϕ_i), and the particle size (m_p).

The low values of $(1 - \phi_{gr})$ and $(1 - \phi_{mm} - \phi_{mp})$ at the end of the reactor indicate that gas-phase reaction is complete, and conversion of monomers to particles is complete. Complete (99%) conversion of the gas-phase reaction is obtained at $t = 2.5\ s$.

Note the flattening out of the gradient $\frac{dm_p}{dt}$ for larger residence times. This is explained by the depletion of particle concentration by coagulation, and the associated decrease in coagulation rate (particle growth rate).

6.9 Comparison with Published Results

Experimental data is not available (in the literature) for the evolution of particle size along the whole length of the reactor, since particle measurements are only made at the reactor exit. Therefore published modelling results are used to verify that the present model gives a reasonable prediction of the evolution of particle size with time.

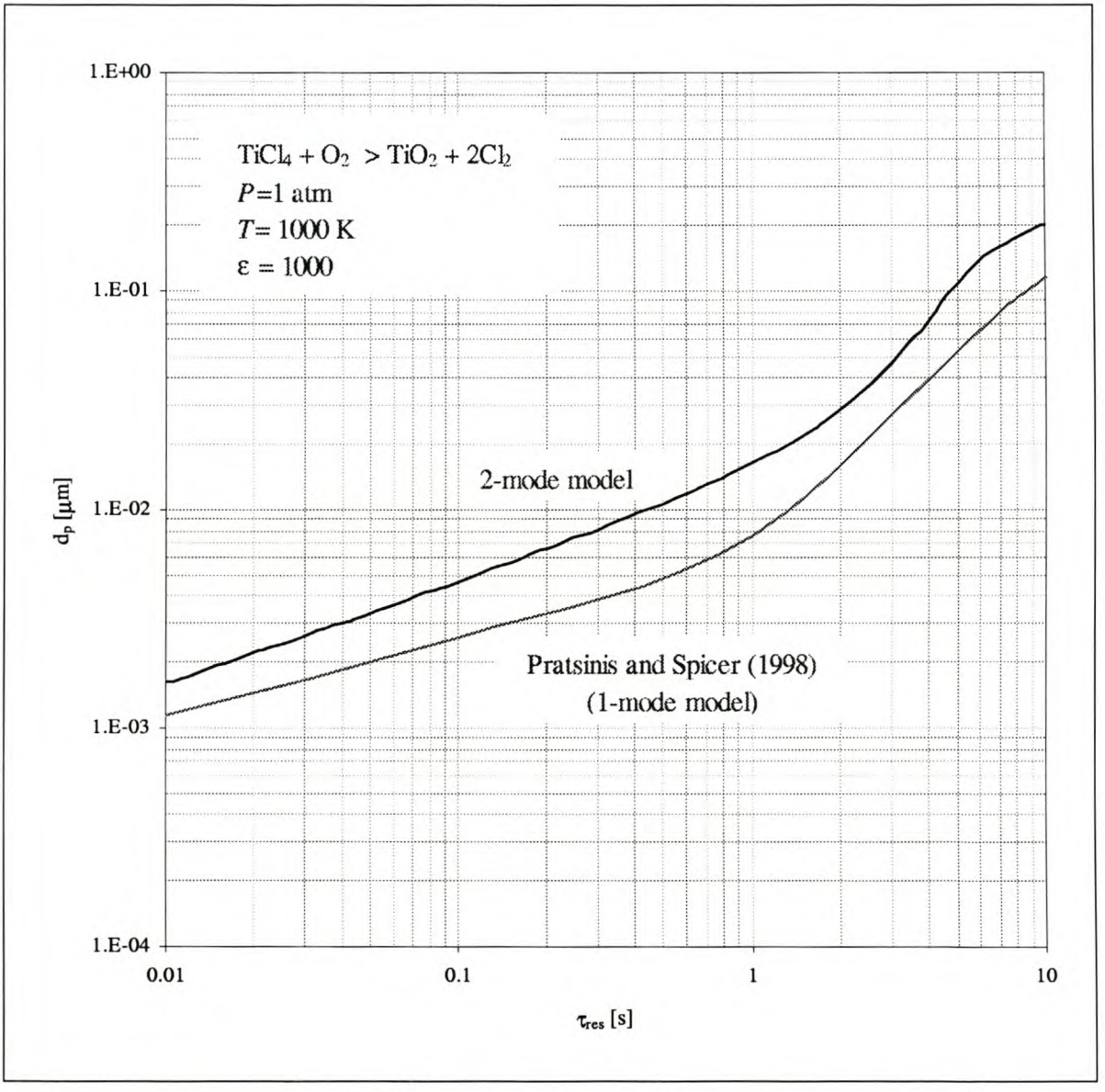

Figure 6.4: Comparison of the Results of the Present 2-Mode Model with a Published 1-Mode Model

Figure 6.4 compares the present simulation results (2-mode model) with the results of the (single-mode) model of Pratsinis and Spicer (1998), in terms of the evolution of particle diameter with residence time.

The two-mode (monomer, monodisperse particles) model in the present work predicts a higher particle size ($\sim$ 80% greater d_p at the reactor exit) than the single-mode (only monodisperse particles) model of Pratsinis and Spicer (1998). This is to be expected, since the (average) size of particles in the two-mode model is not decreased by inclusion of monomers in the calculation of particle size (as is the case for the single-mode model). There is a reasonable correlation between the trends $\left(\frac{dd_p}{dt}\right)$ predicted by the two models.

Note that the model of Pratsinis and Spicer (1998) also incorporated reactant condensation onto particles, and subsequent surface reaction. However, the authors found that surface reaction was negligible at the given conditions.

6.10 Conclusion

A one-dimensional, isothermal aerosol reactor model was developed, that represented the PSD as two modes: monomers and monodisperse particles. The model expresses the aerosol dynamics in terms of 'reaction' conversions, as is typically employed in reactor engineering. The conversions are defined in a sequential manner, analogous to the sequential nature of the different reactions: $gr \rightarrow mm/mp \rightarrow pp$. The whole model was expressed and solved in non-dimensional form.

The modelling results were verified by comparison with results of a similar model from the literature. The present model predicts higher particle sizes, because it considers monomers as a separate mode, whereas the published model considers monomers and particles together in one monodisperse mode.

The model system description (assumptions and approximations) is the same as many other models that represent the PSD as a small number of monodisperse modes [e.g. Wu et al. (1988) , Okuyama et al. (1990), Okuyama et al. (1992)]. The present model is simpler than some existing models of this type, since it neglects clusters dynamics, and does not consider radial effects (velocity profile, diffusion, wall-deposition). The present model is a simplified form of the published more complex models, and therefore it is a valuable tool for understanding the more complex models.

The novel aspect of the present model is the expression of the aerosol dynamic equations in terms of 'sequential reaction conversions'. The choice of these as output variables facilitates the interpretation of data to determine when particle growth becomes coagulation-controlled. Such definition of reactor variables may also have interpretive value in other systems with sequential reactions.

This variable definition complicates the algebraic derivation of model equations, and requires transformation of the differential equations into logarithmic form (since ϕ is scaled from 0 to 1, and some equations divide by $(1-\phi)$). The numerical solution of the resultant equations is *not* computationally intensive.

One expansion possibility of the present model is to incorporate the wall-deposition of monomers by including a constant value for fractional wall-deposition (as is suggested in section 8.4.4, equation 8.41). Another possible expansion is to add a mode for clusters smaller than a k-mer, with characteristic size and concentration. Due to the algebraic difficulty in expressing such a three-mode model in terms of sequential reaction conversions, it may be favourable to use non-sequential reaction conversions.

Part II

Modelling: Seed Growth of Spherical Ceramic Particles

Chapter 7

Description of Problem

Coagulation can produce spherical ceramic particles only up to a maximum fusible particle size, which is determined by the coalescence behaviour of small particles (see section 4.5.5). If coagulation proceeds beyond the maximum fusible size, then fractal-like agglomerates form.

For materials that melt at high temperature, large agglomerate particles in an aerosol can be coalesced by operating close to the melting point [Wu and Flagan (1987)]. However, for non-melting materials or materials that melt only at impractical temperatures (such as many ceramics are), such coalescence is not possible. Coagulation-controlled growth in an aerosol can not be used to produce large non-melting particles.

The feasibility of producing spherical ceramic particles larger than the maximum fusible size by the method of seed growth, as proposed by Zachariah and Dimitriou (1990), is theoretically analysed in the subsequent chapters.

The following **hypothesis** is made:

The method of seed growth makes it possible to grow spherical ceramic particles, with initial size smaller than the maximum fusible size, to a significantly larger size, without coagulation of the seed particles (which will yield unwanted hard agglomerates).

This hypothesis assumes that the desired product is spherical particles larger than the maximum fusible size ($d_{melt} \sim 10 - 30\,nm$ [Zachariah and Dimitriou (1990)]).

Spherical ceramic particles in the order of 1 μm are favourable precursors for bulk electronic applications that require high purity (such as producing ceramic substrates by sintering of powder). The advantages of larger particles ($d_p \sim 1\ \mu m$ *vs.* $d_p < 100\ nm$) are the ease of particle collection and handling, and the reduced risk of contamination with impurities [Alam and Flagan (1986)].

If the hypothesis is proven true, it will indicate that large ($d_p > 100 nm$) spherical ceramic particles can be produced in aerosol reactors, without expensive post-processing (milling) to break *hard* agglomerates into their constituent primary particles. (*Soft* agglomerates will inevitably be formed when the product powder is collected, but the Van der Waal's bonds in soft agglomerates is much easier to break than the bonds formed by neck growth in hard agglomerates).

The strategy employed to evaluate the hypothesis is to establish whether a reactor can be designed that satisfies all the constraints for spherical seed growth.

In chapter 8 simple mathematical analyses are employed to develop a reactor design framework for a laminar flow seed growth reactor, for the production of non-agglomerated particles. This modelling framework gives a clear description of the reactor design problem in terms of design parameters, performance criteria (objective functions) and constraints. As far as possible, mathematical descriptions are used.

In chapter 9 the effect of turbulent intensity on coagulation rates of different species is analysed. A quantitative comparison of collision coefficients is made for varying turbulent intensity. The results are interpreted to indicate whether turbulence is beneficial for spherical seed growth or not.

In chapter 10 the hypothesis of spherical seed growth is evaluated theoretically and by interpretation of published results. The reactor design framework (model of constraints) developed in chapter 8 is used to construct graphs of process constraints in terms of initial reactant concentration and seed concentration, for typical seed growth conditions. Furthermore, the specified particle growth, temperature and pressure are varied to study the effects of these parameters on the process constraints. This simple theoretical analysis is supported by interpretation of experimental data and results of more detailed modelling in the literature.

7.1 Definition of Constant Number Spherical Seed Growth

The *hypothetical method* of spherical seed growth requires preservation of the number of particles (i.e. no formation of new particles that are of comparable size to the seed particles, and no coagulation of seed particles). This method is henceforth referred to as *constant number seed growth*, and is defined by the following constraints:

- Seed particles (initially smaller than the maximum fusible particle size) are exposed to a chemically reacting vapour that produces the product ceramic. Newly formed monomers/clusters (fusible species) deposit onto and coalesce with existing seed particles, thereby facilitating spherical particle growth.
- The growth of new particles is suppressed: new particles can never grow larger than some critical size (much smaller than the seed particle size) before being scavenged by seed particles.
- There is negligible coagulation between seed particles, which would form unwanted agglomerates.

In constant number seed growth the particle size distribution is bimodal, with no overlap between the modes. The mode of larger particles is called the *seed* mode, and the mode of newly formed smaller particles is called the *cluster* mode (monomers and small n-mers). Under such conditions the number of particles (larger than the maximum cluster size) do not change, and the particle size distribution narrows [Kusters and Pratsinis (1995)].

7.2 Constraint for Suppression of Cluster Growth

The constraint that new particles (clusters) should not be able to grow larger than some critical size (much smaller than the seed particle size) before being scavenged by seed particles, is frequently referred to in the literature as *'suppression of homogeneous nucleation'* [Alam and Flagan (1986), Wu and Flagan (1987), Wu et al. (1988), Okuyama et al. (1990), Zachariah and Dimitriou (1990)]. This constraint is experimentally evaluated by counting the number of particles larger than the detection limit of the measuring instrument, which is in the order of $3 - 10\,nm$ [Okuyama et al. (1990), Zachariah and Dimitriou (1990)].

For systems with a thermodynamic barrier for nucleation, homogeneous nucleation can be suppressed by ensuring that clusters larger than the critical nucleation size (from classical nucleation theory) do not form.

In the aerosol synthesis of ceramics, the vapour pressure is typically so low that even clusters of a small number of molecules (e.g. tri-mers) are thermodynamically stable. (Classical nucleation theory cannot predict the critical nucleation size for such systems, in part because the bulk solid surface tension is not applicable to small k-mers.)

However, in conditions where clusters never grow larger than the detectable limit, clusters may possibly grow larger than the critical nucleation size [Wu and Flagan (1987)].

Cluster diffusivity decreases sharply with increasing size ($D_f \propto d^{-2}$). Therefore, if clusters grow larger than a critical size, their diffusivity become so low that they cannot be scavenged by seed particles anymore, and the clusters keep on growing by cluster coagulation (hence unconstrained cluster growth) [Wu and Flagan (1987)].

The above discussion points out that the limit on ceramic cluster size for suppression of *observable* new particle formation is *not* determined by the critical nucleation size, but rather by the (larger) critical cluster size for scavenging by seeds. Therefore this condition is described as *'constrained cluster growth'* in the present text, rather than as *'suppression of homogeneous nucleation'*.

The constraint on cluster growth has received extensive attention in the literature [Alam and Flagan (1986), Wu and Flagan (1987), Wu et al. (1988), Okuyama et al. (1990), Zachariah and Dimitriou (1990)]. It was shown that cluster growth is more effectively suppressed at lower monomer source rate, at higher seed concentration, and with larger seed size. An increasing temperature profile can 'even out' the monomer source rate (or even increase it as the seed particles becomes bigger and more effective at scavenging clusters), thereby constraining cluster growth at higher average monomer source rates (i.e. higher growth rates).

The constraint of negligible seed coagulation, on the other hand, has received little attention in the literature.

Chapter 8

Reactor Design Framework for Constant Number Seed Growth

Published experimental results for seed growth of ceramics (see section 3.4.1) indicate that the reactor design and optimisation problem is multi-dimensional. Multiple design parameters (such as initial reactant concentration, seed concentration and temperature profile) need to be considered to compare different reactor designs, and multiple performance indices (such as yield, reactor volume and heating requirements) need to be evaluated.

This chapter strives to develop a simple framework for the comparison of different seed growth reactor designs. In the present study, this framework is used only to evaluate the hypothesis on spherical seed growth (chapter 10), by assessing whether a reactor can be designed that satisfies all the constraints of constant number seed growth. Future extension of the modelling framework may allow process optimisation for seed growth in general (i.e. not limited to the hypothetical method of constant number spherical seed growth).

A *simplified model system* is defined to represent the characteristics of constant number seed growth, and all the quantities relating to the system are classified. In the present study, the model system (and the resulting reactor design framework) is *limited to isobaric and isothermal conditions*, since comparison of different process conditions is complicated by temperature and pressure profiles.

Yet, as indicated earlier, temperature profile is an important design parameter for seed growth. The extension of the current model system to incorporate temperature profiles will be a major consideration in future development of the reactor design framework.

The model system is further limited by neglecting seed growth in conditions where new particle formation is *not* suppressed (i.e. only *constant number* seed growth is considered). For a fixed temperature profile and initial reactant concentration, more growth per particle may (or may not) be obtained by lowering the seed particle concentration to such an extent that new particle formation is not suppressed anymore (see section 3.4.1).

Having clearly stated which design parameters are not considered for this first attempt on a reactor design framework, the remaining design parameters are evaluated. These are determined by performing an *independence analysis on process parameters.* Seed and product particle sizes are considered as fixed parameters, so as to ensure that *different reactor designs will be compared for the same specifications of precursor and product.* Suitable performance criteria relating to yield losses and growth rate are defined. The set of design parameters is reduced further by decoupling the problem from production rate.

The constraints for constant number seed growth, as well as some more general reactor design constraints, are derived in mathematical form. A simple reactor design model for estimating the required residence time is developed, so as to be able to evaluate constraints which are dependent on residence time.

8.1 Description of Model System

To develop a reactor design framework, a simplified representation (model) of the process is first defined. The *model system* is defined according to the following assumptions and approximations:

8.1.1 Assumptions and Approximations

1. Fully developed (hydrodynamically) laminar flow (see section 8.3.4).
2. Isothermal reactor.
3. Isobaric reactor (negligible pressure drop because of friction).
4. Steady-state conditions.
5. Conservation of number of seed particles (negligible wall-deposition and coagulation of seed particles, no new particle formation). The assumption of negligible wall-deposition of seed particles is based on the low diffusivity of the relatively large particles.
6. No reactant is deposited on the reactor walls (temperature is higher than evaporation temperature of reactant).
7. First-order reaction kinetics, and stoichiometric ratio between limiting reactant and product is unity.
8. Very dilute limiting reactant, by using a large excess of non-limiting reactant and possible also diluent inert gas.
9. Axial mass diffusion is negligible compared to convection.

Comparison of process conditions for different temperature and pressure profiles will be complex. Therefore, since the present work tries to establish a simple reactor design framework, isothermal and isobaric conditions are assumed.

The assumption of negligible axial diffusion is based on the criterion of having a narrow residence time distribution (RTD), so as to obtain a narrow particle size distribution. The reactor design should ensure that the RTD is not significantly broadened by axial diffusion, which implies that there will be a lower limit on velocity of flow.

8.1.2 Phenomena in the Model System

The following phenomena take place in the model system:

1. Monomer formation
2. Cluster formation and growth (by coagulation)
3. Monomer/cluster deposition onto seed particles
4. Monomer/cluster deposition onto reactor wall
5. Radial diffusion (of mass)
6. Axial convection (of mass)

None of the other phenomena are influenced by the rate of axial convection (velocity of flow). These other phenomena are dependent on the radial residence time distribution (RTD) only. The RTD, in turn, is dependent on the average residence time and the reactor diameter only, for fully developed laminar flow (see page 111, equation 8.1). For a fixed residence time ($\bar{\tau}_{res}$), the flow velocity ($\bar{u}$) may be scaled (with corresponding scaling of reactor length: $L = \bar{u}\bar{\tau}_{res}$), without any change in the RTD, as long as the flow is still laminar. The de-coupling of the reactor design problem from velocity is discussed on page 111.

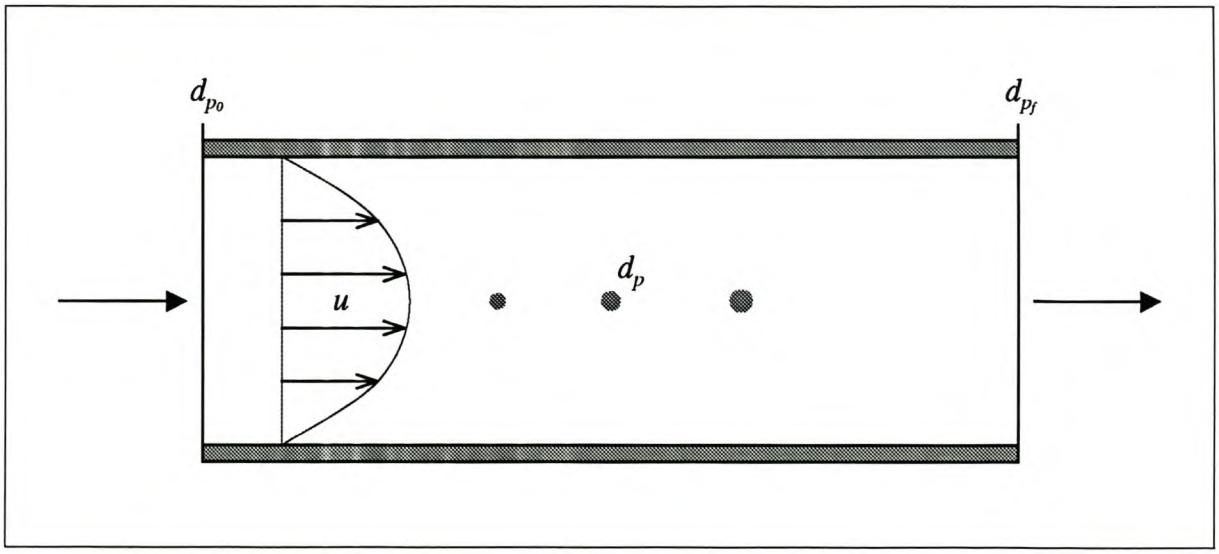

Figure 8.1: Geometry of the Model System

8.1.3 Geometry of the Model System

Figure 8.1 illustrates the increase in particle size with reactor position, as well as the bounds of the reactor in terms of initial (seed) particle size (d_{p_0}) and the required product particle size (d_{p_f}). The parabolic velocity profile for fully developed laminar flow is also shown.

8.2 Quantity Analysis for the Reactor Design Problem

All the quantities of relevance in the model system are classified to differentiate between variables, parameters and constants. Figure 8.2 summarises the classification of quantities. A detailed description and tables of different classes of quantities are given in appendix D.

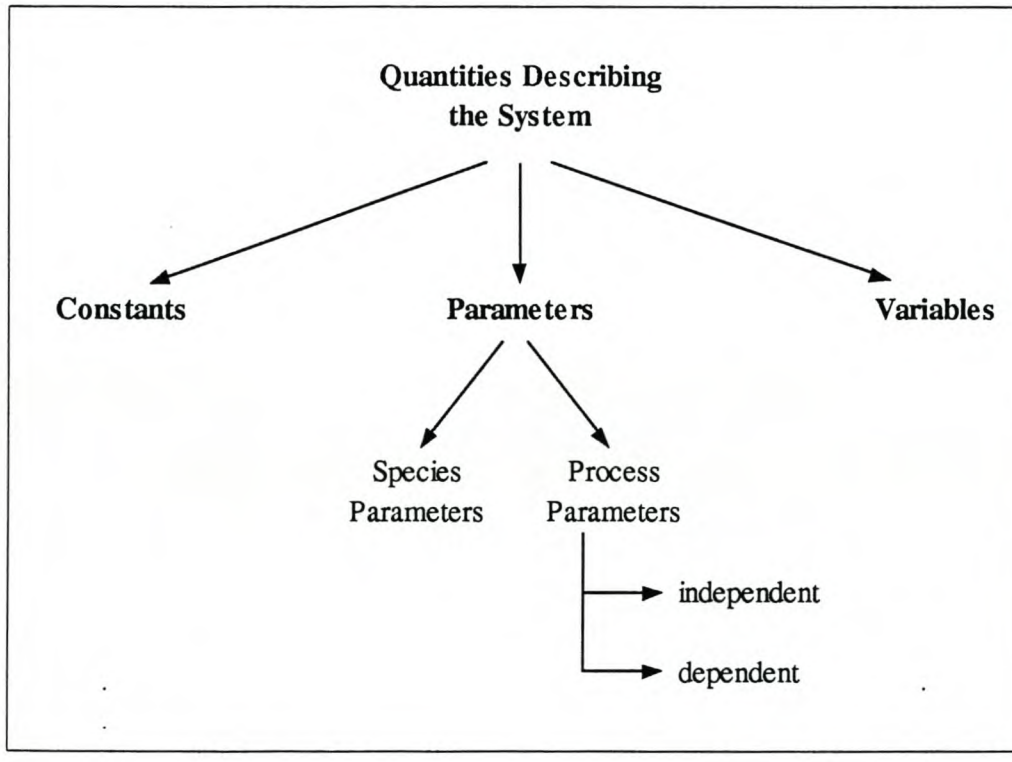

Figure 8.2: Classification of Quantities Describing the System

- Quantities pertaining to the properties of the material in the system are labelled as *species parameters*, e.g. the molecular weight of the product.
- For specified species, the set of quantities that gives a complete description of the reactor design are labelled as *process parameters*.
- The quantities that vary with position in the reactor are labelled as *variables*.

8.2.1 Independent Set of Process Parameters

A set of mutually independent process parameters is derived in appendix D. These are listed in table 8.1. Comparison of experimental/modelling results for different process conditions should be done in terms of the independent process parameters only. This will ensure a comparison without convolution of inter-dependent parameters.

It is necessary to compare different reactor designs for the same initial (seed) particle size and final (product) particle size. Hence both the seed and product particle sizes are considered as process parameters.

$P\ [N/m^2]$	reactor pressure
$T\ [K]$	reactor temperature
$C_0\ [mol/m^3]$	initial reactant concentration
$M_{pr}\ [t/a]$	production rate
$D\ [m]$	reactor diameter
$n_p[\#/m^3]$	seed particle concentration
d_{p0} [m]	initial (seed) particle size
σ_{g_s}	geometric standard deviation of the seed particle size
d_{p_f} [m]	final (product) particle size

Table 8.1: Independent Process Parameters

8.2.2 Variables: Product Requirement and Performance Indices

Quantities that change with position in the reactor are called variables. With a suitable reactor model, the values, at the end of the reactor, of all the variables may be expressed as functions of the independent process parameters. Hence, the set of independent process parameters completely characterises the reactor design (for predetermined species).

The end of the reactor is defined as that point at which the particle size is equal to the required product particle size (d_{p_f}). In a numerical solution of reactor model equations, the reactor length (or residence time) will be incremented until the required (average) product particle size is obtained.

The following values of variables at the end of the reactor are used in calculating the performance indices:

- τ_{res} [s] is the (average) residence time to give the required particle growth: $\Delta m_p = \frac{\pi}{6v_m}(d_{p_f}^3 - d_{p0}^3)$ $[\#_m/\#_p]$, where $d_{p_f} = d_{p_f}(\tau_{res})$.
- W_{dep_f} $[\#/m^3]$ is the average wall-deposition per volume of gas passing through the reactor, from $t = 0$ to $t = \tau_{res}$.
- C_f $[mol/m^3]$ is the reactant concentration at $t = \tau_{res}$.
  For first-order reaction: $C_f = C_0(1 - e^{-k\tau_{res}})$.
- n_{c_f} $[\#/m^3]$ is the cluster concentration at $t = \tau_{res}$.
- m_{c_f} $[\#_m/\#_c]$ is the mass-average cluster size at $t = \tau_{res}$.
- σ_{g_f} is the geometric standard deviation of the particle size, at $t = \tau_{res}$.

The following **performance indices** are proposed:

- Production rate per volume:
$$\frac{n_p}{\tau_{res}} \quad \left[\frac{\#}{m^3 \cdot s}\right]$$
- Yield loss to wall-deposition:
$$\frac{W_{dep_f}}{n_p \Delta m_p}$$
- Yield loss to incomplete reaction:
$$\frac{C_f A_v}{n_p \Delta m_p}$$
- Yield loss to undeposited clusters:
$$\frac{n_{c_f} m_{c_f}}{n_p \Delta m_p}$$
- Geometric standard deviation of the particle size: σ_{g_f}

These five performance indices can be used to compare different reactor designs. The indices may be combined into a cost function for optimisation, but this falls beyond the scope of the present study.

Note that the three yield losses are expressed in non-dimensional form, by scaling with the production rate.

8.2.3 Reducing the Number of Design Parameters for Process Comparison

For pre-defined species, the reactor design of the model system is completely described by the seven independent process parameters in table 8.1. These are also called the *design parameters*. The number of design parameters can be reduced by the following arguments, thereby facilitating simpler comparison of different reactor designs.

Fixed Parameters for Seed and Product Particles

The initial seed particle size (d_{p_0}) is determined by the seed manufacturing process, and the product particle size (d_{p_f}) is specified by the product application. Therefore, these two sizes are treated as constants for comparison of different seed growth reactor designs.

Furthermore, it is reasonable to assume that the seed particles have a self-preserving size distribution for coagulation-controlled growth: $\sigma_g = 1.45$.

De-Coupling of Reactor Design from Production Rate

Production rate and reactor length are both proportional to flow velocity. These three parameters (M_{pr}, L and u) are interchangeable in the set of independent process parameters (table 8.1): any one of them may be considered as an independent parameter, and then the other two will be dependent parameters.

If hydrodynamically fully developed laminar flow is assumed (see justification in section 8.3.4), i.e. a parabolic velocity profile, then the residence time distribution (RTD) is a function of the average residence time and of radial position:

$$\tau_{res}(r) = \left(\frac{L}{\bar{u}}\right) \frac{1}{2[1-(r/r_0)^2]} = \bar{\tau}_{res} \frac{1}{2[1-(r/r_0)^2]} \tag{8.1}$$

For a fixed $\bar{\tau}_{res}$, the residence time distribution of laminar flow is not a function of velocity. Hence, for the same $D(= 2r_0)$ and $\bar{\tau}_{res}$, u may be scaled (implicity also scaling M_{pr} and L), without changing the residence time distribution. Furthermore, all the phenomena taking place in the reactor (monomer formation, deposition on seed particles and deposition on walls) are not affected by velocity (assuming that the flow remains laminar).

Therefore, if only the parameter $M_{pr}$is changed, then the required τ_{res} and wall-deposition will not change, subject to the constraint of laminar flow.

Production rate may be scaled by adjusting the flow velocity, subject to the following constraints on the flow velocity:

- The *upper limit* is set by the constraint of *laminar flow*. Too fast flow will result in turbulence, which will spread out the RTD, and hence will spread out the PSD. An expression for the laminar flow constraint is developed in appendix E.
- The *lower limit* is set by the constraint of *negligible turbulent entry region* or by the constraint of *negligible axial diffusion*, whichever of the constraints imposes the highest lower limit.
  - It was noted in section 3.2.1 that *turbulent reactant mixing* in a tube which is narrower than the reactor is often used. This implies that the gas enters the reactor through a small orifice (compared with the larger reactor diameter), and therefore the entry region of the reactor will be turbulent [Kusters and Pratsinis (1995)]. This turbulent entry region should be short compared with the total reactor length, to avoid spreading out of the PSD. Too slow flow will require too short a reactor length, compared with the length of the turbulent entry region.
  - The constraint of *negligible axial diffusion*, to ensure that the RTD is not spread out by diffusion, was discussed in section 8.1.1.

The production rate may be scaled by using a number of parallel reactors (i.e. a modular design). This will allow a lower Re (and laminar flow) for each reactor, than if the total production rate was delivered by a single reactor with the same diameter.

Reduced Set of Design Parameters

The remaining design parameters are listed in table 8.2.

P $[N/m^2]$	reactor pressure
T $[K]$	reactor temperature
D $[m]$	reactor diameter
C_0 $[mol/m^3]$	initial reactant concentration
n_p $[\#/m^3]$	seed particle concentration

Table 8.2: Reduced Set of Design Parameters

8.3 Constraints

The reactor design constraints for constant number seed growth are presented here in simple functional forms. Some of these constraints may be expressed more accurately by more complex modelling, or by experimentally determined (empirical) expressions.

The effect of reactor diameter (D) will not be investigated, for the following reason: Some of the constraints are dependent on the residence time (τ_{res}) required for growth up to the specified product particle size. Therefore a simple reactor design model is proposed to estimate τ_{res} (section 8.4), so as to be able to evaluate the constraints. This reactor design model assumes that the fractional loss to wall-deposition (W/S) is a constant, and the actual dependence of wall-deposition on D is not incorporated (a possible extension of the model to incorporate this is suggested).

In chapter 10 the constraints will be used to plot the allowable region of reactor designs in terms of the design parameters specified in table 8.2.

In the following derivation of constraint equations, each constraint is finally written in terms of C_0 and n_p, so as to have a convenient format for the plotting of constraints in chapter 10. Also, it is pointed out if a constraint is not a function of D, assuming that the fractional loss to wall-deposition is a constant (i.e. the dependence of wall-deposition on diameter is not indicated).

8.3.1 Reaction Conversion

The *upper limit* of n_p corresponds to having just enough reactant for the required particle growth (d_{p_f}), i.e. complete reaction and consumption of monomers.

The simple reactor design model in section 8.4 defines the maximum particle growth that can be attained for a specified C_0 and n_p (equation 8.53). Rearrangement of this equation expresses the constraint in terms of n_p:

$$n_p < C_0 A_v \frac{6v_1}{\pi(d_{p_f}^3 - d_{p_0}^3)\left(1 + \left(\frac{W}{S}\right)\right)} \neq f(D) \tag{8.2}$$

8.3.2 Constrained Cluster Growth

The growth mechanism can be evaluated by applying the criterion for constant number seed particle growth of Zachariah and Dimitriou (1990) (they called it 'suppression of homogeneous nucleation', see section 4.5.7). This criterion is stated in different form here, and therefore the derivation, which is analogous to that of Zachariah and Dimitriou (1990), is also shown.

Consider a system in which monomers are consumed only by monomer-monomer and monomer-seed collisions (i.e. monomer-cluster and monomer-wall collisions are neglected), and monomer concentration is constant. (This *model system* is a simpler 'subset' of the model system defined in section 8.1. Here, the additional assumptions of constant monomer concentration and negligible wall-deposition are employed, and cluster dynamics are neglected.)

The monomer balance at steady state can be written as:

$$\text{MONOMER FORMATION} = \text{MONOMER CONSUMPTION} \tag{8.3}$$

$$r_m A_v = k A_v C = \beta_{m,p} n_m n_p + 2\beta_{m,m} n_m^2 \left[\frac{\#}{m^3 \cdot s}\right] \tag{8.4}$$

Let f be the minimum ratio between monomer consumption by monomer-particle collisions and monomer consumption by monomer-monomer collisions, to ensure constrained cluster growth. This is identical to the definition of f by Zachariah and Dimitriou (1990).

$$f \leq \frac{\beta_{m,p} n_m n_p}{2\beta_{m,m} n_m^2} \tag{8.5}$$

$$n_m \leq \frac{\beta_{m,p} n_p}{2 f \beta_{m,m}} \tag{8.6}$$

Substitution of equation 8.6 into equation 8.4 allows elimination of monomer number concentration from the monomer balance equation:

$$k A_v C \leq \frac{\beta_{m,p}^2 n_p^2}{2 f \beta_{mm}} + \frac{\beta_{m,p}^2 n_p^2}{2 f^2 \beta_{mm}} \tag{8.7}$$

For constrained cluster growth, f should be much larger than 1, and therefore the second term of equation 8.7 can be neglected. Using this approximation, equation 8.7 is converted to a simple expression for the minimum seed particle concentration required to constrain cluster growth:

$$n_p \geq \frac{(2 f \beta_{m,m} k A_v C)^{\frac{1}{2}}}{\beta_{m,p}} \tag{8.8}$$

Expressing the Cluster Growth Constraint in Dimensions C_0 and n_p

Cluster formation is the most prominent at the start of the reactor, where the reactant concentration (and reaction rate) is the highest. Therefore the constraint on cluster growth (equation 8.8) is espressed for $C = C_0$:

$$n_p \geq \frac{(2 f \beta_{m,m} k A_v C_0)^{\frac{1}{2}}}{\beta_{m,p}} \neq f(D) \tag{8.9}$$

8.3.3 Negligible Seed Coagulation

The fraction of seed particles that undergo coagulation during the residence time should be small. As a first approximation, this constraint is written for the average residence time (the effect of the residence time distribution is neglected). Assuming that the fraction of seed particles that undergo coagulation is very small, this small fraction can be estimated as:

$$\frac{2r_{p,p}\bar{\tau}_{res}}{n_p} \leq \epsilon_{sc} \ , \ 0 < \epsilon_{sc} \ll 1 \tag{8.10}$$

$$2\bar{\beta}_{p,p}n_p\bar{\tau}_{res} \leq \epsilon_{sc} \tag{8.11}$$

Particle size affects the collision frequency, and therefore an average particle size should be used to calculate $\bar{\beta}_{p,p}$, for evaluation of the constraint equation 8.11. This average particle size should be between the initial seed particle size (d_{p_0}) and the final product particle size (d_{p_f}).

As a first approximation, the surface-average diameter is used to calculate the average collision coefficient:

$$\bar{\beta}_{p,p} = \beta_{p,p}(\bar{d}_p) \tag{8.12}$$

$$\bar{d}_p = \left(\frac{d_{p_0}^2 + d_{p_f}^2}{2}\right)^{\frac{1}{2}} \tag{8.13}$$

Expressing the Seed Coagulation Constraint in Dimensions C_0 and n_p

The constraint for negligible seed coagulation (equation 8.11) can be expressed as:

$$n_p \leq \mathrm{f}_{\mathrm{coag}}(C_0) = \frac{\epsilon_{sc}}{2\bar{\beta}_{p,p}\bar{\tau}_{res}(C_0, n_p)} \neq f(D) \tag{8.14}$$

- $\bar{\beta}_{p,p}$ is not a function of C_0 or n_p.
- $\bar{\tau}_{res}$ increases with n_p (more monomer formation is required for the same growth per particle), and decreases with C_0 (higher monomer formation rate).

Therefore:

$$\frac{\mathrm{d}f_{coag}}{\mathrm{d}C_0} > 0 \tag{8.15}$$

8.3.4 Thermodynamic Entry Length

It is necessary that the reactant mixture is fully heated (up to the radial centre of the reactor) in a short part of the reactor, so as to obtain homogeneous reaction and small temperature gradients, thereby ensuring a narrow PSD. This requirement implies that the thermodynamic entry-length for fully developed laminar flow (length after which the thermal boundary layer radially converges) should be a small percentage of the reactor length:

$$\frac{x_{fd,t}}{L} \leq \epsilon_{te} \ , \ 0 < \epsilon_{te} \ll 1 \tag{8.16}$$

$$L = u\tau_{res} \tag{8.17}$$

Incropera and De Witt (1990) give the following expression for the thermodynamic entry length for fully developed laminar flow in circular tubes:

$$x_{fd,t} \approx 0.05 RePrD \ [m] \tag{8.18}$$

The constraint equation 8.16 can be expressed as a function of residence time and Prandtl number by combination with equations 8.17 and 8.18:

$$\frac{x_{fd,t}}{L} = \frac{0.05 RePrD}{u\tau_{res}} \leq \epsilon_{te} \ , \ 0 < \epsilon_{te} \ll 1 \tag{8.19}$$

$$= 0.05 \left(\frac{\rho u D}{\mu}\right)\left(\frac{PrD}{u\tau_{res}}\right) \tag{8.20}$$

The *thermodynamic entry length constraint* is:

$$D < \left[20\epsilon_{te}\tau_{res}\left(\frac{\mu}{\rho Pr}\right)\right]^{\frac{1}{2}} \tag{8.21}$$

Note that the thermodynamic entry length constraint is the only constraint that depends on D, assuming that (W/S) is a constant.

The Prandtl number for typical inert and oxidant gases (air/O_2/N_2) has small temperature dependence. The Prantl number for these gases is bracketed by the following limits, for temperatures from 500 to 1500 K (typical temperatures for aerosol synthesis of ceramics):

$$0.68 \leq Pr \leq 0.75 \tag{8.22}$$

(The data were obtained from the material properties tables of Incropera and De Witt (1990).)

Example of Analysis of Heat Transfer from Reactor Walls

The use of the thermodynamic entry length calculations is illustrated by an example from the literature:

Alam and Flagan (1986) used a reactor consisting of 5 separately heated sections with increasing temperatures. They reported that their reactor had a low enough Peclet number ($Pe = RePr \leq 30$) so that the gas temperature was very close to the wall temperature throughout the reactor. This justified their use of the measured wall temperatures to characterise the gas temperature profile.

The reactor diameter was $9.5mm$ and the length of each section was $50mm$. Substituting these values into equation 8.18 gives $\frac{x_{fd,t}}{L} < 0.3$. Hence for each section, the thermodynamic entry length was less than 30% of the total section length.

Hydrodynamically Fully Developed Flow

Substitution of the limits of the Prandtl number (equation 8.22) into equation 8.18, indicates that the *hydrodynamic entry length for fully developed laminar flow* is smaller than the thermodynamic entry length:

$$x_{fd,h} \approx 0.05ReD < x_{fd,t} \tag{8.23}$$

The specified constraint is that the thermodynamic entry length should be much smaller than the reactor length, and equation 8.23 shows that the hydrodynamic entry length will be even smaller. Therefore the *flow will be hydrodynamically fully developed*, and the residence time distribution will correspond to the parabolic velocity profile of fully developed laminar flow.

Expressing the Entry Length Constraint in Dimensions C_0 and n_p

The dependence of equation 8.21 on C_0 and n_p is that τ_{res} increases with n_p and decreases with C_0. Therefore the thermodynamic entry length constraint can be expressed as:

$$n_p > \mathrm{f}_{\mathrm{entry}}(C_0, n_p, D) \tag{8.24}$$

$$\frac{\mathrm{d}f_{entry}}{\mathrm{d}C_0} > 0 \tag{8.25}$$

8.3.5 Stoichiometric Limit on C_0

The *upper limit* of C_0 is set by the stoichiometric reactant concentration, i.e. no excess gas. This can be expressed by combining equations D.2 and D.5 in appendix D, and setting $\varepsilon = 0$ (no excess gas):

$$C_0 < \left(\frac{P}{k_B A_v T}\right) \frac{\alpha_M}{\alpha_M + \alpha_O} \neq f(n_p, D) \tag{8.26}$$

8.4 Simple Reactor Design Model

A simple reactor design model for estimating the required residence time is developed, so as to be able to evaluate the constraints for negligible seed coagulation and thermodynamic entry length (which are both dependent on residence time).

To derive these expressions, a simple model system is considered. The assumptions and approximations that are specified in section 8.1.1 are used, as well as some additional assumptions/approximations.

8.4.1 Additional Assumptions/Approximations

- The monomer-particle collision rate is approximated with a constant (average) value of the collision coefficient.
- The particle population is represented by two monodisperse modes: monomers and seed particles. The formation of dimers and larger clusters, and the deposition of such clusters onto seeds and the reactor wall, are neglected. Monomers are assumed to be representative of clusters, as they are likely to have the highest concentration of all n-mer clusters, and they are the most likely to diffuse to seeds or to the reactor wall.
- Fractional wall-deposition is a constant.

8.4.2 Reactant Balance at Steady State

The reactant balance is simply expressed according to reaction rate. The resultant differential equation is solved to determine the reactant concentration (C) as a function of time spent in the reactor (t), and employing the initial condition $C|_{t=0} = C_0$:

$$\frac{\mathrm{d}C}{\mathrm{d}t} = -kC \tag{8.27}$$

$$C = C_0 e^{-kt} \tag{8.28}$$

8.4.3 Monomer Balance at Steady State

$$0 = -(\text{CONVECTION}) + (\text{SEED GROWTH}) - (\text{WALL DEPOSITION})$$

$$= \frac{\pi}{4} D^2 u \left(-\frac{\mathrm{d}C_m}{\mathrm{d}V}\right) + r_m - r_{m,p}/A_v \left[1 + \left(\frac{W}{S}\right)\right] \quad \frac{mol}{m^3 \cdot s} \tag{8.29}$$

$$= -\frac{\mathrm{d}C_m}{\mathrm{d}t} + kC - \beta_{m,p} C_m n_p \left[1 + \left(\frac{W}{S}\right)\right] \tag{8.30}$$

Assuming Constant Collision Coefficient

The monomer balance (equation 8.30) can be written as a first-order linear differential equation, by assuming that the collision rate coefficient $\beta_{m,p}$ is constant throughout the reactor. Thereby an analytical solution of the monomer concentration can be obtained.

An average value $\bar{\beta}_{m,p}$ is defined, which should lie between the values of $\beta_{m,p}$ at the reactor entrance and exit. To derive a simple expression for $\bar{\beta}_{m,p}$, the kinetic theory approximation of collisions is employed (see the justification in appendix F). Equation F.17 indicates that $\beta_{m,p} \propto d_p^2$, and therefore $\bar{\beta}_{m,p}$ is calculated by using the surface-average particle diameter ($\bar{d}_p$):

$$\bar{d}_p = \left(\frac{d_{p0}^2 + d_{pf}^2}{2}\right)^{\frac{1}{2}} \tag{8.31}$$

$$\bar{\beta}_{m,p} = \beta_{m,p}(\bar{d}_p) \tag{8.32}$$

Analytical Solution of Differential Equation

Equation 8.30 can now be written as a first-order linear differential equation:

$$\frac{\mathrm{d}C_m}{\mathrm{d}t} + \alpha C_m = f(t) \tag{8.33}$$

$$\alpha = \bar{\beta}_{m,p} n_p \left[1 + \left(\frac{W}{S}\right)\right] \tag{8.34}$$

$$f(t) = kC = kC_0 e^{-kt} \tag{8.35}$$

Integration by the method of an integrating factor is used to solve for the monomer concentration (C_m), with the initial condition $C_m|_{t=0} = 0$:

$$C_m = \frac{kC_0}{(\alpha - k)}\left[e^{-kt} - e^{-\alpha t}\right] \tag{8.36}$$

$$= \frac{kC_0 e^{-kt}}{(\alpha - k)}\left[1 - e^{-(\alpha - k)t}\right] \tag{8.37}$$

For the special case of $\alpha = k$:

$$C_m = kC_0te^{-kt} = ktC \tag{8.38}$$

8.4.4 Mass Balance Over Total Reactor Volume, at Steady State

$$0 = IN_{reactant} - OUT_{unreacted} - OUT_{monomer} - OUT_{seed\ growth} - DEP_{wall} \tag{8.39}$$

$$= C_0 - C_f - C_{m_f} - \frac{n_p}{A_v}(m_{p_f} - m_{p_0})\left[1 + \left(\frac{W}{S}\right)\right] \tag{8.40}$$

Constant Wall-to-Seed Deposition Ratio

The ratio between monomers deposited on the reactor wall and monomers deposited onto seed particles is evaluated for the simple model system. One of the process constraints is that cluster growth (i.e. coagulation of monomers that are not deposited on the wall or onto seeds) should be limited. Therefore it is reasonable to assume that the average time for a monomer to be deposited is much less than the reactor residence time. This implies that the ratio between monomers deposited on the reactor wall and monomers deposited onto seed particles is approximately equal to the probability that a monomer will diffuse to the reactor wall before it diffuses to a seed particle.

Let $P(r)$ be the probability that a monomer at radial position r will diffuse to the wall. The overall probability, for the whole radial distribution of monomers, is expressed by assuming that monomer formation is radially homogeneous, i.e. the radial distribution of monomers is homogeneous.

$$\left(\frac{W}{S}\right) = \frac{1}{\pi r^2}\int_0^{r_0} 2\pi r P(r)\mathrm{d}r = f(n_p, d_p, D, T, P) \tag{8.41}$$

Note that the wall-to-seed deposition ratio, for the simple model system, is not dependent on residence time in the reactor. Therefore $\left(\frac{W}{S}\right)$ is a constant in equation 8.40.

Note further that $\left(\frac{W}{S}\right)$ is not a function of monomer concentration or formation rate. $\left(\frac{W}{S}\right)$ decreases with increasing seed particle concentration and/or size (because of the larger available seed surface area), and decreases with increasing reactor diameter (D).

The present work suggests, but does not pursue, the *a priori* calculation of $\left(\frac{W}{S}\right)$ by deriving an expression for the probability that a monomer will diffuse to the reactor wall before it diffuses to a seed particle.

Deriving a Set of Equations Describing the Residence Time

In analogy to the linear dependence between C_m and C exhibited by the special case of $\alpha = k$ (see equation 8.38), C_{m_f} is expressed as a simple function of C_f:

$$C_{m_f} = \beta C_f \tag{8.42}$$

where β is a function of residence time (see equation 8.45).

An expression for β is derived by combining equations 8.28, 8.37 and 8.42:

$$C_{m_f} = \frac{kC_0 e^{-k\tau_{res}}}{(\alpha - k)}\left[1 - e^{-(\alpha-k)\tau_{res}}\right] \tag{8.43}$$

$$= \beta C_f = \beta C_0 e^{-k\tau_{res}} \tag{8.44}$$

$$\beta = \frac{k}{(\alpha - k)}\left[1 - e^{-(\alpha-k)\tau_{res}}\right] \tag{8.45}$$

For the special case of $\alpha = k$, β is given by combination of equations 8.38 and 8.42:

$$\beta = k\tau_{res} \tag{8.46}$$

The relationship between m_p and d_p is:

$$m_p v_1 = \frac{\pi d_p^3}{6}\ [m^3] \tag{8.47}$$

$$m_p = \frac{\pi d_p^3}{6 v_1} \tag{8.48}$$

An expression for the residence time is derived by substitution of equations 8.28, 8.42 and 8.48 into equation 8.40:

$$C_f = \left[C_0 - \frac{n_p}{A_v} \cdot \frac{\pi}{6v_1}(d_{p_f}^3 - d_{p_0}^3)\left(1 + \left(\frac{W}{S}\right)\right)\right] \frac{1}{(1+\beta)} \tag{8.49}$$

$$= C_0 e^{-k\tau_{res}} \tag{8.50}$$

$$\tau_{res} = -\frac{1}{k} \ln \left[\frac{1 - \frac{n_p}{A_v C_0} \cdot \frac{\pi}{6v_1}(d_{p_f}^3 - d_{p_0}^3)\left(1 + \left(\frac{W}{S}\right)\right)}{1+\beta}\right] \tag{8.51}$$

Iterative Solution of Residence Time

The system is described by two independent equations, equations 8.45 and 8.51, both containing β and τ_{res}. For the special case of $\alpha = k$, equation 8.46 is used instead of equation 8.45. An iterative procedure will be used to re-calculate β and τ_{res} until convergence is obtained. For each iteration, the residence time calculated with the previous iteration is used to calculate β (with equation 8.45 or 8.46), which is in turn used to calculate the new value of τ_{res} (with equation 8.51).

8.4.5 Maximum Product Particle Size

Inspection of equation 8.51 shows that there is a maximum limit on the particle size that can be obtained with initial reactant concentration C_0. The required residence time becomes infinitely large as the maximum particle size (corresponding to complete reaction and consumption of monomers) is approached:

$$1 > \frac{n_p}{A_v C_0} \cdot \frac{\pi}{6v_1}(d_{p_f}^3 - d_{p_0}^3)\left(1 + \left(\frac{W}{S}\right)\right) \tag{8.52}$$

$$d_{p_f} < \left[\frac{A_v C_0}{n_p} \cdot \frac{6v_1}{\pi}\left(\frac{1}{1 + \left(\frac{W}{S}\right)}\right) + d_{p_0}^3\right]^{\frac{1}{3}} \tag{8.53}$$

A similar expression for the maximum product particle size was proposed by Alam and Flagan (1986).

8.4.6 Yield Loss because of Incomplete Reaction and Deposition

In a reactor with finite residence time (i.e. incomplete reaction), there are yield losses due to unreacted reactant and un-deposited monomers/clusters (represented in the model system as monomers) that leave the reactor. Equations 8.28 and 8.43 can be used to calculate the concentrations of unreacted reactant un-deposited monomers at the end of the reactor. The amount of unreacted reactant will determine whether a recycling process is needed. The significance of yield loss to undeposited monomers compared to unreacted reactant is indicated by the ratio $\beta = \frac{C_{m_f}}{C_f}$.

8.5 Summary of Reactor Design Framework

A simple mathematical framework was developed for comparison of different reactor designs for constant number seed growth of spherical ceramic particles. Design parameters for describing a non-constant temperature profile, and a model system which includes conditions of unconstrained cluster growth, were *not* investigated, for simplicity. Future extension of the framework should include these aspects of seed growth reactor design. Since the comparison of reactor designs is based on fixed seed and product particle sizes, future analysis of temperature profiles should express the temperature profiles in terms of particle size $\left(\frac{dT}{dd_p}\right)$, instead of time or position $\left(\frac{dT}{dt}, \frac{dT}{dx}\right)$.

Within the above-mentioned limitations, the remaining design parameters were evaluated. Classification of quantities and an *independence analysis* yielded a set of independent process parameters. This set was reduced by noting that the initial and final particle sizes are fixed, and by proving that the reactor design problem is decoupled from production rate for laminar flow.

The reactor design problem was explored by expressing appropriate process constraints (constraints for constant number seed growth, as well as some more general reactor design constraints) in terms of the design parameters. The final constraint equations explicitly indicate the effects of initial reactant concentration and seed concentration. This will allow a two-dimensional graphical representation of constraints, as applied in chapter 10 (the two-dimensional graphical representation of constraints will be performed for a range of different temperatures and pressures).

In some cases analytical expressions for the constraints exist. For constraints which cannot be analytically expressed, the slopes of the constraint curves (in terms of dimensions n_p and C_0) are evaluated to characterise the behaviour of the constraint curves.

A simple reactor design model was proposed to determine the residence time necessary for the required particle growth, since some of the constraint functions are dependent on τ_{res}. The effect of reactor diameter on wall-deposition is not incorporated in this model (a possible extension of the model to incorporate this is suggested), and a constant value for fractional wall-deposition is assumed .

8.5.1 Constraints

Reaction Conversion (equation 8.2)

$$n_p < C_0 A_v \frac{6v_1}{\pi(d_{pf}^3 - d_{p0}^3)\left(1 + \left(\frac{W}{S}\right)\right)} \neq f(D)$$

Constrained Cluster Growth (equation 8.9)

$$n_p \geq \frac{(2f\beta_{m,m}kA_vC_0)^{\frac{1}{2}}}{\beta_{m,p}} \neq f(D)$$

Negligible Seed Coagulation (equation 8.14)

$$n_p \leq \mathrm{f}_{\mathrm{coag}}(C_0) = \frac{\epsilon_{sc}}{2\bar{\beta}_{p,p}\bar{\tau}_{res}(C_0, n_p)} \neq f(D) \ , \ 0 < \epsilon_{sc} \ll 1$$

$$\frac{\mathrm{d}f_{coag}}{\mathrm{d}C_0} > 0$$

Negligible Thermodynamic Entry Length (equation 8.21)

$$D < \left[20\epsilon_{tc}\tau_{res}\left(\frac{\mu}{\rho Pr}\right)\right]^{\frac{1}{2}} \quad , \quad 0 < \epsilon_{te} \ll 1$$

$$n_p > \mathrm{f}_{\mathrm{entry}}(C_0, n_p, D)$$

$$\frac{\mathrm{d}f_{entry}}{\mathrm{d}C_0} > 0$$

Stoichiometric Limit on C_0 (equation 8.26)

$$C_0 < \left(\frac{P}{k_B A_v T}\right)\frac{\alpha_M}{\alpha_M + \alpha_O} \neq f(n_p, D)$$

8.5.2 Reactor Design Model

$$\begin{aligned}
\alpha &= \bar{\beta}_{m,p} n_p \left[1 + \left(\frac{W}{S}\right)\right] \\
\beta &= \frac{k}{(\alpha - k)}\left[1 - e^{-(\alpha-k)\tau_{res}}\right] \\
\tau_{res} &= -\frac{1}{k}\ln\left[\frac{1 - \frac{n_p}{A_v C_0}\cdot\frac{\pi}{6v_1}(d_{p_f}^3 - d_{p0}^3)\left(1 + \left(\frac{W}{S}\right)\right)}{1+\beta}\right]
\end{aligned} \tag{8.54}$$

An iterative procedure will be used to re-calculate β and τ_{res} until convergence is obtained.

Chapter 9

Analysis of Turbulent Coagulation

The purpose of this chapter is to determine whether it is beneficial to employ turbulent flow in constant number seed growth. The contribution of turbulent coagulation to the overall coagulation rate is investigated by comparing turbulent and Brownian collision coefficients for varying turbulent intensity. This comparison is done quantitatively by considering typical conditions for seed growth (growth of $Ti0_2$ seed particles at atmospheric pressure and $773K$) [Okuyama et al. (1990)]. The results are interpreted in terms of minimising reactor volume (maximising seed and reactant concentrations), and in terms of the acoustic limit on velocity of flow.

9.1 Modelling the Interplay of Brownian and Turbulent Forces in Collisions

The collision rate between two particles i and j is expressed as:

$$r_{ij} = \beta_{ij} n_i n_j \ [\#_c \, m^{-3} \, s^{-1}] \tag{9.1}$$

where β_{ij} is the collision coefficient.

Collision Coefficients

The interplay of Brownian and turbulent forces in particle movement (and subsequent collisions) is approximated by the following simple additive expression for the collision coefficient, as was used by Xiong and Pratsinis (1991):

$$\beta = \beta_B + \beta_T \tag{9.2}$$

The Brownian collision coefficient, β_B, is described by the Fuchs interpolation formula for Brownian collisions from the free-molecular to the continuum regimes (see section 2.4.6).

$$\beta_{B_{ij}} = f(T, P, d_i, d_j) \tag{9.3}$$

The turbulent collision coefficient, β_T, is described by the following expressions [Xiong and Pratsinis (1991)]:

$$\beta_{T_{ij}} = K_T \left(v_i^{\frac{1}{3}} + v_j^{\frac{1}{3}} \right)^3 = f(T, P, d_i, d_j, u, D) \tag{9.4}$$

$$K_T = 2.3 \left(\frac{3}{4\pi} \right) \left(\frac{\varepsilon_d \rho_g}{\mu} \right)^{\frac{1}{2}} \tag{9.5}$$

$$\varepsilon_d = \frac{4}{D} \left(\frac{f_F}{2} \right)^{\frac{3}{2}} u^3 \tag{9.6}$$

$$f_F = \frac{0.0791}{\mathrm{Re}^{\frac{1}{4}}} = 0.0791 \left(\frac{\mu}{\rho_g u D} \right)^{\frac{1}{4}} \tag{9.7}$$

The following special terminology is used in equations 9.4 to 9.7:

v $[m^3/\#_p]$	particle volume
ε_d $[m^2/s^3]$	turbulent energy dissipation rate
ρ_g $[kg/m^3]$	gas density
f_F	Fanning friction factor

The dependence of the turbulent collision coefficient on different independent parameters is demonstrated by combination of equations 9.4 to 9.7:

$$\beta_{T_{ij}} \propto \frac{u^{21/16}}{D^{11/16}} \left(\frac{\rho_g}{\mu} \right)^{5/16} (d_i + d_j)^3 \tag{9.8}$$

Note that turbulent collision rate increases with u and decreases with D, and therefore does not necessarily increase with $\mathrm{Re} \propto uD$ (the Reynolds number enables a one-dimensional distinction between laminar and turbulent flow, but it is not on its own an indication of turbulent intensity).

For the present analysis of turbulence, the choice of species and the reactor temperature and pressure are treated as constants: hence the kinematic viscosity (μ/ρ_g) is treated as a constant.

The comparison of Brownian and turbulent collision coefficients should indicate how turbulence affects particles of different sizes. To allow a simple comparison, the distribution of particle sizes is represented by two monodisperse modes, monomers and (seed) particles. Therefore collision coefficients will be calculated for any combination of monomers and particles (*m-m* / *m-p* / *p-p*). The particle diameters d_i and d_j represent the colliding particles in equation 9.8. Monomer diameter is constant, and a constant particle diameter is assumed.

For specified species, temperature, pressure and seed particle size, the design parameters that influence the turbulent collision frequency (β_T) are velocity (u) and reactor diameter (D). Note that the Brownian collision coefficient is not a function of u or D. Hence β_T for different u and D should be compared to constant β_B, for the collision combinations *m-m*, *m-p* and *p-p*.

The basis for comparing different turbulent intensities is a fixed total mass flow rate, thereby reducing the number of independent design parameters to unity. Velocity (u) is considered as the independent parameter, from which reactor diameter (D) is inferred. For a large excess gas, the total mass flow rate is proportional to the density of the bulk gas:

$$M_{flow} = 3600\frac{\pi}{4}D^2 u\rho_g \tag{9.9}$$

$$D = \left(\frac{M_{flow}}{3600}\frac{4}{\pi}\frac{1}{u\rho_g}\right)^{1/2} \tag{9.10}$$

Typical Process Conditions for Calculations

The calculations are done for typical conditions for seed growth: growth of $Ti0_2$ seed particles ($d_p = 80\,nm$) at atmospheric pressure and $773K$ [Okuyama et al. (1990)].

Upper Limit of Flow Velocity

The speed of sound is used as a conservative upper limit on flow velocity. The speed of sound is approximated according to the ideal gas law [De Nevers (1991)]:

$$u_{ac} = \left(\frac{k k_b A_v T}{M W_{bg}} \right) \tag{9.11}$$

where $k \approx 1.4$ for diatomic gases.

Note that for velocities close to the speed of sound, the flow cannot be isothermal [De Nevers (1991), p.310]. Therefore the coagulation coefficients calculated for such high velocities are inaccurate, since they are calculated by assuming isothermal and isobaric conditions.

The purpose of the present analysis is to determine the significance of turbulent coagulation for realistic velocities, well below the speed of sound. Therefore the inaccuracy discussed above is not relevant for the present analysis.

9.2 Results

Figure 9.1 gives a quantitative comparison of collision coefficients for different turbulent intensities. The calculations are given in spreadsheet form in appendix H.

Changes are made to the independent parameter u, equation 9.10 is used calculate D to ensure a constant mass flow rate, and the resulting β_T is calculated with equations 9.4 to 9.7. The ratio between the turbulent and Brownian collision coefficients (β_B/β_T) is an indication of how significant turbulent coagulation is compared with Brownian coagulation. This ratio is calculated for the collision combinations m-m, m-p and p-p.

Broad shaded lines are used to indicate the inaccuracy at high velocities (close to the speed of sound) due to the assumption of isothermal flow.

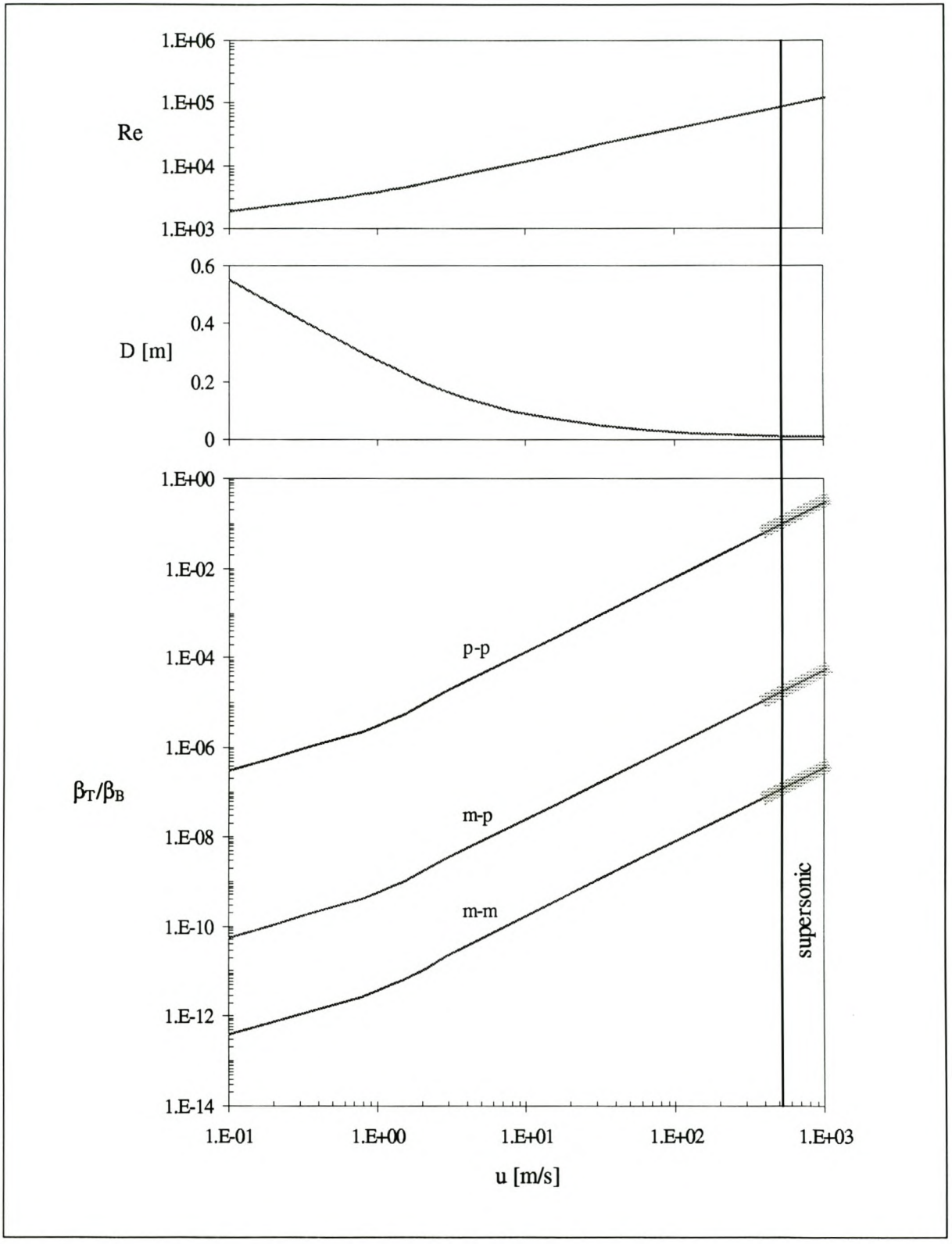

Figure 9.1: The Significance of Turbulent Coagulation in Seed Growth:
Growth of 80 nm $Ti0_2$ seed particles at $P = 1\,atm$ and $T = 773\,K$, $M_{flow} = 100\,kg/h$.

9.3 Interpretation of Results

The results are interpreted for the specific process conditions of the simulation, and the interpretation does therefore not constitute a rigourous general proof. Such a general proof may be possible, but falls beyond the scope of the present work. The analysis in the present work indicates a trend with respect to the significance of turbulent coagulation for different particle sizes, which is supported by modelling results from the literature. This trend is interpreted in terms of constant number seed growth, so as to justify the proposition that laminar flow is preferable for conditions similar to the simulation conditions. The simple mathematical format of the analysis (identification of design parameters, dimensions used for graphical presentation, definition of constraint) is a useful tool for reproducing the analysis of turbulence for different conditions.

Negligible Turbulent Coagulation Below Speed of Sound

For the specific reactor conditions, it is shown that turbulent coagulation is negligible for velocities lower than the speed of sound. However, it is possible that turbulent coagulation will become significant below the speed of sound for lower mass flow rates, because then D will be smaller for the same u, and turbulent intensity will be increased (see equation 9.8).

Seed Coagulation

It is shown that as turbulence is increased, the seed coagulation rate is the first coagulation rate to be significantly enhanced by turbulence. This is in agreement with the results of Xiong and Pratsinis (1991), who stated that the larger the particle size is, the lower is the turbulent intensity required for turbulence to increase the collision rate significantly (more than the Brownian collision rate).

For turbulent flow, as opposed to laminar flow, the increase in seed coagulation rate implies that lower seed concentrations (i.e. higher reactor volume per production rate) are required to ensure negligible seed coagulation.

Hence it is favourable to employ laminar flow for constant number seed growth, so as to have a larger allowable region of design parameters (less stringent process constraints). The velocity should be as low as possible, so as to minimise reactor size. The *lower* limit on velocity was discussed in section 8.2.3, page 112.

Chapter 10

Evaluation of Hypothesis on Non-Agglomerating Seed Growth

The existing literature on seed growth focuses on characterising the suppression of new particle formation (constrained cluster growth) [Alam and Flagan (1986), Wu and Flagan (1987), Wu et al. (1988), Okuyama et al. (1990), Zachariah and Dimitriou (1990)]. The work of Alam and Flagan (1986) and Wu and Flagan (1987) also considered the constraint on the amount of particle growth that can be obtained by complete reaction conversion. In chapter 8, these and other constraints for constant number seed growth reactors were defined. Notably, the constraint for negligible seed coagulation (agglomeration) was defined, something which has not yet been considered in the literature on *spherical* seed particle growth. The constraints are applied here to test the hypothesis that significant growth of spherical (non-agglomerated) particles can be obtained by constant number seed growth (see page 100).

The strategy employed to evaluate the hypothesis is to establish whether a reactor can be designed that satisfies all the constraints for spherical seed growth.

In section 10.1 the process constraints are explored theoretically, by applying the constraint equations derived in chapter 8 (for an isothermal reactor). The constraints are evaluated for the temperature and pressure values ($T = 773\,K$, $P = 1\,atm$) that were used by Okuyama et al. (1990), so as to allow a comparison of the present theoretical results with the published experimental results. Furthermore, a range of temperatures and pressures ($T = 673 - 773\,K$, $P = 0.25 - 5\,atm$) are investigated to search for suitable conditions for spherical seed growth.

In section 10.2, the theoretical analysis is supported by experimental and simulation results for seed growth from the literature.

The work of Okuyama et al. (1990) is the only published experimental work on the growth of presumedly spherical seed particles. Their experimental work included both isothermal ($T = 773\,K$) and increasing ($T = 323 - 873\,K$) temperature profiles. They did not report the particle shape, but the small seed particle size that they employed ($d_{pg} = 50\,nm$) may well be below the maximum fusible particle size. For lack of any experimental work on seed growth that explicitly reports spherical particle shape, it is assumed here that the seed particles of Okuyama et al. (1990) were spherical.

The maximum growth obtained by Okuyama et al. (1990) in conditions of constrained cluster growth was $53 - 64\,nm$. It is noted here that more significant can be obtained by operating at lower temperature (slower reaction), so as to allow a higher ratio of reactant concentration to seed concentration, whilst still constraining cluster growth. Published results of agglomerate seed growth are interpreted to asses the viability of obtaining more significant spherical seed growth (not considering the seed coagulation constraint) than that obtained by Okuyama et al. (1990).

The present work evaluates more constraints than are discussed in the literature, and therefore the data in the literature are manipulated and re-interpreted in terms of the additional constraints. To this end, typical experimental measurements for an aerosol reactor are translated to characteristic variables commonly used in reactor design.

10.1 Theoretical Investigation

10.1.1 Design Parameters

Table 8.2 lists the reduced set of independent design parameters describing the system. Isothermal and isobaric reactor conditions are assumed, since comparison of different process conditions (for the same specified particle growth) would be complicated by temperature and pressure profiles. The effect of reactor diameter (D) on wall-deposition is not investigated, because this requires a modelling effort which falls beyond the scope of the present work.

The constraint equations (derived in chapter 8) explicitly indicate the effects of initial reactant concentration (C_0) and seed concentration (n_p). This allows a two-dimensional graphical representation of constraints.

10.1.2 Constraints

The following constraints are evaluated (see section 8.5.1):

- Reaction conversion
- Constrained cluster growth
- Stoichiometric reactant concentration
- Negligible seed coagulation
- Thermodynamic entry length

Model Equations to Evaluate Constraints

To evaluate the constraints, Brownian collision coefficients (β_B) are calculated by the Fuchs interpolation formula (see section 2.4.6), for the collision combinations m-m, m-p and p-p.

The equation describing the constraint on cluster growth (equation 8.9) was derived from severe modelling simplifications (neglecting of cluster dynamics), and employs an empirical parameter f. Zachariah and Dimitriou suggested a value of $f = 300$. The sensitivity of the allowable region (in terms of C_0 and n_p) is investigated by plotting the constraint for both $f = 300$ and $f = 30$.

The simple reactor design model developed in section 8.4 is used to calculate the residence time (τ_{res}), which is used to evaluate the constraint of negligible seed coagulation. (The parameter $\beta = \frac{C_{m_f}}{C_f}$ was found to be negligible, which indicates that the yield loss to undeposited clusters is negligible. See appendix H.2.)

Reactor diameter is not specified in the present analysis, and therefore the thermodynamic entry length constraint cannot be evaluated. Instead, the constraint equation is used to calculate the maximum reactor diameter to ensure that the entry length is less than 10% of the reactor length (the residence time is used in this calculation).

10.1.3 Parameter Evaluation

The evaluation of constraints for conditions similar to the experimental conditions of Okuyama et al. (1990) (figure 3, for seed growth of TiO_2 in an isothermal reactor) uses the following parameter values:

$$\begin{aligned} T &= 773\,K \\ P &= 1\,atm \\ k &= 3.96 \times 10^5 \exp\left(-\frac{7.05 \times 10^4}{k_B A_v T}\right)\,[s^{-1}] \\ MW_{bg} &= 28\,g/mol\ \ (N_2) \\ d_{pg_0} &= 53.3\,nm\ ,\ \sigma_g = 1.49 \end{aligned} \tag{10.1}$$

The reaction rate constant (k) describes first-order reaction rate for the thermal decomposition of titanium tetraisopropoxide (TTIP): $Ti(OC_3H_7)_4 \rightarrow TiO_2 + 4C_3H_6 + 2H_2O$

Note that Okuyama et al. (1990) specified the seed particle size distribution in terms of the geometric mean particle size (d_{pg_0}) and geometric standard deviation (σ_g). These parameters are commonly used in aerosol science to describe the approximately log-normal particle size distribution resulting from coagulation. In the present study, the volume-average particle size is used as it facilitates calculation of conversion (see appendix H.1, equation H.5):

$$d_{pg_0} = 53.3\,nm\,, \sigma_g = 1.49 \quad \equiv \quad d_{pv_0} = 67.3\,nm \tag{10.2}$$

The final particle size is also inferred from the data of Okuyama et al. (1990), with the calculations shown in see appendix H.1 (equations H.6 to H.9):

$$d_{pv_f} = 76\,nm \tag{10.3}$$

Gas Properties

The model equations employ the density (ρ) and the viscosity (μ) of the bulk gas (N_2). These parameters are evaluated by first considering the reduced temperature and pressure of the gas, for the range $T = 673 - 773\,K$ and $P = 0.2 - 5\,atm$ (the range considered in calculations with the model of constraints).

The critical properties of N_2 are: $T_c = 126\,K$, $P_c = 34\,bar$ [Reid, Prausnitz and Polling (1986)]. The reduced temperature and pressure are:

$$T_r = T/T_c > 5$$

$$P_r = P/P_c < 0.15$$

For such high temperature and low pressure, the ideal gas law is valid and viscosity is a very weak function of pressure [Reid, Prausnitz and Polling (1986)]. Hence the ideal gas law is used to calculate density, and viscosity is assumed not to be a function of pressure.

The following values for viscosity are obtained from Incropera and De Witt (1990):

$$\mu(673\,K) = 3.13 \times 10^{-5}\,Pa \cdot s$$

$$\mu(773\,K) = 3.43 \times 10^{-5}\,Pa \cdot s$$

10.1.4 Results

The headings of the following subsections indicate where the values for design parameters of Okuyama et al. (1990) were used. In the cases where design parameters are not indicated as fixed, the present theoretical analysis considers a range of different parameter values. Hence the evaluation of the hypothesis is not only for one specific set of process conditions, but considers a range of values for the design parameters T, P, $d_{p_0} \rightarrow d_{p_f}$, C_0 and n_p.

The quantitative evaluation of the different constraints is shown in appendix H.

Fixed parameters: T, P, $d_{p_0} \rightarrow d_{p_f}$

Figure 10.1 shows the constraints of reaction conversion, stoichiometric reactant concentration and constrained cluster growth, and the *allowable region* defined by these constraints (shaded). The experimental conditions (C_0 and n_p) of Okuyama et al. (1990) are indicated.

Figure 10.1 also shows the fractional excess gas (ε) at the cross-over of the reaction conversion and cluster growth constraints (the maximum allowable dilution), for different values of the empirical constant for constrained cluster growth (f).

The table at the bottom of figure 10.1 shows values for fractional seed coagulation (ϵ_{sc}) corresponding to points on the cluster growth constraint. The minimum value of ϵ_{sc} is observed for the maximum allowable C_0 (the stoichiometric limit). The increase of ϵ_{sc} with decreasing C_0 is characterised by considering the value of ϵ_{sc} corresponding to 99% reaction conversion (near the cross-over of the cluster growth and reaction conversion constraints).

If the seed coagulation constraint is violated at every position on the cluster growth constraint in the allowable region, then it is violated everywhere in the allowable region. This is because a higher n_p (for the same C_0) requires a longer residence time, and such simultaneous increase in n_p and τ_{res} will increase the seed coagulation.

The seed coagulation constraint cannot be plotted on figure 10.1, since it is severely violated ($\epsilon_{sc} \gg 1$) everywhere in the allowable region defined by the other constraints, and it is not defined outside this allowable region.

Figure 10.2 shows detail of the allowable region. The required residence times and maximum reactor diameters for thermodynamic entry length less than 10% of reactor length, are shown for different positions on the cluster growth constraint.

Fixed parameters: T, P

Figure 10.3 shows the effect of product particle size on the constraints.

Fixed parameters: $d_{p_0} \rightarrow d_{p_f}$

Figure 10.4 shows the effect of different temperatures and pressures on the process constraints. The purpose of this figure is to indicate whether there may be a certain T and P for which *spherical* seed growth is possible (the *hypothesis*). In order to obtain a *conservative dis*proof of the hypothesis, the following parameter values are chosen, with justification:

$f = 30$: The effect of f on ϵ_{sc} is tabulated below figure 10.1, which shows that less seed coagulation may be achieved with a lower f.

$d_{pv} = 67 - 76\,nm$: Figure 10.3 shows that specifying a lower product particle size enlarges the allowable region in terms of the maximum allowable reactant dilution (ε_{max}).

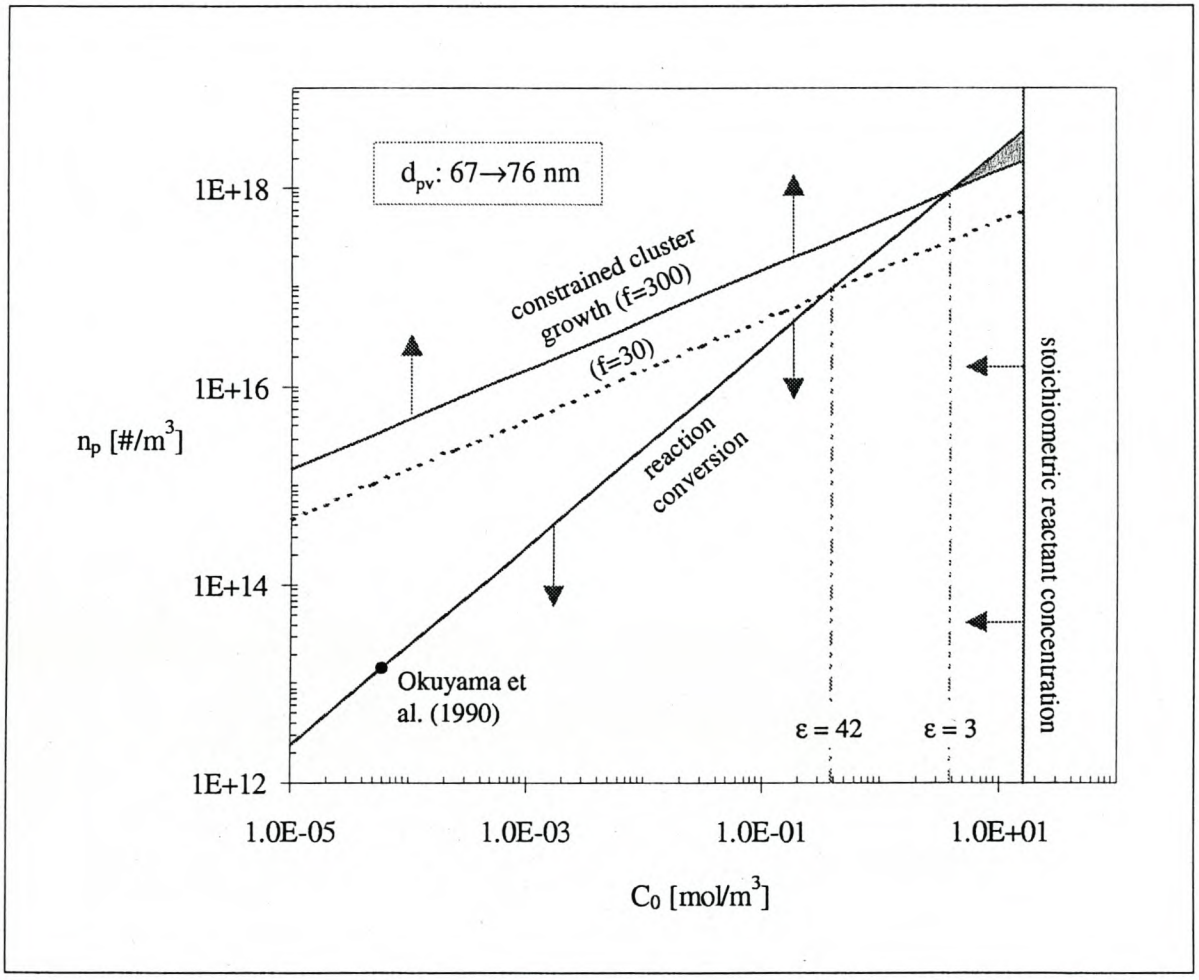

Seed Coagulation for Points on Cluster Growth Constraint		
f = 300	99% reaction conversion: $\epsilon_{sc} = 4000$	max. (stoichiometric) C_0: $\epsilon_{sc} = 1200$
f = 30	99% reaction conversion: $\epsilon_{sc} = 405$	max. (stoichiometric) C_0: $\epsilon_{sc} = 90$

Figure 10.1: Constraints for Constant Number Seed Growth ($P = 1\ atm$, $T = 773\ K$)

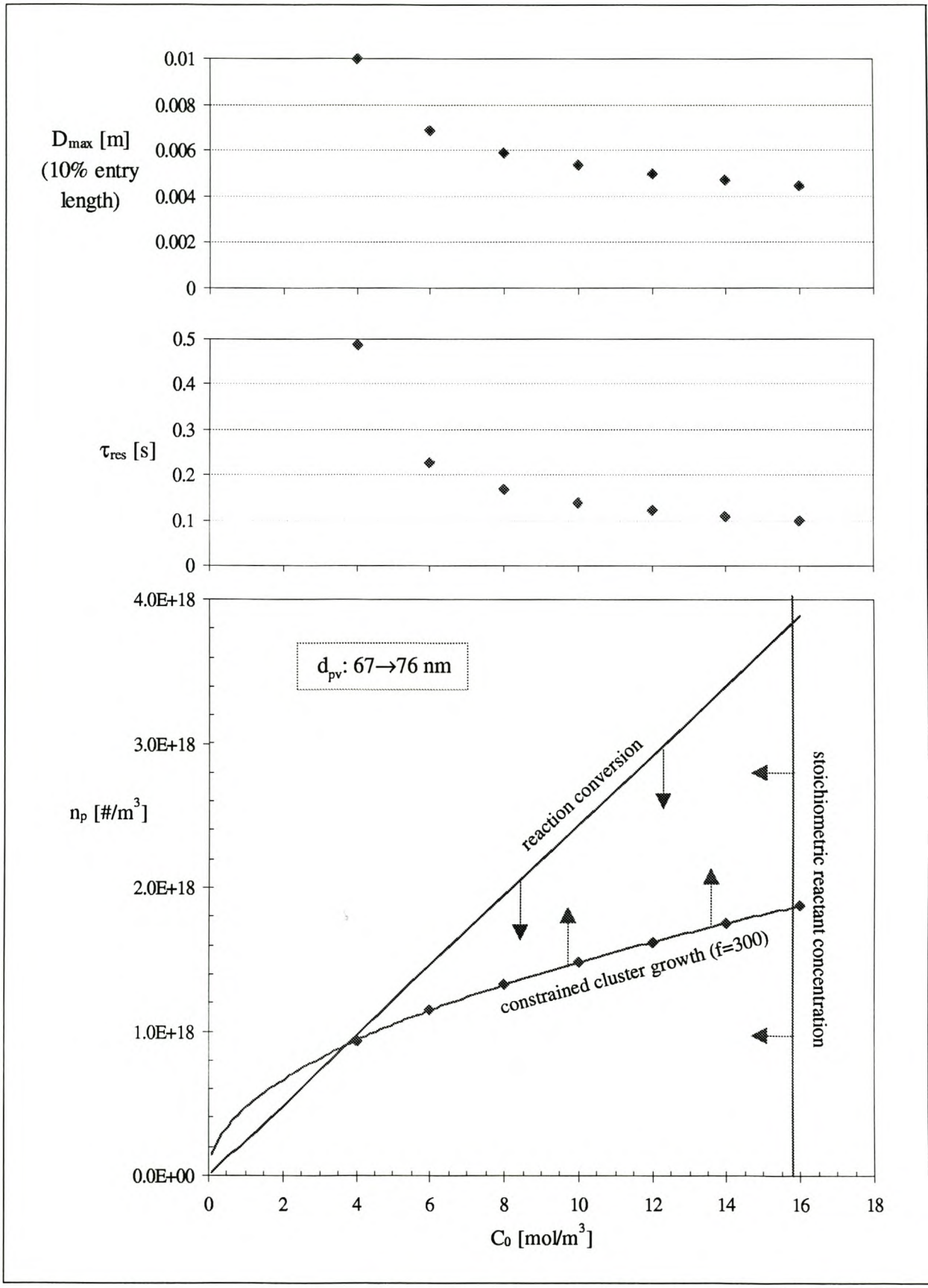

Figure 10.2: Detail of Constraints for Constant Number Seed Growth ($P = 1atm$, $T = 773K$)

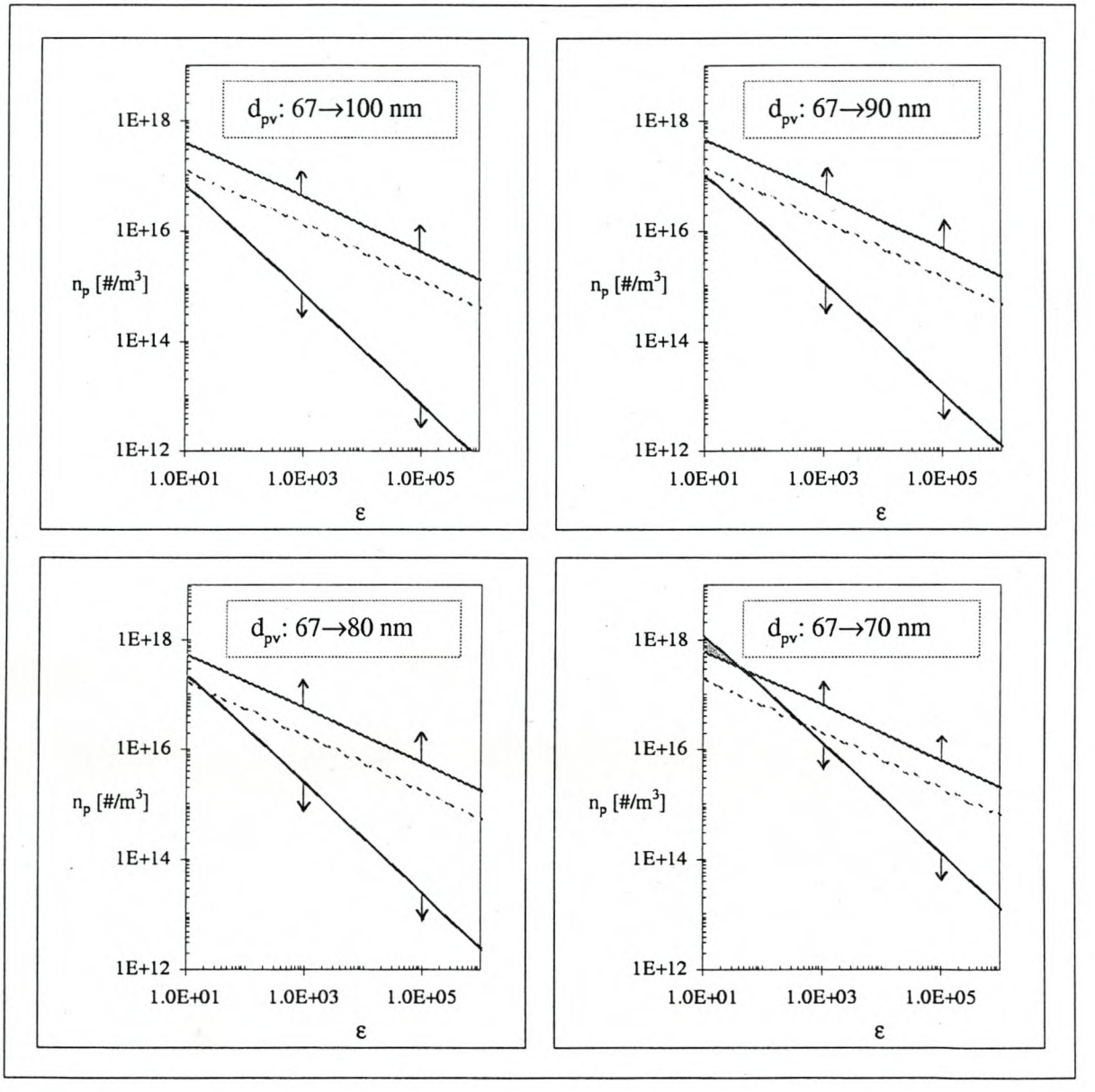

Figure 10.3: Constraints for Constant Number Seed Growth in Terms of Excess Gas: Effect of Final Particle Size ($P = 1\ atm$, $T = 773\ K$)

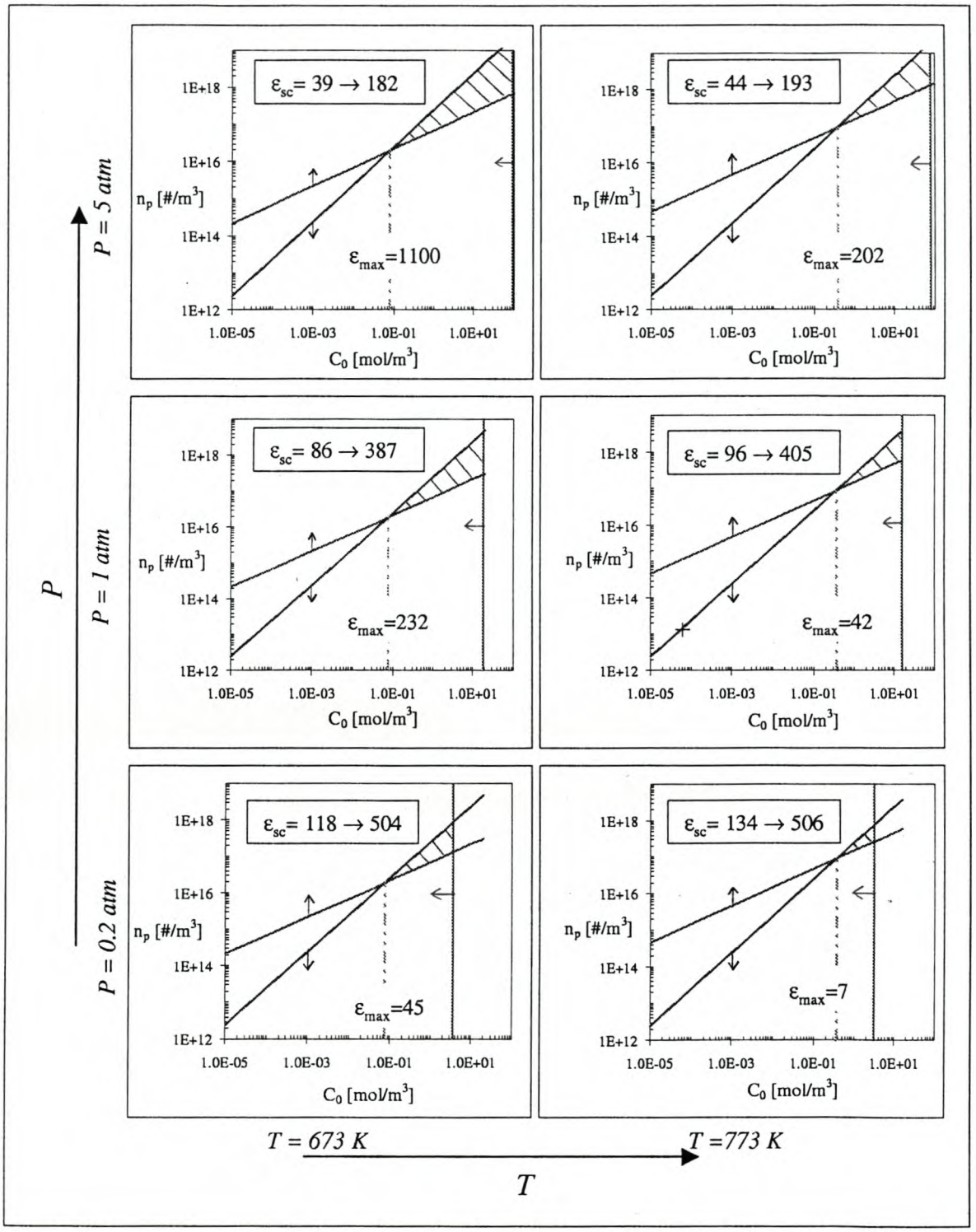

Figure 10.4: Constraints for Constant Number Seed Growth:

Effect of Different Temperatures and Pressures ($f = 30$, $d_{pv} = 67 \rightarrow 76\, nm$).

10.1.5 Interpretation

Sensitivity of Cluster Growth Constraint

Figure 10.1 shows that a tenfold decrease in the empirical parameter for constrained cluster growth ($f = 300 \rightarrow 30$), results in an approximately tenfold increase in the maximum fractional excess gas ($\varepsilon = 3.3 \rightarrow 42$), indicating that the allowable region is sensitive to this empirical parameter. This, combined with the modelling simplifications (neglecting of cluster dynamics) for the cluster growth constraint, indicates that the cluster growth constraint is likely to be inaccurate. Yet, the theoretical results are interpreted in terms of the seed growth hypothesis, and this interpretation will later be verified by analysis of published experimental and modelling data.

Seed Coagulation

The values for fractional seed coagulation (ϵ_{sc}) were calculated with a model that assumes that the number of seed particles is approximately constant (see section 8.3.3). For significant seed coagulation ($\epsilon_{sc} > 1$) this is inappropriate, and therefore the magnitude of ϵ_{sc} (for $\epsilon_{sc} > 1$) cannot be physically interpreted. It can just be inferred that if $\epsilon_{sc} > 1$, then seed coagulation is significant.

For $T = 773\ K$ and $P = 1\ atm$, the table at the bottom of figure 10.1 shows that the seed coagulation constraint is violated ($\epsilon_{sc} \gg 1$) at every position on the cluster growth constraint in the allowable region (see appendix H.2), and it is thus violated everywhere in the allowable region (as was discussed earlier). This significant seed coagulation occurs even for the very small amount of specified seed growth ($67 - 76\ nm$).

The evaluation of different temperatures and pressures, in figure 10.4, indicates that seed coagulation cannot be avoided within the parameter range of $T = 673 - 773\ K$ and $P = 0.2 - 5\ atm$, even for the very small amount of specified seed growth ($67 - 76\ nm$).

The magnitude of the minimum obtainable ϵ_{sc} decreases with increasing pressure and decreasing temperature. It was noted earlier that the magnitude of ϵ_{sc} should not be physically interpreted. However, this observed trend in decreasing ϵ_{sc} may merit a future search for suitable spherical seed growth conditions at higher pressures and lower temperatures. In such a study, limitations on the maximum practical pressure and the minimum allowable temperature (for an realistic residence time) will need to be considered.

Thermodynamic Entry Length

Figure 10.2 shows that, for the indicated positions on the cluster growth constraint curve, reactor diameters in the order of $4 - 10\,mm$ are required to ensure that the thermodynamic entry length is less than 10% of reactor length. These diameters are realistic for experimental reactors (Okuyama et al. (1990) employed a reactor diameter of $11.5\,mm$), but may be unrealistically small for industrial-size reactors.

Note that these diameters were calculated for very little seed growth ($67 - 76\,nm$), since the constraints did not allow more growth per particle.

A higher seed particle concentration (n_p) than the minimum set by the cluster growth constraint will result in increase in the residence time, and hence also an increase in the maximum allowable reactor diameter. But such conditions will result in more seed coagulation.

Agglomerate Seed Growth

If seed coagulation is deemed inevitable, and the reactor is intentionally designed for agglomerate seed growth, it will be beneficial to operate with the highest n_p allowed by the reaction conversion constraint (and not to consider the seed coagulation constraint). This will minimise the reactor volume per production rate, and allow higher reactor diameters (corresponding to higher production rates).

Amount of Growth Possible

Figure 10.3 indicates how the allowable region (defined by the reaction conversion and cluster growth constraints) changes with the specified product particle size. Instead of initial reactant concentration (C_0), the fractional excess gas (ϵ) is used for the x-axis.

Experimental aerosol reactors commonly use a large degree of reactant dilution, in the order of 0.01 mole of limiting reactant to 1 mole total gas, i.e. $\varepsilon \sim 100$ [e.g. Kobata, and Kusakabe and Morooka (1991); Xiong, Pratsinis and Weimer (1992)]. For constructing figure 10.3, the minimum fractional excess gas is arbitrarily set at $\epsilon = 10$, which implies a tightening of the constraint for stoichiometric reactant concentration ($\epsilon = 0$).

The maximum excess gas for the allowable region (corresponding to the cross-over of the reaction conversion and cluster growth constraints) decreases with product particle size. In fact, for growth more than 67 nm to 80 nm, an allowable region does not exist for $\epsilon > 10$ (using the value of $f = 30$ for the cluster growth constraint).

Figure 10.4 indicates how the allowable region can be changed, by the choice temperature and pressure, so that the specified growth may be obtained for higher reactant dilution. A lower temperature lowers the cluster growth constraint (because of reduced reaction rate), and therefore higher reactant dilution may be used. A higher pressure increases the stoichiometric limit on reactant concentration, and therefore also allows higher reactant dilution.

Note that the specified growth for figure 10.4 is very small ($67 - 76 nm$), so this figure does not represent significant seed growth. More significant growth may be obtained by lowering the temperature, as long as the temperature is still higher than the vaporisation temperature of the reactant. The penalty for lowering the temperature is increased residence time (i.e. greater reactor volume).

Summary

For the specific temperature and pressure used by Okuyama et al. (1990), significant growth cannot be obtained, and seed coagulation cannot be avoided.

The investigation of a range of different temperatures and pressures ($T = 673 - 773\ K$ and $P = 0.2 - 5\ atm$) did not indicate the existence of conditions for which seed coagulation is negligible.

There is a possibility that higher pressures and lower temperatures than was considered in the present work may allow significant spherical seed growth, if such conditions are practical. An investigation of this possibility should define appropriate constraints for the maximum practical pressure, and the minimum temperature for a maximum realistic residence time. Such a study falls beyond the scope of the present work.

10.2 Comparison with Data in Literature

10.2.1 Isothermal Reactors

Okuyama et al. (1990), figure 3, isothermal reactor

The (isothermal reactor) conditions of Okuyama et al. (1990) are indicated on figure 10.1. They did not explicitly state that product particles were spherical. Yet, the small seed particle size ($d_{pg} = 50\,nm$) may well be below the maximum fusible particle size, and it is assumed here that the seed particles were spherical.

They showed experimentally, by measuring the initial (seed) and final particle concentrations, that cluster growth was not constrained for these conditions. This observation is in agreement with the theoretical violation of the cluster growth constraint, as indicated on figure 10.1.

The data from Okuyama et al. (1990) are manipulated to determine the final particle size, so as to represent this data on the same plot as the theoretical constraints (figure 10.1).

The necessary data manipulation includes calculation of the following (equations and tabulated results are given in appendix H.1):

1. Residence time:

$$\tau_{res} = 1.98\,s$$

2. Reaction conversion:

$$X \approx 1$$

3. Conversion of geometric mean particle size, with associated geometric standard deviation, to volume-average particle size (so as to calculate the total mass of particles):

$$d_{pg_0} = 53.3\,nm\,,\sigma_g = 1.49 \quad \rightarrow \quad d_{pv_0} = 67.3\,nm$$

4. Yield loss to wall-deposition (by evaluating the difference between the converted reactant and the obtained total particle mass, for the experiments without seed particles):

$$X_{wd} = 0.12$$

5. Final seed particle size (volume-average):

$$d_{pv_f} = 76\,nm$$

6. Ratio of thermodynamic entry length to total reactor length:

$$\epsilon_{te} = 0.032$$

Zachariah and Dimitriou (1990), figures 5 and 6

Zachariah and Dimitriou (1990) modelled seed growth at isothermal and isobaric conditions, using a sectional representation of the particle size distribution. They assumed a constant monomer source rate ($R_M = 1.3 \times 10^{16}\ \#cm^{-3}s^{-1}$), and evaluated the effect of seed particle concentration (for $d_{p_0} = 92\,nm$) on suppression of new particle formation (only new particles larger than $10\,nm$ were counted). They showed that, for these conditions, new particle formation was effectively suppressed (i.e. constrained cluster growth) with a seed concentration of $n_p = 7.18 \times 10^8\ \#cm^{-3}$.

Yet, the seed growth obtained at these conditions corresponds to an *increase* in the width of the particle size distribution (the original seeds were assumed to be monodisperse), and the size distribution asymptotically approached the self-preserving size distribution for *coagulation-controlled growth*. In contrast, constant number seed growth is expected to approach a monodisperse size distribution asymptotically. The cluster deposition rate is approximately homogeneous on all seed particle surface area, and therefore the increase in seed diameter will be approximately the same for seeds of all sizes, resulting in a *decrease* in the geometric standard deviation [Kusters and Pratsisnis (1995)].

Although Zachariah and Dimitriou (1990) determined conditions with constrained cluster growth, these conditions resulted in significant seed coagulation, as was indicated by the characteristic size distribution development for coagulation-controlled growth (this interpretation was not given by Zachariah and Dimitriou). In an actual reactor with incomplete sintering of colliding seed particles, this seed coagulation would produce hard agglomerates.

10.2.2 Increasing Temperature Profile

The problem of the high seed concentration (with the resulting small amount of growth per particle) needed to constrain cluster growth can be resolved by operating at lower temperature, i.e. slower monomer formation but the same overall monomer formation (for complete reaction conversion).

To minimise the required residence time (reactor size), the initially low temperature can be gradually increased as reactant concentration becomes lower and seed particles become larger. The increased efficiency of larger particles to scavenge clusters allows the temperature to be increased by even more than is required for a constant reaction rate.

Okuyama et al. (1990) conducted several experiments with an increasing temperature profile. The maximum seed growth that they reported for conditions with constrained cluster growth was $d_p = 53 \rightarrow 64\,nm$ (figure 4b). Hence the reaction rate with the ramped temperature profile was also too high to allow significant growth per particle, for conditions of constrained cluster growth. Okuyama et al. (1990) also reported results for conditions with unconstrained cluster growth, and in these cases more particle growth was obtained (up to $d_p = 53 \rightarrow 81nm$).

It is noted here that by operating with a similarly ramped temperature profile, but with a lower temperature at each position in the reactor, cluster growth can be constrained with a lower seed concentration. If, in addition to using such lower temperature and seed concentration, the reactor length would be extended so as to allow complete reaction conversion for the slower reaction rate, then more growth per particle could be obtained.

The seed coagulation constraint may be evaluated by considering the results from the reaction-coagulation model for seed growth of Okuyama et al. (1990). This model represented the particle population as four monodisperse modes: monomers, clusters below k-mer, particles above $(k+1)$-mer, and seeds. The model was used to simulate the experimental reactor conditions which were discussed above ($d_p = 53 \rightarrow 64\,nm$, figure 4b). The simulation showed a significant decrease in the seed particle concentration: $n_p/\rho = 3 \times 10^{11} \rightarrow 5 \times 10^{10}$ [#/g dry gas], i.e. the number of seeds was more than halved. Hence significant seed coagulation was predicted, which would in practice form hard agglomerates.

The lack of any published information on significant *spherical* seed growth can be attributed to seed coagulation, and is *not* an indication that significant growth per particle cannot be obtained. The agglomerate seed growth reactors of Alam and Flagan (1986) and Wu and Flagan (1987) clearly demonstrated that the size of primary particles in agglomerates could be increased greatly by cluster deposition onto agglomerate seed particles. Similarly, the modelling of cluster deposition onto agglomerates by Rogak (1997) indicated that up to a fourfold increase in primary particle diameter could be obtained.

10.3 Evaluation of Hypothesis of Constant Number Seed Growth

The following **hypothesis** was made by Zachariah and Dimitriou (1990), and the validity thereof was evaluated in this chapter:

The method of seed growth makes it possible to grow spherical ceramic particles, with initial size smaller than the maximum fusible size, to a significantly larger size, without coagulation of the seed particles (which will yield unwanted hard agglomerates).

The *model of constraints* was applied quantitatively for values of temperature ($T = 773\,K$, *isothermal*) and pressure ($P = 1\,atm$) that were used in an experimental study in the literature [Okuyama et al. (1990)]. This indicated that significant growth per particle (*more* than $67 - 80\,nm$) could *not* be obtained for any C_0 and n_p (within the *allowable region* defined by the constraints of reaction conversion, stoichiometric reactant concentration and constrained cluster growth). This is because of the high seed particle concentration needed to constrain cluster growth at the specified temperature (reaction rate increases with temperature). Furthermore, it was shown that *significant seed coagulation* cannot be avoided for the specified T and P, for any realistic amount of particle growth.

The experimental results of Okuyama et al. (1990) for an *increasing reactor temperature profile* ($T = 323 \rightarrow 873\,K$, $P = 1\,atm$) also indicated *insignificant seed growth* ($53 - 64\,nm$). Furthermore, their reactor model indicated that *seed coagulation was significant* at these conditions.

The modelling of an isothermal seed growth reactor by Zachariah and Dimitriou (1990) also indicated *significant seed coagulation.*

The evaluation of the hypothesis discussed above is limited to the temperatures and pressures from two literature sources on supposedly spherical seed growth (for lack of any other published work on spherical seed growth).

In order to do a more thorough search for reactor conditions for spherical seed growth, a *range of different temperatures and pressures* ($T = 673 - 773\ K$ and $P = 0.2 - 5\ atm$) were investigated with the *model of constraints*. It was shown that *significant seed coagulation* cannot be avoided within this range, even for a small specified particle growth ($67 - 76\ nm$). Future investigation of a wider range of temperatures and pressures will allow a more comprehensive evaluation of the hypothesis, and suitable limits on pressure and temperature should be defined for such an investigation.

Significant growth due to cluster deposition can be obtained, but not without seed coagulation. The experimental and modelling results for *agglomerate seed growth* in the literature [Alam and Flagan (1986), Wu and Flagan (1987), Rogak (1997)] demonstrated significant growth per primary particle.

To summarise the **evaluation of the hypothesis**:

The theoretical analysis in the present work, as well as experimental and modelling results from the literature, could not demonstrate that significant seed growth is possible without agglomeration (seed coagulation).

Chapter 11

Conclusion and Continuation

A comprehensive review of aerosol reactor engineering has been performed, from the perspective of producing micron-sized spherical ceramic particles (materials that cannot melt). The critical review delivered useful insights, which may be well-known to aerosol experts, but which an uninitiated reader may not easily infer from the available literature.

- The onset of agglomeration in an aerosol reactor (for solid-state ceramics) is characterised by the maximum fusible particle size, which is commonly observed experimentally. Particles smaller than this size coalescence rapidly and completely. Current sintering models cannot predict the sintering rate of particles smaller than this size.
- For non-densely packed particles larger than the maximum fusible size, solid-state sintering (without the aid of sintering additives) continues only to a meta-stable equilibrium, i.e. complete coalescence cannot be obtained.
- Condensation-like growth can be obtained in conditions with no thermodynamic barrier for nucleation, by scavenging of newly formed clusters by seed particles.

An experimental method to determine the maximum fusible particle size, as well as the temperature dependence thereof, has been suggested. Such experimental work is imperative for characterising the coalescence behaviour of very small particles (rapid and complete coalescence), which is not accounted for by current solid-state sintering models. (See section 4.5.5.)

A simple two-mode (numerical) model of simultaneous chemical reaction and coagulation was developed. Model predictions, for the evolution of particle size with time, were shown to be comparable to that of another simple model in the literature. The model is a simplified form of more complex models (in the literature) that represent the PSD as a small number of monodisperse modes, and it is therefore a valuable tool for understanding the more complex models.

The novel aspect of the present model is the expression of the aerosol dynamic equations in terms of 'sequential reaction conversions'. The choice of these as variables facilitates the interpretation of results to determine when particle growth becomes coagulation-controlled. The manner of variable definition and derivation of equations are similar to what is generally applied in reactor engineering. The model therefore serves to translate aerosol dynamics into the terminology of reactor engineering.

The final model equations were expressed in terms of 'logarithmic' variables $(-\ln|1 - \mathit{conversion}|)$, which resulted in high numerical resolution for conversions close to 1 (corresponding to complete conversion). The 'logarithmic' output variables were all of comparable magnitude, and scaled between 0 and 25.

The variable definition (sequential reaction conversions) and logarithmic transformation complicate the algebraic derivation of model equations, and may hinder expansion of the model to include more modes.

The main contribution of the present work is the evaluation of the hypothesis of Zachariah and Dimitriou (1990) that it is possible to grow isolated spherical particles larger than the maximum fusible size by the method of seed growth. A simple theoretical analysis of process constraints was conducted to evaluate the hypothesis, for an isothermal laminar-flow reactor.

The analysis of constraints is based on a mathematical framework for comparison of different values of reactor design parameters. This framework constitutes the proposal of a simplified model system, a rigourous classification of quantities in the system, and isolating an independent set of design parameters. The reactor design problem is decoupled from production rate, with justification, thereby reducing the number of design parameters. The comparison of different values of reactor design parameters is done on the basis of fixed initial (seed) and final (product) particle sizes.

The final constraint equations explicitly indicate the effects of two design parameters (initial reactant concentration and seed concentration), to facilitate two-dimensional graphical representation of the constraints.

An analysis of turbulent and laminar collision coefficients for colliding species of different sizes indicated that turbulent seed coagulation lowers the maximum seed concentration allowed for negligible seed coagulation. This is used as justification for considering only laminar flow in the modelling of constraints for constant number seed growth.

The modelling of constraints in the present work (for the range of temperatures and pressures under investigation), as well as experimental and modelling results from the literature, could not demonstrate that significant spherical seed growth is possible without seed coagulation.

An investigation of the effects of temperature and pressure on the process constraints indicated that increase in pressure and decrease in temperature allows a higher reactant dilution to be used.

The following continuing work is suggested, which will use and expand the model of constraints developed in the present work:

- Significant spherical seed growth may be possible at higher pressures and lower temperatures than were considered in the present work, if such conditions are practical. An investigation of this possibility should define appropriate constraints for the maximum practical pressure, and the minimum temperature for a maximum realistic residence time. These extra constraints should be combined with the existing model of constraints.

- The model of constraints may be applied to optimisation of a seed growth reactor, e.g. to minimise losses to wall-deposition. A suitable reactor model, such as that developed by Okuyama et al. (1992), should be employed to predict the values of performance indices for different values of design parameters. (See chapter 8.)

References

[1] M.K. Alam and R.C. Flagan. Controlled nucleation in aerosol reactors: Production of bulk silicon. *Aerosol Science and Technology*, 5(2):237–248, 1986.

[2] D.R. Askeland. *The Science and Engineering of Materials.* Chapman & Hall, London, 3 edition, 1996.

[3] P.W. Atkins. *Physical Chemistry.* Oxford University Press, Oxford, 5 edition, 1994. Chptrs. 24&28.

[4] A. Bensberg, P. Roth, R. Brink, and H. Lange. Modeling of particle evolution in aeosol reactors with coflowing gaseouys reactants. *AIChE Journal*, 45(10):2097–2107, Oct. 1999.

[5] R.M. Cannon and W.C. Carter. Interplay of sintering microstructures, driving forces, and mass transport mechnisms. *Journal of the American Ceramic Society*, 72(8):1550–1555, 1989.

[6] Y.C. Chang, M.B. Ranade, and J.W. Gentry. Thermophoretic deposition of aerosol particles on transport tubes. *Journal of Aerosol Science*, 21,S1:S81–S84, 1990.

[7] M. Chen, C. Hwang, and Y. Shih. A wavelet-galerkin method for solving population balance equations. *Computers & Chemical Engineering*, 20(2):131–145, 1996.

[8] Y-M. Chiang, D.P. Birnie, and W.D. Kingery. *Physical Ceramics: Principles for Ceramic Science and Engineering.* John Wiley&Sons, New York, 1997.

[9] W.S Coblenz, J.M. Dynys, R.M. Cannon, and R.L. Coble. Initial stage solid state sintering models: A critical analysis and assesment. In G.C. Kuczynski, editor, *Sintering Processes, Materials Science Research*, volume 13, pages 141–157, New York, 1980.

Plenum Press. Proceedings of the Fifth International Conference on Sintering and Related Phenomena.

[10] N. De Nevers. *Fluid Mechanics for Chemical Engineers.* 2 edition.

[11] J.M. Douglas. *Conceptual Design of Chemical Processes.* McGraw-Hill, New York, 1988.

[12] H. Fissan. Synthesis of nanoparticles in the gas phase for functional materials. Tutorial at the European Aerosol Conference 2000, Process- and Aerosol Measurement Technology, Gerhard-Mercator-University Duisburg, 47048 Duisberg, Germany, September 2000.

[13] R.C. Flagan. Gas phase synthesis processes: Thermochemistry and kinetics. In A.W. Weimer, editor, *Carbide, Nitride and Boride Materials Synthesis and Processing*, chapter 11. Chapman&Hall, London, 1997.

[14] R.C. Flagan and M.M. Lunden. Particle structure control in nanoparticle synthesis from the vapor phase. *Materials Science & Engineering*, A204:113–124, 1995.

[15] S.K. Friedlander. *Smoke, Dust and Haze.* Wiley, New York, 1977.

[16] F. Gelbard and J.H. Seinfeld. Numerical solution of dynamic equation for particulate systems. *Journal of Computational Physics*, 28:357–375, 1978.

[17] F. Gelbard, Y. Tambour, and J.H. Seinfeld. Sectional representations for simulating aerosol dynamics. *Journal of Colloid and Interface Science*, 76:541–556, Aug. 1980.

[18] A. Gomez and D.E Rosner. Thermophoretic effects on particles in counterflow laminar diffusion flames. *Combustion Science and Technology*, 89:335–362, 1993.

[19] A. Gurav, T. Kodas, T. Pluym, and Y. Xiong. Aerosol processing of materials. *Aerosol Science and Technology*, 19:411–452, 1993.

[20] M.J. Hounslow. A discretized population balance for continuous systems at steady state. *AIChE Journal*, 36(1):106–116, Jan. 1990.

[21] F.P. Incropera and D.P. De Witt. *Fundamentals of Heat and Mass Transfer.* 3 edition.

[22] S. Jain, T.T. Kodas, M.K. Wu, and P. Preston. Role of surface reaction in aerosol synthesis of titanium dioxide. *Journal of Aerosol Science*, 28(1):133–146, 1997.

[23] J.I. Jeong and M. Choi. A sectional method for the analysis of growth of polydisperse non-spherical particles undergoing coagulation and coalescence. *Journal of Aerosol Science*, 32:565–582, 2001.

[24] B.J. Kelett and F.F. Lange. Thermodynamics of densification: I, sintering of simple particle arrays, equilibroum configurations, pore stability, and shrinkage. *Journal of the American Ceramic Society*, 72(5):725–734, 1989.

[25] A. Kobata, K. Kusakabe, and S. Morooka. Growth and transformation of TiO_2 crystallites in aersol reactor. *AIChE Journal*, 37(3):347–359, Mar. 1991.

[26] W. Koch and S.K. Friedlander. The effect of particle coalescence on the surface area of a coagulating aerosol. *Journal of Aerosol Science*, 20(8):891–894, 1989.

[27] W. Koch and S.K. Friedlander. The effect of particle coalescence on the surface area of a coagulating aerosol. *Journal of Colloid and Interface Science*, 140(2):419–427, Dec. 1990.

[28] T.T. Kodas and S.K. Friedlander. Design of tubular flow reactors for monodisperse aerosol production. *AIChE Journal*, 34(4):551–557, April 1988.

[29] M. Kostoglou and A.G. Konstandopoulos. Brownian coagulation of fractal aggregates. In *Journal of Aerosol Science*, volume 31, S1, pages S574–S575, Sept. 2000.

[30] F.E. Kruis, K.A. Kusters, S.E. Pratsinis, and B. Scarlett. A simple model for the evolution of the characteristics of aggregate particles undergoing coagulation and sintering. *Aerosol Science & Technology*, 19:514–526, 1993.

[31] F.E. Kruis, A. Maisels, and H. Fissan. Direct simulation monte carlo method for particle coagulation and aggregation. *AIChE Journal*, 46(9):1735–1742, Sep. 2000.

[32] K.A. Kusters and S.E. Pratsinis. Strategies for control of ceramic powder sysnthesis by gas-to-particle conversion. *Powder Technology*, 82:79–91, 1995.

[33] J.D. Landgrebe, S.E. Pratsinis, and S.V.R. Mastrangelo. Nomographs for vapor synthesis of ceramic powders. *Chemical Engineering Science*, 45(9):2931–2941, 1990.

[34] F.F. Lange. Powder processing science and technology for increased reliability. *Journal of the American Ceramic Society*, 72(1):3–15, 1989.

[35] B.W. Lee, J.I. Jeong, J.Y. Hwang, M. Choi, and S.H. Chung. Analysis of growth of non-spherical silica particles in a counterflow diffusion flame considering chemical reaction, coagulation and coalescence. *Journal of Aerosol Science*, 32:165–185, 2001.

[36] Kruis F.E. Maisels, A. and H. Fissan. Synthesis of composite nanoparticle pairs. In *Journal of Aerosol Science*, volume 31, S1, pages S1007–S1008, Sept. 2000.

[37] T. Matsoukas and S.K. Friedlander. Dynamics of aerosol agglomerate formation. *Journal of Colloid and Interface Science*, 146(2):495–506, Oct. 1991.

[38] P. Meakin. Fractal aggregates. *Advances in Colloid and Interface Science*, 28:249–331, 1988.

[39] R.D. Mountain, G.W. Mulholland, and H. Baum. Simulation of aerosol agglomeration in the free molecular and continuum flow regimes. *Journal of Colloid and Interface Science*, 114(1):67–81, Nov. 1986.

[40] M. Nicmanis and M.J. Hounslow. Finite-element methods for steady-state population balance equations. *AIChE Journal*, 44(10):2258–2272, Oct. 1998.

[41] K. Okuyama, R. Ushio, Y. Kousaka, R.C. Flagan, and J.H. Seinfeld. Particle generation in chemical vapor deposition process with seed particles. *AIChE Journal*, 36(3):409–419, Mar. 1990.

[42] K. Okuyama, R. Ushio, Y. Kousaka, J.H. Seinfeld, and R.C. Flagan. Evaluation of fine particle formation by cvd in a laminar-flow aerosol reactor. *International Chemical Engineering*, 32(4):750–758, Oct. 1992.

[43] H.M. Park and D.E. Rosner. Boundary layer coagulation effects on the size distribution of thermophoretically deposited particles. *Chemical Engineering Science*, 44(10):2225–2231, 1989.

[44] S.E. Pratsinis. Flame aerosol synthesis of ceramic powders. *Progess in Energy and Combustion Science*, 24(3):197–219, 1998.

[45] S.E. Pratsinis and P.T. Spicer. Competition between gas phase and surface phase oxidation of $TiCl_4$ during the synthesis of TiO_2 particles. *Chemical Engineering Science*, 53(10):1861–1868, 1998.

[46] S.E. Pratsinis and S. Vemury. Particle formation in gases: a review. *Powder Technology*, 88(3):267–273, 1996.

[47] T.E. Ramabhadran, T.W. Peterson, and J.H. Seinfeld. Dynamics of aerosol and coagulation and condensation. *AIChE Journal*, 22(5):840–851, Sept. 1976.

[48] A.D. Randolph and M.A. Larson. *Theory of Particulate Processes: Analysis and Techniques of Continuous Crystallization.* Academic Press Inc., San Diego, 1998.

[49] Prausnitz J.M. Reid, R.C. and B.E. Polling. *The Properties of Gases and Liquids.* McGraw-Hill, New York, 4 edition, 1986.

[50] S.N. Rogak. Modelling small cluster deposition on the primary particles of aerosol agglomerates. *Aerosol Science and Technology*, 26:127+, 1997.

[51] S.N. Rogak and R.C. Flagan. Coagulation of aerosol agglomerates in the transition regime. *Journal of Colloid and Interface Science*, 151(1):203–224, June 1992.

[52] D.E. Rosner and S. Yu. Mc simulation of aerosol aggregation and simultaneous spheroidization. *AIChE Journal*, 47(3), March.

[53] M. Sadataka, Y.B. Xu, and A. Harano. A systematic approach for the design of aerosol reactors. *Powder Technology*, 88:261–266, 1996.

[54] A. Schmidt-Ott. Aerosol instrumentation. Tutorial at the European Aerosol Conference 2000, Institute for Combustion and Gas Dynamics, Gerhard-Mercator-University Duisberg, 47048 Duisberg, Germany, September 2000.

[55] J.H. Seinfeld. *Atmospheric Chemistry and Physics: from Air Pollution to Climate Change.* Wiley, New York, 1998.

[56] M. Smith and T. Matsoukas. Constant-number monte carlo simulation of population balances. *Chemical Engineering Science*, 53(9):1777–1786, 1998.

[57] Van Ness H.C. Smith, J.M. and M.M. Abbott. *Introduction to Chemical Engineering Thermodynamics.* McGraw-Hill, New York, 5 edition, 1996.

[58] P. Stamatakis, C.A. Natalie, B.R. Palmer, and W.A. Yuill. Research needs in aerosol processing. *Aerosol Science and Technology*, 14:316–321, 1991.

[59] P. Tandon and D.E. Rosner. Monte carlo simulation of particle aggregation and simultaneous restructuring. *Journal of Colloid and Interface Science*, 213:273–286, 1999.

[60] G.D Ulrich and N.S. Subramanian. Particle growth in flames iii: Coalescence as a rate-controlling process. *Combustion Science and Technology*, 17:119–126, 1977.

[61] M. Wilck and F. Stratmann. A 2-d multicomponent modal aerosol model and its application to laminar flow reactors. *Journal of Aerosol Science*, 28(6):959–972, 1997.

[62] J.J. Wu and R.C. Flagan. Onset of runaway nucleation in aerosol reactors. *Journal of Applied Physics*, 61(4):1365–1371, 1987.

[63] J.J. Wu, H.V. Nguyen, R.C. Flagan, K. Okuyama, and Y. Kousaka. Evaluation and control of particle properties in aerosol reactors. *AIChE Journal*, 34(8):1249–1256, Aug. 1988.

[64] Y. Xiong and S.E. Pratsinis. Gas-phase production of particles in reactive turbulent flows. *Journal of Aerosol Science*, 22(5):637–655, 1991.

[65] Y. Xiong, S.E. Pratsinis, and A.W. Weimer. Modelling the formation of boron carbide particles in an aerosol flow reactor. *AIChE Journal*, 38(11):1685–1692, Nov. 1992.

[66] M.R. Zachariah and P. Dimitriou. Controlled nucleation in aerosol reactors for suppression of agglomerate formation: A numerical study. *Aerosol Science and Technology*, 13:413–425, 1990.

Part III

Appendices

Appendix A

Maximum Contraction of a Bi-Particle Agglomerate

The maximum decrease in length of a bi-particle agglomerate, because of coalescence, is predicted by the contact angle relaxation model, for the centre-to-centre approach mechanism (see section 2.5.2, figure 2.3).

Figure A.1 is a scale-drawing to determine the fractional decrease in the length of a bi-particle agglomerate ($\Delta L/L_0$), for the metastable equilibrium geometry corresponding to a dihedral angle of $\psi_e = 120^0$:

$$\frac{\Delta L}{L_0} = \frac{L_0 - L}{L_0} = 0.21 \tag{A.1}$$

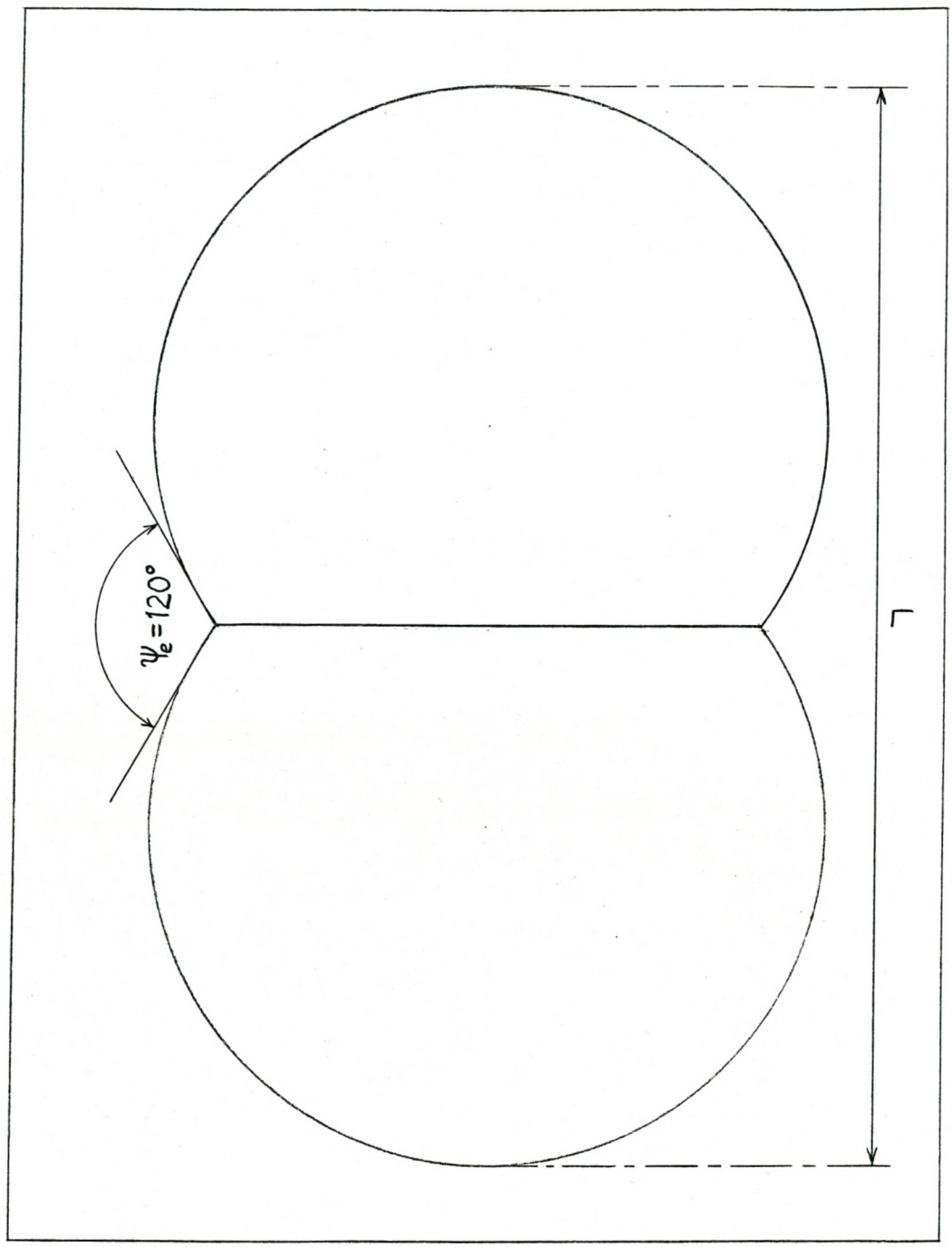

Figure A.1: Maximum Contraction of a Bi-Particle Agglomerate

Appendix B

Geometry of Bi-Particle Coalescence with Zero Neck Curvature

The geometry of a bi-particle agglomerate, undergoing coalescence according to the *neck curvature model* (see section 2.5.2, figure 2.2), is evaluated for the case where the neck curvature is zero, i.e. when the neck length is equal to the neck radius:

$$\ell_n = x \tag{B.1}$$

This is the geometry that was presumably used by Kobata et al. (1991) to calculate the characteristic sintering time (see page 57).

Figure B.1 is a scale-drawing to show the ratio between neck radius and initial particle radius (ℓ_n/r_i) for neck growth corresponding to $\ell_n = x$. The accurate value of the ratio was calculated, but the mathematical analysis is not shown here.

$$\ell_n/r_i = 0.814 \tag{B.2}$$

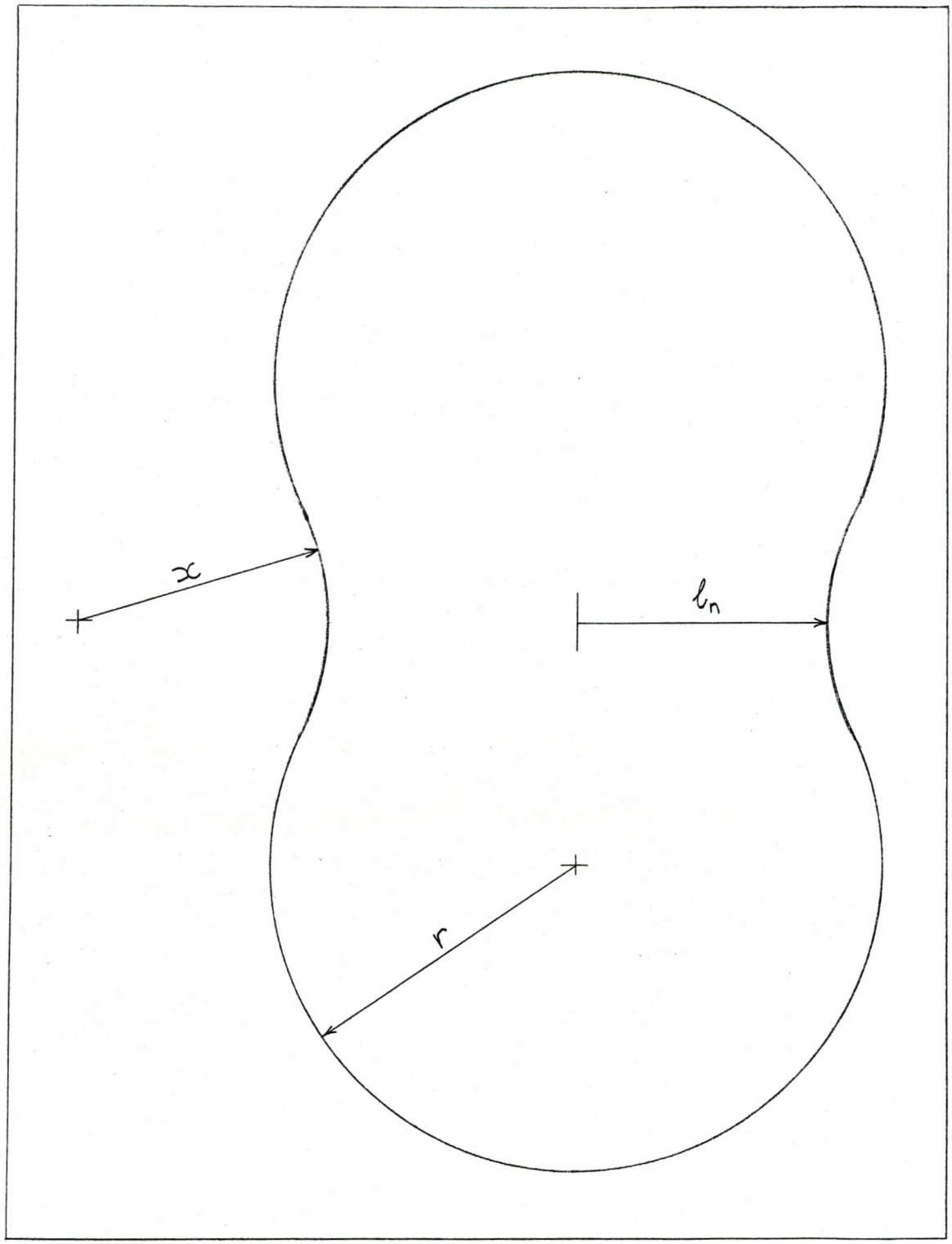

Figure B.1: Geometry of Bi-Particle Coalescence with Zero Neck Curvature

Appendix C

Code for Numerical Simulations

Invocation of numerical integration algorithm:

```
» TSPAN=[0,1];
» Y0=[-log(1-1e-5) 0 -log(1-1e-6) 0];
» [T,Y]=ODE15s('TwoMode',TSPAN,Y0)
```

Aerosol reactor model equations:

```
function zdot = TwoMode(T,Y)

%Non-dimensional Parameters
Kg=1.898e4;
Kc=2.12E+12;
l0d1=0.951;
Kn0=1635;
eps=1000;

%Particle size
mp=exp(Y(2))

%Conversions
Xg=1-exp(-Y(1));
Xmp=1-exp(-Y(3));
Xmm=2*Xmp/exp(Y(2)-Y(4));
Xpp=1-exp(-Y(4));

%Number Concentrations
nT=exp(-Y(1))/(1+eps);
nm=Xg*exp(-Y(3))/(1+eps);
np=0.5*Xg*Xmm*exp(-Y(4))/(1+eps);

%Gas-phase Reaction Rate
Rg=Kg*nT;

%Auxiliary Variables for Collisions
Dfm=(5+4*Kn0+6*Kn0^2+18*Kn0^3)/(5-Kn0+(8+pi)*Kn0^2);
Knp=Kn0/mp^(1/3);
Dfp=(5+4*Knp+6*Knp^2+18*Knp^3)/(5-Knp+(8+pi)*Knp^2)/mp^(1/3);
cmp=sqrt(1+1/mp);
cpp=sqrt(2/mp);
gm=((1+l0d1.*Dfm)^3-(1+l0d1.^2.*Dfm.^2).^(3/2))./(3.*Dfm.*l0d1)-1;
gp=((mp.^(1/3)+l0d1.*Dfp.*mp.^(1/2))^3-(mp.^(2/3)+l0d1.^2.*Dfp.^2.*mp).^(3/2))...
   ./(3.*Dfp.*mp.^(5/6).*l0d1)-mp.^(1/3);
gmm=sqrt(2).*gm;
gmp=sqrt(gm.^2+gp.^2);
gpp=sqrt(2).*gp;
Bbmm=8*pi.*Dfm/(1/(1+gmm)+pi.*l0d1.*Dfm./sqrt(2));
Bbmp=2*pi.*(Dfm+Dfp).*(1+mp.^(1/3))/...
   ((1+mp.^(1/3))./(1+mp.^(1/3)+2.*gmp)+pi.*l0d1.*(Dfm+Dfp)./cmp./(1+mp.^(1/3)));
Bbpp=8*pi.*Dfp.*mp.^(1/3)/...
    (mp.^(1/3)./(mp.^(1/3)+gpp)+pi.*l0d1.*Dfp./cpp./mp.^(1/3));

%Collision rates
Rmm=Kc*Bbmm*nm^2;
Rmp=Kc*Bbmp*nm*np;
Rpp=Kc*Bbpp*np^2;

%CHANGE IN CONVERSION

zdot=[Rg/exp(-Y(1))
   (2*Rmm+Rmp+(Rpp-Rmm)*mp)/(Xg*Xmp)
   (2*Rmm+Rmp-Rg*Xmp)/(Xg*exp(-Y(3)))
   2*(Rpp-Rmm*Xpp)/(Xg*Xmm*exp(-Y(4)))];
```

Appendix D

Analysis of Process Parameters

The purpose of this appendix is to determine an independent set of *process parameters* for the model in chapter 8. Before this is done, the different quantities in the model system are classified.

D.1 Quantities Describing the System

The basic classification of quantities is to differentiate between variables, parameters and constants. Sections D.1.1 to D.1.3 discuss the classification of quantities. Figure D.1 summarises the classification of quantities.

D.1.1 Variables

The quantities that describe the changing particle population and gas composition are variables. The model will be used to simulate spatial change of the variables.

D.1.2 Parameters

There are some quantities which are remain constant during any simulation with the model. However, these quantities may be different for different simulations. These quantities are called parameters.

A classification is made between parameters relating to the process conditions and geometry, parameters relating to the specific species involved in the reaction, and parameters that represent model simplifications.

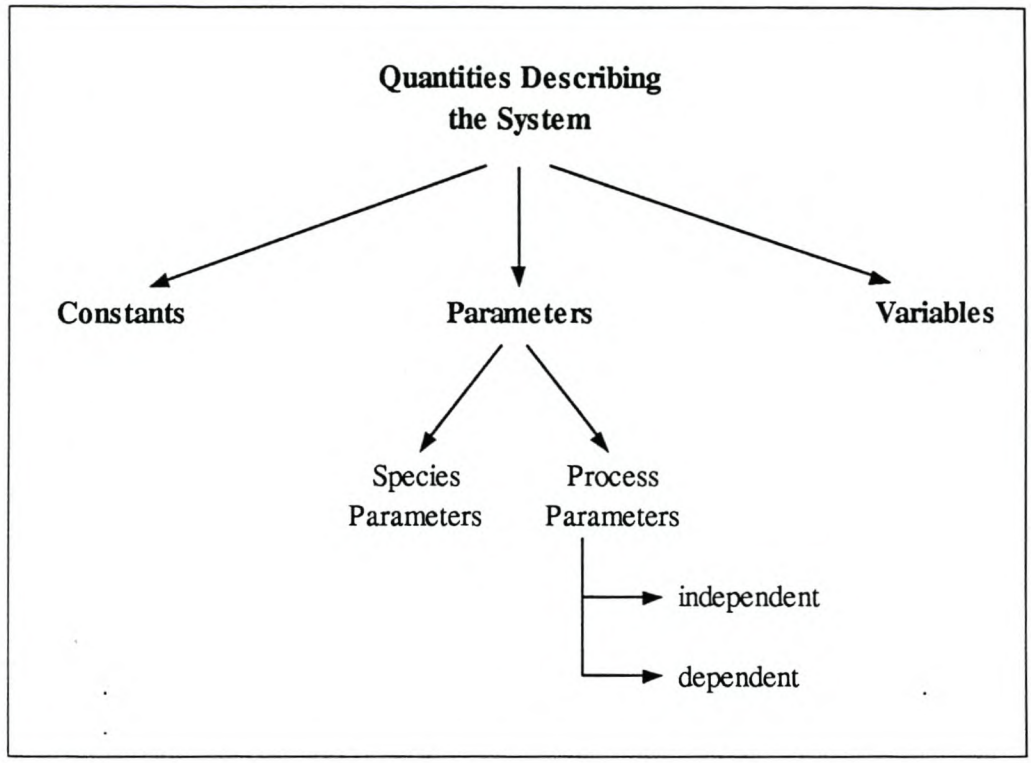

Figure D.1: Classification of Quantities Describing the System

Species Parameters

Species parameters depend only on the species involved in the reaction.

Process Parameters

Parameters relating to process conditions and reactor geometry are called process parameters. Many process parameters are inter-related, and thus does not constitute an independent set (in mathematical terms). In section D.2 equations are given that shows the interdependence of process parameters. The equations are written in such a form so as to identify an *independent set of process parameters*. This independent set of process parameters, as well as a list of dependent process parameters, are summarised in tabular format in section D.3.

Model Parameter

A certain parameter is introduced to describe the approximate representation of clusters in the model.

The formation di-mers and larger clusters, and the deposition of such clusters onto seeds and the reactor wall, are neglected. A model parameter, f, compensates for this approximation by quantifying the ratio between monomer consumption by seed-monomer collision and monomer consumption by monomer-monomer collision. This parameter originated from the simplified (and abstract) representation of the real system by the model system. Therefore this parameter is called a *model parameter*. Because of the uncertainty of the value of this parameter, it will be subjected to sensitivity analysis.

D.1.3 Constants

Some *universal constants* are used, such as the Avogadro number.

D.2 Interdependence of Process Parameters

Consult the tables in section D.3 for definition of terminology, and classification of quantities.

Fractional Excess Gas

The total gas concentration, C_T is approximated to be constant throughout the reactor. This approximation is based on the assumptions of large excess gas and constant temperature and pressure. The initial concentration of the limiting reactant ($C_0 = C_{M_0}$) is calculated as a fraction of the total gas concentration:

$$C_0 = \left(\frac{C_0}{C_T}\right) C_T \quad \left[\frac{mol}{m^3}\right] \tag{D.1}$$

C_T is the total gas concentration, and is calculated according to the ideal gas law.

$$C_T = \frac{P}{k_B A_v T} \quad \left[\frac{mol}{m^3}\right] \tag{D.2}$$

The following notation is used to describe the chemical reaction:

$$\alpha_M M + \alpha_O O \rightarrow m + \alpha_{bp}(byproduct\ gas) \tag{D.3}$$

where M is the metal-containing reactant, O is the the oxidant reactant, and m is a product monomer. α_i is the stoichiometric coefficient.

The volume (mole) fraction of the limiting reactant M is a function of the excess gas:

$$\frac{C_0}{C_T} = \frac{C_{M_0}}{C_{M_0} + C_{O_0}} \tag{D.4}$$

$$= \frac{1}{1 + \frac{\alpha_O}{\alpha_M}(1+\varepsilon)} \tag{D.5}$$

$$\approx \frac{\alpha_M}{\alpha_O \varepsilon} \tag{D.6}$$

The approximation in equation D.6 is based on the assumption of large excess non-limiting reactant O (and possibly inert gas): $\varepsilon \gg 1$.

Combination of equations D.1, D.2 and D.6 gives the expression for the fractional excess non-reacting gas (ε) in terms of other process parameters. These other parameters are independent of each other, and this equation shows that (ε) is a dependent process parameter:

$$C_0 = \frac{\alpha_M}{\alpha_O \varepsilon}\left(\frac{P}{k_B A_v T}\right) \tag{D.7}$$

$$\varepsilon = \left(\frac{P}{k_B A_v T}\right)\frac{\alpha_M}{\alpha_O C_0} \tag{D.8}$$

Initial Number Flux of Limiting Reactant

Number flux is expressed as a function of the production rate. An operating time of 8150 hr/a is assumed [Douglas (1988), p. 73].

$$N_0\left[\frac{\#}{s}\right] = M_{pr}\left[\frac{t}{a}\right]\cdot 10^6\left[\frac{g}{t}\right]\cdot\frac{1}{MW_{product}}\left[\frac{mol}{g}\right]\cdot A_v\left[\frac{\#}{mol}\right]\cdot\frac{1}{8150}\left[\frac{a}{h}\right]\cdot\frac{1}{3600}\left[\frac{h}{s}\right] \tag{D.9}$$

$$N_0 = 0.0341\frac{M_{pr}A_v}{MW_{product}}\left[\frac{\#}{s}\right] \tag{D.10}$$

Residence Time

The residence time for production of the required particle size can be determined by simulation with an appropriate model. The residence time is a function of all the independent process parameters (see the table in section D.3):

$$\tau_r = \tau_r(P, T, C_0, M_{pr}, u, d_s, d_{p_f}) \; [s] \tag{D.11}$$

Gas Density

Gas density is calculated by assuming constant total gas flux (see equation 6.10), and that the limiting reactant has negligible effect on the total gas density:

$$\rho = \frac{C_T MW_O}{1000} \left[\frac{kg}{m^3}\right] \tag{D.12}$$

$$= \frac{PMW_O}{1000 k_B A_v T} \tag{D.13}$$

Reynolds Number

The Reynolds number is a function of u and D:

$$Re = \frac{\rho u D}{\mu} \tag{D.14}$$

$$uD = \frac{Re\mu}{\rho} \left[\frac{m^2}{s}\right] \tag{D.15}$$

Flow Velocity

In addition to equation D.15, another relationship between u and D is determined by N_0:

$$N_0 \left[\frac{\#}{s}\right] = C_0 \left[\frac{mol}{m^3}\right] \cdot \frac{\pi}{4} D^2 \left[m^2\right] \cdot u \left[\frac{m}{s}\right] \cdot A_v \left[\frac{\#}{mol}\right] \tag{D.16}$$

Substitution of C_0 with equation D.7 gives:

$$N_0 = \frac{P}{k_B A_v T} \frac{\alpha_M}{\alpha_O \varepsilon} \frac{\pi}{4} D^2 u A_v \left[\frac{\#}{s}\right] \tag{D.17}$$

Rearrangement gives:

$$uD^2 = N_0 \frac{k_B T}{P} \frac{\alpha_O \varepsilon}{\alpha_M} \frac{4}{\pi} \left[\frac{m^3}{s}\right] \quad \text{(D.18)}$$

$$= N_0 \frac{k_B T}{P} \frac{\alpha_O \varepsilon}{\alpha_M} \frac{4}{\pi} \cdot \left(\frac{Re\mu}{\rho u D}\right) \quad \text{(D.19)}$$

Dividing equations D.18 and D.19 by equation D.15:

$$D = \left(\frac{N_0}{Re}\right) \frac{\rho}{\mu} \frac{k_B T}{P} \frac{\alpha_O \varepsilon}{\alpha_M} \frac{4}{\pi} \; [m] \quad \text{(D.20)}$$

$$= \left[\frac{N_0}{u} \frac{k_B T}{P} \frac{\alpha_O \varepsilon}{\alpha_M} \frac{4}{\pi}\right]^{\frac{1}{2}} \; [m] \quad \text{(D.21)}$$

$$u = \frac{N_0}{D^2} \frac{k_B T}{P} \frac{\alpha_O \varepsilon}{\alpha_M} \frac{4}{\pi} \; [m/s] \quad \text{(D.22)}$$

Reactor Volume

The reactor volume is a function of flow velocity and residence time:

$$V = \frac{\pi}{4} D^2 u \tau_r \; [m^3] \quad \text{(D.23)}$$

D.3 Tables of Quantities

Independent Process Parameters

P $[N/m^2]$	reactor pressure
T $[K]$	reactor temperature
C_0 $[mol/m^3]$	initial reactant concentration
M_{pr} $[t/a]$	production rate
D $[m]$	reactor diameter
n_p $[\#/m^3]$	seed particle concentration
d_{p_0} [m]	initial (seed) particle size
d_{p_f} [m]	final (product) particle size

Dependant Process Parameters

ε	fractional excess gas	see eq. D.8
N_0 $[\#/s]$	initial flux of limiting reactant	see eq. D.10
τ_r $[s]$	residence time	see eq. D.11
ρ $[kg/m^3]$	gas density	see eq. D.13
u $[m/s]$	flow velocity	see eq. D.22 (and D.10)
Re	Reynolds number	see eq. D.14 (and D.22)
V $[m^3]$	reactor volume	see eq. D.23

Species Parameters

A_g $[s^{-1}]$	reaction constant
E_g [J/mol]	reaction activation energy
MW_i [g/mol]	molecular weight: i = metal- containing reactant (M) *or* oxidant gas (O) *or* product
v_1 $[m^3/mol]$	product molar volume (in bulk solid phase)
α_i	stoichiometric coefficient of reactant i
μ [Pa·s]	gas viscosity

Universal Constants

A_v $[\#/mol]$	Avogadro number
k_B $[J/\#\cdot K]$	Boltzmann constant

Appendix E

Constraint of Laminar Flow

Turbulent flow must be avoided as it will spread out the PSD. It is generally accepted that single-phase flow in a circular tube is laminar for $Re \leq 2000$ [De Nevers (1991)]. The flow in an aerosol reactor consists of two phases: the bulk gas and the small particles suspended therein. It can be expected that the presence of these particles will cause turbulent flow at lower Reynolds numbers than for single-phase flow. The maximum Reynolds number (or functional description thereof) for laminar flow of an aerosol is not known. Here, as a first approximation, the maximum Reynolds number is chosen to be half that for single-phase flow:

$$Re = \frac{\rho u D}{\mu} < 1000 \tag{E.1}$$

This constraint is written in terms of the independent set of process parameters by using equations D.8, D.10 and D.22 in appendix D:

$$u = \frac{N_0}{D^2}\frac{k_B T}{P}\frac{\alpha_O \varepsilon}{\alpha_M}\frac{4}{\pi} \; [m/s] \tag{E.2}$$

$$\varepsilon = \left(\frac{P}{k_B A_v T}\right)\frac{\alpha_M}{\alpha_O C_0} \tag{E.3}$$

$$N_0 = 0.0341\frac{M_{pr} A_v}{MW_{product}} \tag{E.4}$$

$$u = 0.0341\frac{M_{pr}}{MW_{product}}\frac{4}{\pi D^2 C_0} \tag{E.5}$$

The laminar flow constraint can be now be written in terms of the design parameters D and C_0, by substituting equation E.5 into equation E.1:

$$Re = 0.0341 \frac{M_{pr}}{MW_{product}} \frac{4}{\pi D^2 C_0} \frac{\rho D}{\mu} < 1000 \tag{E.6}$$

$$DC_0 > 0.0341 \frac{M_{pr}}{MW_{product}} \frac{4}{\pi} \frac{\rho}{\mu} \frac{1}{1000} \tag{E.7}$$

Appendix F

Kinetic Theory Approximation of Collision Coefficient

In section 2.4 an expression for monomer-particle collision frequency (equation 2.52) was derived for systems where evaporation is negligible (i.e. in conditions of uninhibited coagulation). This expression corresponds to the modelling of Kodas and Friedlander (1988).

$$\beta_{m,p} = 2\pi D_m d_p F(\mathrm{Kn}) \left[\frac{m^3}{\# \cdot s}\right] \tag{F.1}$$

$$F(\mathrm{Kn}) = \frac{1+\mathrm{Kn}}{1+1.71\mathrm{Kn}+\frac{4}{3}\mathrm{Kn}^2} \tag{F.2}$$

$$\mathrm{Kn} = \frac{2\lambda}{d_p} \tag{F.3}$$

- For the *continuum regime* (particles are big compared to the mean free path of the gas):

$$\mathrm{Kn} \to 0 \;\; ; \;\; F(\mathrm{Kn}) \to 1 \tag{F.4}$$

- For the *kinetic theory regime* (particles are small compared to the mean free path of the gas):

$$\mathrm{Kn} \to \infty \;\; ; \;\; F(\mathrm{Kn}) \to \frac{3}{4\mathrm{Kn}} \tag{F.5}$$

To derive a simplified expression for β_{mp}, the value of $F(\mathrm{Kn})$ is evaluated at typical conditions for constant number seed growth of ceramic particles in an aerosol reactor. Conditions similar to the experimental conditions of Okuyama et al. (1990) are chosen:

$$\begin{aligned} T &= 773\,K \\ P &= 1\,bar \\ \text{product} &= TiO_2 \\ MW_{bg} &= 28\,g/mol\ \ (N_2) \\ \mu &= 3.4 \cdot 10^{-5}\ N \cdot s/m^2 \\ d_p &= 53\,nm \end{aligned}$$

First, the mean free path of the bulk gas, λ, is approximated according to the kinetic theory of gases [Seinfeld (1998), p.455]:

$$\lambda = \frac{2\mu}{P}\left(\frac{\pi k_B A_v T}{8MW_{bg} \times 10^{-3}}\right)^{\frac{1}{2}} \tag{F.6}$$

$$= \frac{2 \times 3.4 \cdot 10^{-5}}{10^5}\left(\frac{\pi k_B A_v 773}{8 \times 0.028}\right)^{\frac{1}{2}} \tag{F.7}$$

$$= 2.04 \cdot 10^{-7}\ [m] \tag{F.8}$$

Now Kn and $F(\mathrm{Kn})$ are calculated:

$$\mathrm{Kn} = \frac{2\lambda}{d_p} = 7.7 \tag{F.9}$$

$$F(\mathrm{Kn}) = \frac{1 + \mathrm{Kn}}{1 + 1.71\mathrm{Kn} + \frac{4}{3}\mathrm{Kn}^2} = 0.093 \tag{F.10}$$

$$\frac{3}{4Kn} = 0.097 \tag{F.11}$$

$$F(\mathrm{Kn}) \approx \frac{3}{4Kn} \tag{F.12}$$

A comparison of the numerical values of equations F.10 and F.11 is used to evaluate the applicability of approximating the monomer-particle collision rate with the kinetic theory of gases (see equation F.5). It can be seen that it is appropriate to use the kinetic theory approximation of the collision coefficient expression, for the specified numerical conditions.

Note that for larger particle sizes, the approximation becomes less accurate:

$$\begin{aligned} d_p &= 200\,nm \\ \mathrm{Kn} &= 2.04 \\ F(\mathrm{Kn}) &= 0.30 \\ \frac{3}{4Kn} &= 0.37 \end{aligned} \tag{F.13}$$

Furthermore, the approximation is limited to the specific process conditions and material properties, and therefore this approximation is not necessarily true for all constant seed growth systems.

$$\beta_{m,p} = 2\pi D_m d_p F(\mathrm{Kn}) \tag{F.14}$$

$$\approx 2\pi D_m d_p \left(\frac{3}{4Kn}\right) \tag{F.15}$$

$$= 2\pi D_m d_p \left(\frac{3d_p}{4 \cdot 2\lambda}\right) \tag{F.16}$$

$$= \frac{3\pi D_m d_p^2}{4\lambda} \tag{F.17}$$

The monomer-particle collision coefficient is approximately proportional to the square of the particle diameter.

Appendix G

Analysis of Turbulent Coagulation

Constants

k_B [J #$^{-1}$K^{-1}]	1.38E-23
A_v [#/mol]	6.02E+23

Species Parameters

M_{pr} [kg/mol]	0.080
MW_{bg} [kg/mol]	0.028
v_m [m3/#]	3.12E-29
d_m [m]	3.9E-10
μ (T=773K, P= 1atm [Pa.s]	3.41E-05
ρ (T=773K, P= 1atm [kg/m^3]	0.465

Process Parameters

T [K]	773
P	1.00E+05
d_p [m]	8.0E-08
m_p	8.6E+06
v_p [m^3/#]	2.7E-22
u_{ac} *[m/s]*	*5.7E+02*

Brownian Collision Coefficients

$=f(T,P,d_i)$

β_{Bmm} [m^3#$^{-1}$s^{-1}]	3.06E-16
β_{Bmp} [m^3#$^{-1}$s^{-1}]	2.292E-12
β_{Bpp} [m^3#$^{-1}$s^{-1}]	3.274E-15
λ [m]	2.0E-07
D_{fm} [m^2/s]	1.4E-04
Kn_m	1.0E+03
c_m [m/s]	4.5E+02
c_{mm} [m/s]	6.4E+02
l_m [m]	8.1E-07
g_m [m]	8.1E-07
g_{mm} [m]	1.1E-06
c_{mp} [m/s]	4.5E+02
g_{mp} [m]	8.1E-07
D_{fp} [m^2/s]	3.7E-09
Kn_p	5.1E+00
c_p [m/s]	1.5E-01
c_{pp} [m/s]	2.2E-01
l_p [m]	6.1E-08
g_p [m]	4.2E-08
g_{pp} [m]	5.9E-08

Design Parameters

M_{flow} [kg/h]	100						
D [m]	0.55	0.28	0.14	0.07	0.03	0.02	0.0086
u [m/s]	0.25	1	4	16	64	256	1024
Re	*1.9E+03*	*3.8E+03*	*7.5E+03*	*1.5E+04*	*3.0E+04*	*6.0E+04*	*1.2E+05*

Turbulent Collision Coefficients

$=f(T,P,d_i,D,u)$

β_{Tmm} [$m^3\#^{-1}s^{-1}$]	1.2E-28	1.2E-27	1.1E-26	1.1E-25	1.1E-24	1.1E-23	1.1E-22
β_{Tmp} [$m^3\#^{-1}s^{-1}$]	1.3E-22	1.3E-21	1.3E-20	1.2E-19	1.2E-18	1.2E-17	1.2E-16
β_{Tpp} [$m^3\#^{-1}s^{-1}$]	1.0E-21	9.9E-21	9.9E-20	9.8E-19	9.7E-18	9.7E-17	9.6E-16
K_T [1/s]	4.7E-01	4.6E+00	4.6E+01	4.6E+02	4.5E+03	4.5E+04	4.5E+05
ε_d [m^2/s^3]	5.3E-05	5.2E-03	5.1E-01	5.1E+01	5.0E+03	4.9E+05	4.9E+07
f	1.2E-02	1.0E-02	8.5E-03	7.1E-03	6.0E-03	5.1E-03	4.2E-03

Comparison of Turbulent Collision Coefficient vs. Brownian Collision Coefficient

D [m]	0.55	0.28	0.14	0.07	0.03	0.02	0.01
u [m/s]	0.10	1	4	16	64	256	1024
Re	*1.9E+03*	*3.8E+03*	*7.5E+03*	*1.5E+04*	*3.0E+04*	*6.0E+04*	*1.2E+05*
β_{Tmm}/β_{Bmm}	3.8E-13	3.8E-12	3.7E-11	3.7E-10	3.7E-09	3.7E-08	3.6E-07
β_{Tmp}/β_{Bmp}	5.5E-11	5.5E-10	5.5E-09	5.4E-08	5.4E-07	5.3E-06	5.3E-05
β_{Tpp}/β_{Bpp}	3.1E-07	3.0E-06	3.0E-05	3.0E-04	3.0E-03	3.0E-02	2.9E-01

Appendix H

Analysis of Seed Growth in an Isothermal Reactor

H.1 Manipulation of Seed Growth Data

H.1.1 Equations

Reaction Conversion

For first-order reaction kinetics:

$$X = 1 - \exp(-k\tau_{res}) \tag{H.1}$$

Fractional Excess Gas

$$\varepsilon = \frac{\frac{P}{k_B A_v T} - C_0}{C_0} \tag{H.2}$$

Thermodynamic Entry Length

$$\epsilon_{tc} = 0.05 \frac{Pr\rho D^2}{\mu\tau_{res}} \tag{H.3}$$

Volume-Average Particle Size

The log-normal distribution is a good approximation of the particle size distribution created by coagulation-controlled growth. Therefore aerosol size distributions are commonly characterised by the geometric mean (d_{pg}) and geometric standard deviation (σ_g), the parameters of the log-normal distribution:

$$f(\ln d_p) = \frac{1}{\sqrt{2\pi}\ln\sigma_g}\exp\left[-\frac{\ln^2(d_p/d_{pg})}{2\ln^2\sigma_g}\right] \tag{H.4}$$

Integration of the particle volume over all particle sizes, using the log-normal distribution, gives the following expression for the volume-average particle diameter:

$$d_{pv} = \left[\frac{1}{\sqrt{2\pi}\ln\sigma_g}\int_0^\infty d_p^2\exp\left(-\frac{\ln^2(d_p/d_{pg})}{2\ln^2\sigma_g}\right)\mathrm{d}d_p\right]^{\frac{1}{3}} \tag{H.5}$$

This integral is solved numerically.

Yield Loss to Wall-Deposition (for experiments without seeds)

Since no seeds are present, the term *'yield loss to wall-deposition'* (X_{wd}) is used instead of the *'wall-to-seed deposition ratio'* (W/S). These two quantities both indicate the ratio between wall-deposition and particle yield/growth. In the presence of seeds, wall-deposition will be suppressed in the same manner that cluster growth is suppressed. Hence, (W/S) [with seeds] $< X_{wd}$ [with no seeds]. For the specific data that is evaluated here, cluster growth is not completely constrained. Therefore a value for (W/S) that is just slightly smaller than X_{wd} is assumed is the subsequent calculations.

To calculate X_{wd}, the particle yield is first calculated:

$$\text{particle yield} = \frac{n_{pn}}{A_v}\cdot\frac{\pi}{6v_1}d_{pn}^3 \tag{H.6}$$

The fractional wall-deposition is inferred from the different between the particle yield and the reaction yield:

$$X_{wd} = \frac{C_0X - (\text{particle yield})}{(\text{particle yield})} \tag{H.7}$$

Final (Product) Particle Size

To calculate d_{p_f}, the new particle yield is first calculated:

$$\text{new particle yield} = \frac{n_{pn}}{A_v} \cdot \frac{\pi}{6v_1} \cdot d_{pn}^3 \tag{H.8}$$

$$d_{p_f} = \left[\frac{(C_0 X - (\text{new particle yield}))\, A_v}{n_p} \cdot \frac{6v_1}{\pi} \left(\frac{1}{1 + \left(\frac{W}{S}\right)} \right) + d_{p0}^3 \right]^{\frac{1}{3}} \tag{H.9}$$

H.1.2 Results of Data Manipulation

Data from Okuyama et al. (1990):

Reactor dimensions

D [m]	0.0115
L [m]	0.55

Transform

V [m^3]	5.71E-05

Reactor conditions

P [Pa]	1.01E+05
T_{in}[K]	313
T [K]	773
$C_{0,in}$ [mol/cm^3]	1.51E-10
$Q_{0,in}$ [cm^3/min]	700

k [s^{-1}]	6.76
C_0 (T) [mol/m^3]	6.11E-05
Q(T) [m^3/s]	2.88E-05
τ_{res} *[s]*	***1.98***
X	***0.999998***
ε_{excess}	***2.6E+05***
ε_{te}	***0.032***

Homogeneously nucleated particles (in absence of seeds)

d_{pn} (geometric mean) [m]	2.55E-08
σ_{gn} (geom. standard deviation)	1.61
n_{pn}/ρ [#/g]	9.18E+10

d_{pn} (volumetric mean) [m]	3.58E-08
n_{pn}(T) [$\#/m^3$]	4.27E+13
particle yield [mol/m^3]	5.46E-05
X_{wd}	***0.120***

Seed particles

d_{p0} (geometric mean) [m]	5.33E-08
σ_g (geom. standard deviation)	1.49
n_p/ρ (seeds) [#/g]	3.00E+10
n_{pt}/ρ (total) [#/g]	4.20E+10

d_{p0} (volumetric mean) [m]	6.73E-08
n_p(T) [$\#/m^3$]	1.40E+13
$(W/S)_{assumed}$	0.1
n_{pn}/ρ (new particles) [#/g]	1.20E+10
n_{pn}(T) [$\#/m^3$]	5.58E+12
d_{pn} (assumed) [m]	1.79E-08
new particle yield [mol/m^3]	8.92E-07
d_{pf} (volumetric mean) [m]	***7.64E-08***

Required particle growth

d_{p0} (vol) [m] 6.73E-08

d_{pf} (vol.) [m] 7.60E-08

d_p(av) [m] 7.18E-08

Wall-to-seed deposition ratio

(W/S) 0.1

CONSTRAINTS

C_0 [mol/m^3]	1.0E-05	5.0E-05	2.5E-04	1.3E-03	6.3E-03	3.1E-02	1.6E-01	7.8E-01	**3.9E+00**	1.6E+01	1.6E+01

Stoichiometric reactant concentration C_0(max) [mol/m^3] 15.8

ε	1.6E+06	3.2E+05	6.3E+04	1.3E+04	2.5E+03	5.0E+02	1.0E+02	1.9E+01	3.0E+00	5.3E-04	2.2E-05

Reaction conversion

n_p(max) [#/m^3]	2.43E+12	1.22E+13	6.08E+13	3.04E+14	1.52E+15	7.6E+15	3.8E+16	1.9E+17	9.5E+17	3.83E+18	3.84E+18

Constrained cluster growth f = 300

n_p(min) [#/m^3]	1.5E+15	3.3E+15	7.4E+15	1.7E+16	3.7E+16	8.3E+16	1.9E+17	4.1E+17	9.3E+17	1.9E+18	1.9E+18

Constrained cluster growth f = 30

n_p(min) [#/m^3]	4.7E+14	1.0E+15	2.3E+15	5.2E+15	1.2E+16	2.6E+16	5.9E+16	1.3E+17	2.9E+17	5.9E+17	5.9E+17

CONSTRAINTS: detail of allowable region

											cross-over of constraints	
											f=300	*f=30*
C_0 [mol/m^3]	0.1	0.5	1	4	6	8	10	12	14	16	*3.71*	*0.37*

Stoichiometric reactant concentration C_0(max) [mol/m^3] 15.8

ε	1.6E+02	3.1E+01	1.5E+01	2.9E+00	1.6E+00	9.7E-01	5.8E-01	3.1E-01	1.3E-01	-1.4E-02	*3.3*	*42*

Reaction conversion

n_p(max) [#/m^3]	2.4E+16	**1.2E+17**	2.4E+17	**9.7E+17**	1.5E+18	1.9E+18	2.4E+18	2.9E+18	3.4E+18	3.9E+18	*9.0E+17*	*9.0E+16*

Constrained cluster growth f = 300

n_p(min) [#/m^3]	1.5E+17	3.3E+17	4.7E+17	**9.4E+17**	1.1E+18	1.3E+18	1.5E+18	1.6E+18	1.8E+18	1.9E+18	*9.0E+17*	
X				0.963	0.786	0.681	0.609	0.556	0.515	0.481		
ε_{sc}				2975	1708	1460	1342	1271	1222	1187	violation of seed coagulation constraint	
α				1.9E+06	2.3E+06	2.7E+06	3.0E+06	3.3E+06	3.6E+06	3.8E+06		
β				3.55E-06	2.9E-06	2.51E-06	2.25E-06	2.05E-06	1.9E-06	1.78E-06		
τ_{res}' [s]				0.49	0.23	0.17	0.14	0.12	0.11	0.10		
τ_{res} [s]				0.49	0.23	0.17	0.14	0.12	0.11	0.10		
D (10% entry) [m]				0.0100	0.0069	0.0059	0.0053	0.0050	0.0047	0.0045		

Constrained cluster growth f = 30

n_p(min) [#/m^3]	4.7E+16	**1.0E+17**	1.5E+17	3.0E+17	3.6E+17	4.2E+17	4.7E+17	5.1E+17	5.5E+17	5.9E+17	2.8E+17	9.0E+16